

Copyright
by
Jarrett Lawrence Johnson
2009

The Dissertation Committee for Jarrett Lawrence Johnson
certifies that this is the approved version of the following dissertation:

Star Formation in the Assembly of the First Galaxies

Committee:

Volker Bromm, Supervisor

Neal J. Evans II

Lars Hernquist

Eiichiro Komatsu

Pawan Kumar

J. Craig Wheeler

Star Formation in the Assembly of the First Galaxies

by

Jarrett Lawrence Johnson, B.S., M.A.

DISSERTATION

Presented to the Faculty of the Graduate School of

The University of Texas at Austin

in Partial Fulfillment

of the Requirements

for the Degree of

DOCTOR OF PHILOSOPHY

THE UNIVERSITY OF TEXAS AT AUSTIN

May 2009

Dedicated to my fiancée, Kristi.

Acknowledgments

I am delighted to have had the chance to come to Austin and work with some of the most talented, hardworking people in the fields into which I have ventured, and I hope that I have made the most possible of this rare experience. I would like to thank Volker Bromm for his thorough and expert guidance, as well as for his unwavering encouragement. I would also like to thank Pawan Kumar for his valuable instruction and for an enriching collaboration, as well the other members of my research committee, Neal Evans, Lars Hernquist, Eiichiro Komatsu, and Craig Wheeler, for useful discussions, suggestions, and wisdom. This dissertation is the fruit of a number of collaborations, and I gratefully acknowledge the colleagues without whom both the depth and breadth of this work would have greatly suffered, among them Thomas Greif, Ralf Klessen, Anna Frebel, and Torgny Karlsson. I should rightly thank the people at the Texas Advanced Computing Center, too, for their prompt and skillful help in carrying out the simulations that went into this research.

Finally, I consider myself extraordinarily privileged to have had the abundant support of my family, who from an early age nurtured my interest in astronomy and helped set the trajectory that I have followed to this point.

Star Formation in the Assembly of the First Galaxies

Publication No. _____

Jarrett Lawrence Johnson, Ph.D.
The University of Texas at Austin, 2009

Supervisor: Volker Bromm

The character of the first galaxies at redshifts $z \geq 10$ strongly depends on the star formation which takes place during their assembly. Conducting cosmological hydrodynamics simulations, we study how the radiative output and chemical enrichment from the first stars impacts the properties of the first galaxies. We find that the radiative feedback from the first stars suppresses the star formation rate at redshifts $z \geq 15$ by a factor of only a few. In turn, this suggests that a large fraction of the first galaxies may form from gas which has already been enriched with the first heavy elements ejected by primordial supernovae. In order to characterize the properties of primordial dwarf galaxies, we carry out radiation hydrodynamics simulations which allow to determine how the luminosities in hydrogen and helium emission lines depend on the initial mass function of the stars in the galaxy. As well, we show that the chemical abundance patterns observed in metal-poor Galactic

halo stars contain the signature of the first supernovae, and we use this data to indirectly probe the properties of the first stars.

Table of Contents

Acknowledgments	v
Abstract	vi
Chapter 1. Overview	1
Chapter 2. Radiative Feedback in the Formation of the First Galaxies	4
2.1 Introduction	4
2.2 Methodology	7
2.2.1 Cosmological Initial Conditions and Resolution	7
2.2.2 Radiative Feedback	10
2.2.2.1 Photoionization	10
2.2.2.2 Photodissociation	13
2.2.3 Sink Particle Formation	17
2.3 Results	18
2.3.1 The First H II Region and Lyman-Werner Bubble	19
2.3.2 Thermal and Chemical Evolution of the Gas	20
2.3.3 Shielding of Molecules by Relic H II Regions	26
2.3.4 Black hole accretion	29
2.3.5 HD cooling in relic H II regions	32
2.3.6 Star Formation in the Presence of Radiative Feedback	35
2.4 Summary and Discussion	37
Chapter 3. The Occurrence of Primordial Galaxies in the Early Universe	42
3.1 Introduction	42
3.2 The Lyman-Werner Background	45
3.2.1 The Critical LW Flux	46

3.2.2	The Maximum Background Flux	47
3.2.3	Self-consistent Models of the LW Background	51
	3.2.3.1 Self-regulation	53
	3.2.3.2 Shielding from Relic H II Regions	57
3.2.4	The Expected Pop III Star Formation Rate	63
3.3	Methodology of Simulations	64
	3.3.1 Sink Particles	65
	3.3.2 Implementation of Background Radiation	66
3.4	Testing the Self-Regulated Model	68
	3.4.1 Initial Conditions	68
	3.4.2 Results	71
3.5	Galaxy Formation in the Early Universe	72
	3.5.1 Initial Conditions	73
	3.5.2 Formation of the First Star	73
	3.5.3 Local Stellar Feedback on Minihaloes	76
	3.5.4 Self-shielding and Molecule Formation	79
3.6	Implications for the Assembly of the First Galaxies	83
	3.6.1 The Protogalactic Star Formation Rate	83
	3.6.2 Supernova Feedback and Metallicity	84
	3.6.3 Black Hole Formation	87
3.7	Summary and Conclusions	89

Chapter 4. The First Galaxies: Signatures of the Initial Starburst 93

4.1	Introduction	93
4.2	Methodology	96
	4.2.1 The simulations	96
	4.2.2 Deriving the observational signature	103
	4.2.2.1 Escape fraction of ionizing photons	103
	4.2.2.2 Luminosity in recombination lines	104
	4.2.2.3 Recombination line equivalent widths	106
4.3	Results and Implications	107
	4.3.1 Evolution of gas inside the galaxy	107

4.3.2	Star formation rate indicators	112
4.3.3	Initial mass function indicators	118
4.3.4	Detectability of Recombination Radiation	123
4.4	Summary and Conclusions	129
Chapter 5.	Stellar Archaeology	133
5.1	The Minimum Observable Metallicity of Stars in the Galaxy	133
5.1.1	Introduction	133
5.1.2	Minimum Stellar Metallicity	136
5.1.3	Data on Metal-Poor Stars	139
5.1.4	Role of Accretion	142
5.1.5	Implications	146
5.2	The Chemical Signature of the First Stars in the Universe	149
5.2.1	Introduction	149
5.2.2	The Cosmological Context	152
5.2.3	Modeling Early Chemical Enrichment	156
5.2.3.1	The Basic Model	157
5.2.3.2	Density Evolution	161
5.2.3.3	Initial Mass Functions and Stellar Yields	161
5.2.3.4	Star Formation Rates	164
5.2.4	Results	169
5.2.4.1	Comparison with Observed Metal-Poor Stars	171
5.2.4.2	Characteristics of PISN-Dominated Stars	173
5.2.4.3	Observational Constraints on Pop III Supernovae	176
5.2.4.4	Parameter Dependence and Sensitivity	181
5.2.5	Discussion and Summary	184
Chapter 6.	Outlook	190
	Bibliography	193
	Vita	211

Chapter 1

Overview

The epoch of the formation of the first galaxies stands as one of the primary frontiers of cosmology today. In addition to confirming the success of the standard Λ CDM cosmology at describing the Universe at very large scales, detailed measurements of the cosmic microwave background (CMB) have given us a detailed picture of the state of the universe a few hundred thousand years after the Big Bang, at the onset of the Cosmic Dark Ages. As well, direct observations of distant galaxies, quasars, and gamma-ray bursts have revealed the tantalizing degree of evolution that the Universe underwent in the first billion years. The reionization of the intergalactic medium by the first generations of stars, the rapid chemical enrichment of massive galaxies, and the vigorous growth of supermassive black holes had all taken place by this early time. As of yet, however, there is little direct observational evidence detailing how the first stars and galaxies brought an end to the relatively simple state of the Universe during the Cosmic Dark Ages and began the transformation of the Universe to the complex state which is observed today.

In the following Chapters, we investigate the role that the first generations of stars play in shaping the formation of the first galaxies, which form

at redshifts $z \geq 10$, several hundred million years after the Big Bang. The primary technique that we employ in this investigation is the simulation of the growth of cosmological structure, and of the processes associated with the star formation that accompanies the formation of structure. In particular, we focus on the effects of the radiation emitted by stars during their lives and on the effects of the dispersal of the first heavy chemical elements which occurs at their deaths.

Chapters 2 and 3 concern the impact of the high-energy radiation emitted by the first stars, believed to have masses of the order of $100 M_{\odot}$. Such massive stars live for only ≤ 3 Myr and shine extraordinarily brightly, with luminosities of the order of a million times that of our Sun. They emit copious amounts of both ionizing radiation and molecule-dissociating radiation, each of which can dramatically impact their surroundings and the subsequent evolution of the Universe. In Chapter 2 we present a simulation which captures the effects of these forms of high-energy radiation in the local vicinity of a primordial protogalaxy, while in Chapter 3 we consider the impact that a cosmological background of molecule-dissociating radiation has on the formation of the first generations of stars, and in turn on the nature of the first galaxies.

Chapters 4 and 5 concern the observational signatures of the first stars and galaxies. Some fraction of the first dwarf galaxies, with masses of the order of $10^8 M_{\odot}$, is likely to form from primordial gas which has not yet undergone enrichment by Population III (Pop III) supernovae. These galaxies will host what may be the only purely Pop III stellar clusters, and direct detection of the

radiation from these clusters thus represents one of the few ways that we may directly probe the properties of primordial stars. In Chapter 4 we present the results of simulations which capture the radiative signature of such clusters, and we discuss how observations of this signature may be used to constrain the stellar initial mass function (IMF) and the star formation rate in the first galaxies.

Some fraction of primordial stars explode as supernovae, thereby ejecting the first heavy elements into the primordial gas, from which subsequent generations of stars form. Stars formed from such metal-enriched gas are likely to be much lower in mass than the first stars, some of them having masses lower than that of the Sun, thereby surviving to the present-day. Chemical abundance analyses of ancient metal-poor stars in the halo of the Milky Way can thus reveal the composition of the gas from which these stars formed, which in turn reflects the chemical signature of the first supernova explosions and so the masses of the first stars themselves. In Chapter 5 we present two studies, the first of which seeks to validate this practice of stellar archaeology as a means to learn about the properties of primordial stars, in addition to offering a prediction for the lowest metallicity stars which may be observed in the Galaxy. The second describes a model for the chemical evolution of the first galaxies which is used, in conjunction with the measured chemical abundances of metal-poor stars, to place constraints on the fraction of very massive stars exploding as supernovae in the early Universe.

Chapter 2

Radiative Feedback in the Formation of the First Galaxies

2.1 Introduction

The formation of the earliest galaxies plays a key role in a number of the most important questions being addressed in cosmology today. The first galaxies are predicted to have been the dominant sources of the radiation which reionized the universe (e.g. Ciardi et al. 2006), and they may have hosted the majority of primordial star formation (Greif & Bromm 2006; but see also Jimenez & Haiman 2006). They are the likely sites for the formation of the most metal-poor stars that have recently been found in our Galaxy (e.g. Christlieb et al. 2002; Beers & Christlieb 2005; Frebel et al. 2005), and possibly for the first efficient accretion onto the stellar black holes (see Johnson & Bromm 2007) which may have been the seeds for the $\sim 10^9 M_{\odot}$ black holes that are inferred at redshifts $z \geq 6$ (Fan et al. 2004, 2006). Furthermore, an understanding of the formation of the first galaxies is crucial for the interpretation of galaxies now beginning to be observed at $z \geq 6$ (e.g. Mobasher et al. 2005; Iye et al. 2006; Bouwens & Illingworth 2006), as well as of the objects at redshifts $z \geq 10$ which are expected to be detected with upcoming telescopes such as the *James Webb Space Telescope (JWST)* (Gardner et al.

2006). Among these systems there promise to be some of the first metal-free objects that will be observable, and as such it is important that theoretical predictions of their properties are made.

What were the effects of the radiative feedback from the first generations of stars on the formation of the first galaxies? It is now widely held that the first stars (termed Population III) were likely very massive, and therefore emitted copious amounts of radiation which profoundly affected their surroundings (Bromm et al. 1999, 2002; Abel et al. 2002; Yoshida et al. 2006; Gao et al. 2007). Recent work has demonstrated that the H II regions surrounding the first stars were able to evacuate the primordial gas from the minihalos that hosted these objects (Whalen et al. 2004; Kitayama et al. 2004; Alvarez et al. 2006; Abel et al. 2006). The impact of these H II regions on second generation star formation is complex (e.g. Ricotti, Gnedin & Shull 2001; Oh & Haiman 2003; Ahn & Shapiro 2006; Susa & Umemura 2006). While initially the density in these regions is suppressed and the gas within heated to $\geq 10^4$ K, vigorous molecule formation can take place once the gas begins to cool and recombine after the central Pop III star has collapsed to form a massive black hole, leading to the possibility of the formation of low-mass primordial stars (Nagakura & Omukai 2005; O’Shea et al. 2005; Johnson & Bromm 2006, 2007; Yoshida et al. 2007).

An additional radiative feedback effect from the first stars is the photo-dissociation of the fragile hydrogen molecules which allow the primordial gas to cool and collapse into minihalos, with virial temperatures $\leq 8,000$ K (e.g.

Barkana & Loeb 2001). The effects of the molecule-dissociating radiation from the first stars can reach far beyond their H II regions (e.g. Ciardi et al. 2000), and thus star formation in distant minihalos may have been delayed or quenched altogether (e.g. Haiman et al. 1997, 2000; Mackey et al. 2003). Interestingly, however, while the general intergalactic medium (IGM) at the epoch of the first stars becomes optically thick to Lyman-Werner (LW) photons only over vast distances (e.g. Haiman et al. 2000; see also Glover & Brand 2001), the high molecule fraction that persists inside the first relic H II regions leads to a high optical depth to these photons, potentially allowing star formation to take place in minihalos down to lower redshifts than would otherwise be possible (Ricotti et al. 2001; Oh & Haiman 2002; Machacek et al. 2001, 2003; Johnson & Bromm 2007).

In the present work, we self-consistently track the formation of, and the radiative feedback from, individual Pop III stars in the course of the formation of a primordial protogalaxy. We compute in detail the H II regions and LW bubbles of each of these sources, and follow the evolution of the primordial gas as it becomes incorporated into the protogalaxy. In § 2, we describe our numerical methodology. Our results are presented in § 3, while we summarize our conclusions and discuss their implications in § 4.

2.2 Methodology

2.2.1 Cosmological Initial Conditions and Resolution

We employ the parallel version of GADGET for our three-dimensional numerical simulations. This code includes a tree, hierarchical gravity solver combined with the smoothed particle hydrodynamics (SPH) method for tracking the evolution of the gas (Springel, Yoshida & White 2001). Along with H_2 , H_2^+ , H , H^- , H^+ , e^- , He , He^+ , and He^{++} , we have included the five deuterium species D , D^+ , D^- , HD and HD^- , using the same chemical network as in Johnson & Bromm (2006, 2007).

We carry out a three-dimensional cosmological simulation of high- z structure formation which evolves both the dark matter and baryonic components, initialized according to the λCDM model at $z = 100$. As in earlier work (Bromm et al. 2003; Johnson & Bromm 2007), we adopt the cosmological parameters $\Omega_m = 1 - \Omega_\Lambda = 0.3$, $\Omega_B = 0.045$, $h = 0.7$, and $\sigma_8 = 0.9$, close to the values measured by *WMAP* in its first year (Spergel et al. 2003). Here we use a periodic box with a comoving size $L = 460 h^{-1}$ kpc, but unless stated explicitly, we will always refer to physical distances in the present work. Our simulation uses a number of particles $N_{\text{DM}} = N_{\text{SPH}} = 128^3$, where the SPH particle mass is $m_{\text{SPH}} \sim 740 M_\odot$.

We have determined the maximum density of gas that can be reliably resolved in this simulation by carrying out a cosmological simulation from $z = 100$, in which we allow the gas to cool and collapse into minihalos without including radiative effects. We then compare the minimum resolved mass,

which we take to be $\sim 64 m_{\text{SPH}}$, with the Bonnor-Ebert mass, given by (see, e.g., Palla 2002)

$$M_{\text{BE}} \simeq 700 M_{\odot} \left(\frac{T}{200 \text{ K}} \right)^{3/2} \left(\frac{n}{10^4 \text{ cm}^{-3}} \right)^{-1/2}, \quad (2.1)$$

where n and T are the number density and temperature of the gas, respectively. As shown in Figure 2.1, the gas evolves according to the canonical behavior of primordial gas collapsing in minihalos (see, e.g., Bromm et al. 2002). We expect the gas in our simulations with radiative feedback to behave similarly as it collapses to high densities, since it is the formation of, and cooling by, molecules which will drive the collapse in both cases. Thus, we take the maximum density that we can reliably resolve to be that at which the Bonnor-Ebert mass becomes equal to the resolution mass. As is evident in Figure 2.1, this criterion results in a maximum resolvable density of $n_{\text{res}} \sim 20 \text{ cm}^{-3}$. This density is four orders of magnitude higher than the background mean density at a redshift of $z \geq 15$, and such overdensities only occur in the minihalos within which the first Pop III stars form (see, e.g., Bromm & Larson 2004; Yoshida et al. 2006). We take it here that one Pop III star, assumed to have a mass of $100 M_{\odot}$, will form from this dense, collapsing primordial gas inside a minihalo, consistent with recent work which shows that, in general, only single stars are expected to form in minihalos under these conditions (Yoshida et al. 2006). Pop III stars with this mass are predicted to directly collapse to a black hole, and therefore produce no supernova explosion (e.g. Heger et al. 2003), which allows us to self-consistently neglect the possibility of ejection of metals

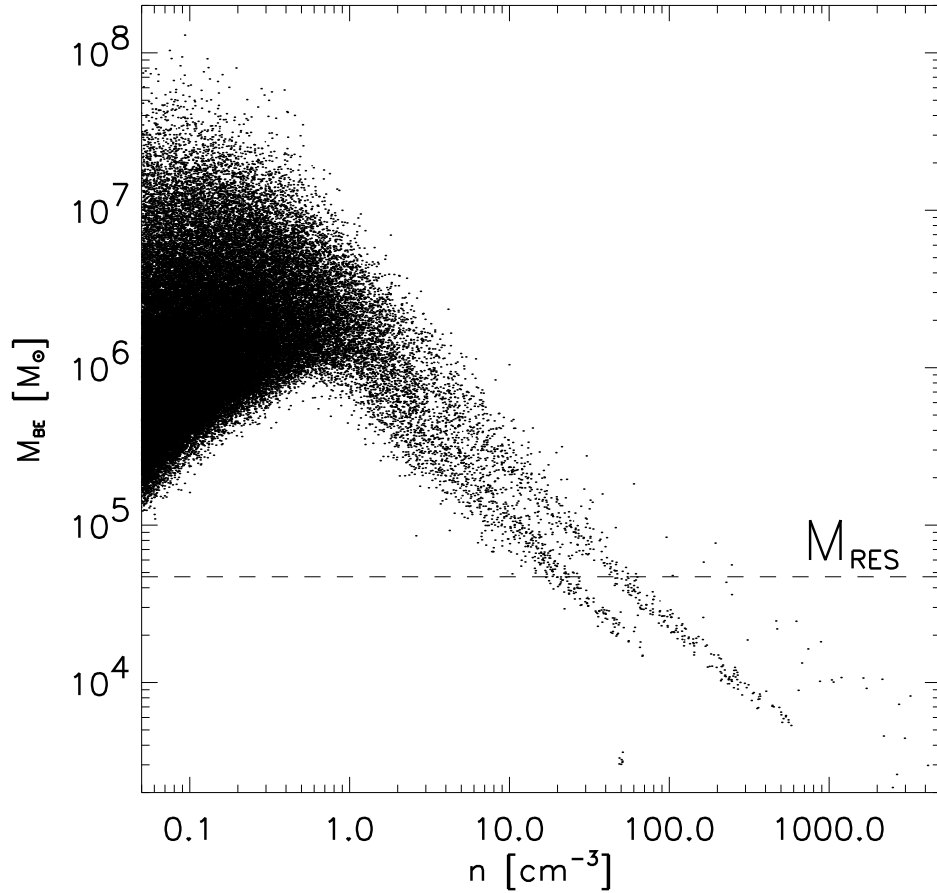


Figure 2.1: Determining the maximum density resolvable in our simulations. To reliably resolve the properties of the gas in our simulation, the Bonnor-Ebert mass, similar to the Jeans mass, must be larger than the mass in the SPH smoothing kernel. For added assurance, we take the minimum resolvable mass to be twice the mass in the kernel. This value for the resolution mass is shown by the dashed horizontal line. For densities higher than $n_{\text{res}} \sim 20 \text{ cm}^{-3}$, the Bonnor-Ebert mass may be exceeded by the resolution mass, and so we take it that we can only resolve the properties of the gas at densities below this value. We note that the two structures emerging at high densities are two spatially distinct halos of different mass which are undergoing collapse.

into the primordial gas. We will consider this possibility in future work. In the present work, we focus on the radiative feedback from the first stars.

2.2.2 Radiative Feedback

In our simulations with radiative feedback, we assume that stars are formed in minihalos which acquire densities higher than $n_{\text{res}} = 20 \text{ cm}^{-3}$. In order to account for the radiative feedback from a star formed in a minihalo, the gas surrounding the star is first photo-heated. We then calculate the extent of the H II region, as well as of the LW bubble around the star. We carry out this procedure every time a star forms in the simulation. The Pop III star will soon die, and we then let the simulation evolve once more, allowing recombination to take place in the relic H II region, and for molecules to reform within the relic LW bubble. We expect that this procedure will provide reliable results, as the ≤ 3 Myr lifetime of a Pop III star is short compared to the typical dynamical times of the gas in this simulation.

2.2.2.1 Photoionization

To account for the presence of a $100 M_{\odot}$ Pop III star in the minihalos in which the gas collapses to a density of n_{res} , we first photoheat and photoionize the gas within 500 pc of the gas particle which first reaches this density for a duration of the lifetime of the star, using the same heating and ionization rates as in Johnson & Bromm (2007). Our choice of a 500 pc radius ensures that the entire gas within the source minihalo, with virial radius ~ 150 pc, is

photoheated, but that we do not photoheat the dense, neutral gas in neighboring halos. Just as in this previous work, we reproduce the basic density and velocity structure of the gas within 500 pc of the central source that has been found in detailed one-dimensional radiation hydrodynamics calculations (Kitayama et al. 2004; Whalen et al. 2004).

Once this density structure is in place around the point source, we employ a ray-tracing technique to solve for the H II region that surrounds the star at the end of its life. We cast rays in $N_{\text{ray}} \sim 100,000$ directions from the central source, and divide each ray into 500 segments. Then, we add up all of the recombinations that take place over the course of the star's lifetime in each bin along each of the N_{ray} rays, taking the number of recombinations to be

$$N_{\text{rec}} = \alpha_{\text{B}} n_{\text{mean}}^2 \frac{4\pi}{N_{\text{ray}}} t_* r^2 dr , \quad (2.2)$$

where α_{B} is the case B recombination coefficient, r is the distance of the bin from the star, dr is length of the bin in the direction radial to the star, and t_* is the lifetime of the star, here taken to be 3 Myr (Schaerer 2002). We compute n_{mean} , the average number density of hydrogen atoms in a bin, as

$$n_{\text{mean}} = \frac{\sum n_{\text{H}}}{N_{\text{part}}} . \quad (2.3)$$

Here N_{part} is the number of SPH particles in the bin and n_{H} is the number density of hydrogen of the individual SPH particles in that bin.

Next, we assume that the star radiates an equal number of photons in every direction, and we take the total number of ionizing photons that it radiates in its lifetime to be

$$N_{\text{ion}} = Q_{\text{ion}} t_* , \quad (2.4)$$

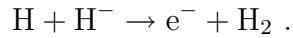
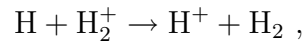
where we have chosen Q_{ion} , the average number of ionizing photons emitted per second by the star, to be 10^{50} s^{-1} (see Bromm et al. 2001; Schaerer 2002). We then add up the recombinations in all of the bins, along each of the rays, beginning with those closest to the star and moving outward, until the number of recombinations along a ray equals the number of ionizing photons that are emitted along that ray. If the number of recombinations in the bin falls below the number of atoms in the bin, then we count the number of atoms in the bin against the number of photons as well. Doing this for each of the rays, we solve in detail for the H II region of the star. We set the free electron fraction to unity for each of the SPH particles that lie within the H II region. We set the temperature of the SPH particles within the H II region, but outside of the 500 pc photo-heated region, to $T = 18,000 \text{ K}$, roughly the value at the outer edge of the photo-heated region. As well, the fraction of molecules in the H II region is set to zero, as we assume that all molecules are collisionally dissociated at the high temperatures in the H II region.

2.2.2.2 Photodissociation

To find the region in which the LW radiation from the star destroys H_2 and HD molecules, the “LW bubble” in our terminology, we carry out a ray-tracing procedure similar to the one used to solve for the H II region. We use the same bins as in that procedure, but now we evaluate the formation time of H_2 molecules in each bin and compare this both to the lifetime of the star and to the dissociation time of the molecules. For each bin, we compute the H_2 formation time as

$$t_{\text{form,H}_2} = \sum \frac{n_{\text{H}_2}}{n_{\text{H}}(k_1 n_{\text{H}_2^+} + k_2 n_{\text{H}^-})} / N_{\text{part}} , \quad (2.5)$$

where $n_{\text{H}_2^+}$ and n_{H^-} are the number densities of H_2^+ and H^- , respectively. The sum is over all the particles in the bin, N_{part} , and k_1 and k_2 are the rate coefficients for the following two main reactions that produce H_2 :



We adopt the following values for these rate coefficients (de Jong 1972; Karpas et al. 1979; Haiman et al. 1996):

$$k_1 = 6.4 \times 10^{-10} \text{cm}^3 \text{s}^{-1} , \quad (2.6)$$

$$k_2 = 1.3 \times 10^{-9} \text{cm}^3 \text{s}^{-1} . \quad (2.7)$$

The dissociation time for the molecules is obtained by finding the flux of LW photons from a $100 M_\odot$ Pop III star, assumed to be a blackbody emitter with radius $R_* \simeq 3.9R_\odot$ and effective temperature $T_* \simeq 10^5$ K (e.g., Bromm et al. 2001). The dissociation time for unshielded molecules at a distance R from the star is then given by (Abel et al. 1997)

$$t_{\text{diss,H}_2} \sim 10^5 \text{yr} \left(\frac{R}{1 \text{kpc}} \right)^2 . \quad (2.8)$$

Next, we note that for molecules to be effectively dissociated by the LW radiation, the dissociation time of the molecules must be shorter than both the lifetime of the star and the formation time of the molecules. Therefore, we compare all of these timescales for each bin along each ray and set the fraction of molecules to zero if $t_{\text{diss,H}_2} \leq t_{\text{form,H}_2}$ and $t_{\text{diss,H}_2} \leq t_*$. If this condition is not satisfied, then the molecule fraction is left unchanged from its value before the formation of the star. This allows for the possibility of the effective shielding of H_2 molecules because it accounts for the build-up of H_2 column density, for instance, in relic H II regions or in collapsing minihalos where the formation time of H_2 is relatively short.

We take into account the effects of self-shielding by adding up the H_2 column density $N(\text{H}_2)$ along the ray contributed by each bin in which the

molecules are not effectively dissociated. We then adjust the dissociation time for the molecules in shielded bins according to (Draine & Bertoldi 1996):

$$t_{\text{diss,H}_2} \sim 10^5 \text{ yr} \left(\frac{R}{1 \text{ kpc}} \right)^2 \left(\frac{N(\text{H}_2)}{10^{14} \text{ cm}^{-2}} \right)^{0.75}, \quad (2.9)$$

when the column density of molecules between the bin and the star is $N(\text{H}_2) \geq 10^{14} \text{ cm}^{-2}$.

The ionic species H^- and H_2^+ , which are reactants in the main reactions which form H_2 , can also, in principle, be destroyed by the radiation from the star. The photo-dissociation times for these species are given in terms of the temperature of the star T_* , the source of thermal radiation in our case, and the distance from the star R , as (Dunn 1968; de Jong 1972; Galli & Palla 1998)

$$t_{\text{diss,H}_2^+} = 5 \times 10^{-2} T_*^{-1.59} \exp\left(\frac{82000}{T_*}\right) \left(\frac{R}{R_*}\right)^2 \text{ s}, \quad (2.10)$$

$$t_{\text{diss,H}^-} = 9.1 T_*^{-2.13} \exp\left(\frac{8823}{T_*}\right) \left(\frac{R}{R_*}\right)^2 \text{ s}. \quad (2.11)$$

For the $100M_\odot$ star, we find that $t_{\text{diss,H}_2^+} \sim 5 \times 10^3 \text{ yr} \left(\frac{R}{1 \text{ kpc}}\right)^2$ and $t_{\text{diss,H}^-} \sim 9 \times 10^2 \text{ yr} \left(\frac{R}{1 \text{ kpc}}\right)^2$. The formation times for these species, on the other hand, are

$$t_{\text{form,H}^-} = n_{\text{H}^-} \left(\frac{dn_{\text{H}^-}}{dt} \right)^{-1} \sim 3 \times 10^3 \text{ yr}, \quad (2.12)$$

$$t_{\text{form,H}_2^+} = n_{\text{H}_2^+} \left(\frac{dn_{\text{H}_2^+}}{dt} \right)^{-1} \sim 4 \times 10^3 \text{yr} , \quad (2.13)$$

for primordial gas at a temperature of $T = 100$ K and a density of $n_{\text{H}} = 10^{-2}$ cm^{-3} , typical for gas at the outskirts of a collapsing minihalo. These formation timescales become much shorter for gas deeper inside minihalos, where the densities and temperatures are generally higher. It is in these regions, in and around minihalos, where the presence of molecules is most important for cooling the gas. Within these regions the photo-dissociation times for these ionic species are less than their formation times only if they are located ≤ 2 kpc from the star. Thus, photo-dissociation of these species will become ineffective at distances ≥ 2 kpc from the star, a distance comparable to the size of the H II region of a Pop III star (Alvarez et al. 2006; Abel et al. 2006). Since we assume that molecules are collisionally destroyed inside the H II region, and since the LW bubble will generally be larger than the H II region, we ignore the photo-dissociation of H^- and H_2^+ in our calculations.

LW photons can also be absorbed by hydrogen atoms, through the Lyman series transitions, as discussed in detail by Haiman et al. (1997, 2000). However, this atomic absorption will only have a significant effect on the LW flux over distances large enough that the Hubble expansion causes many of the LW photons to redshift to wavelengths of the Lyman series transitions. The light-crossing time for our cosmological box is much shorter than the Hubble time at the redshifts that we consider. Thus, LW photons will be negligibly redshifted as they cross our cosmological box and we can safely neglect the

minimal atomic absorption of these photons that may take place.

It has also been found that a shell of H_2 molecules may form ahead of the expanding H II regions surrounding the first stars (see Ricotti et al. 2001). These authors find that such shells may become optically thick to LW photons. However, Kitayama et al. (2004) have discussed that such shells are likely short-lived, persisting for only a small fraction of the lifetime of the star. Thus, for our calculations we neglect the possible formation of such a shell, as we expect that the opacity to LW photons through this shell will be very small when averaged over the lifetime of the star. Additionally, as we show in section 2.3.1, the regions affected by the LW feedback from a single Pop III star extend, at most, only a few kiloparsecs beyond the H II region of such a star, which itself extends ~ 5 kpc. If an H_2 shell forms ahead of the H II region, then the extent of the LW bubble will only be suppressed by, at most, a factor of a few in radius.

2.2.3 Sink Particle Formation

We have carried out two simulations, one with radiative feedback and one in which the simulation evolves without including radiative effects. For the former simulation, we allow stars to form when the density reaches n_{res} , and the expansion of the gas around the star due to photo-heating suppresses the density so that our resolution limit is not violated. For the simulation without radiative feedback we allow sink particles to form when the density of the gas reaches n_{res} . Since the sink particles will form only in minihalos which

are expected to form Pop III stars, we are able to track the star formation rate in the case without feedback by tracking the formation of sink particles. We can then compare the sites, and rates, of star formation in each of the simulations in order to elucidate the effect that radiative feedback has on Pop III star formation.

2.3 Results

In this section we discuss the evolution of the primordial gas under the influence of the radiative feedback which arises as the first stars are formed in a region destined to subsequently be incorporated into the first protogalaxy. Indeed, other effects will become important in the course of the buildup of the first galaxies. Among them is the ejection of metals into these systems by the first supernovae (e.g. Bromm et al. 2003). However, we consider the early regime in which Pop III star formation dominates, and the effects of metals might not yet be important. Initially only taking into account the stellar radiative feedback, and neglecting chemical enrichment, relies on our simplifying assumption that only $100 M_{\odot}$ black hole-forming Pop III stars form, which are predicted not to yield supernovae, and therefore not to eject metals into their surroundings (Heger et al. 2003).

Although the initial mass function (IMF) of the first generation of stars is not known with any certainty yet, there is mounting theoretical evidence that Pop III stars were very massive, and thus it is very likely that many of these stars ended their lives by collapsing directly to black holes, emitting

few or no metals into the IGM (see Fryer et al. 2001; Heger et al. 2003). Here we assume that all of the stars that form within our cosmological box are black hole-forming stars which do not enrich the IGM with metals, and which therefore allow subsequent metal-free star formation to occur. Eventually, however, stars which create supernovae will form, and the ejected metals will be incorporated into the first protogalaxies, thus drawing the epoch of metal-free star formation to a close. In light of this, we end our simulation after the formation of the eighth star in our box at a redshift of $z \sim 18$, as we expect that at lower redshifts the effects of the first metals ejected into the primordial gas will become important (but see Jappsen et al. 2007). Also, at lower redshifts global LW feedback, due to star formation at distances far larger than our cosmological box, will become increasingly important. That said, by tracking the formation of individual Pop III stars in our box, we are able to find a variety of novel results concerning the local radiative feedback from the first generations of stars.

2.3.1 The First H II Region and Lyman-Werner Bubble

The first star appears in our cosmological box at a redshift of $z \sim 23$. It forms inside a minihalo with a total mass $\leq 10^6 M_\odot$ and the gas within this halo is evaporated due to the photo-heating from the star. The H II region that is formed around the star can be seen in Figure 2.2, which shows the electron fraction, H_2 fraction, temperature, and density of the gas, in projection. The H II region, which has a morphology similar to those found in previous studies,

extends out to ~ 4 kpc from the star, also similar to results found in previous works (Alvarez et al. 2006; Wise et al. 2006; Yoshida et al. 2007).

As shown in Figure 2.2, the molecules within ~ 5 kpc are photodissociated by the LW radiation from the first star, and the LW bubble extends to only ~ 1 kpc outside of the H II region. Noting that the formation timescale for H_2 in the neutral IGM at these redshifts is of the order of ~ 300 Myr, much longer than the lifetime of the massive stars that we consider here, we can estimate the distance through the IGM that the LW bubble should extend, R_{LW} , by evaluating the criterion for the effective dissociation of molecules at this distance from the first star: $t_{\text{diss},\text{H}_2} = t_*$. Using equation (2.8) and taking the lifetime of the star to be 3 Myr gives $R_{\text{LW}} \sim 5$ kpc, consistent with the result we find for the first star, shown in Figure 2.2 (see also Ferrara 1998). Outside of this LW bubble molecules will not be dissociated effectively by the single Pop III star, owing largely to its short lifetime. Only when continuous star formation sets in will the LW bubbles of the first generations of stars merge and become large enough to establish a more pervasive LW background flux (see e.g. Haiman et al. 2000).

2.3.2 Thermal and Chemical Evolution of the Gas

The properties of the primordial gas within our box are strongly time-dependent, as any gradual evolution of the gas is disrupted each time a star turns on and heats the gas, ionizes atoms, and photodissociates molecules. Certain robust patterns, however, do emerge in the course of the evolution of

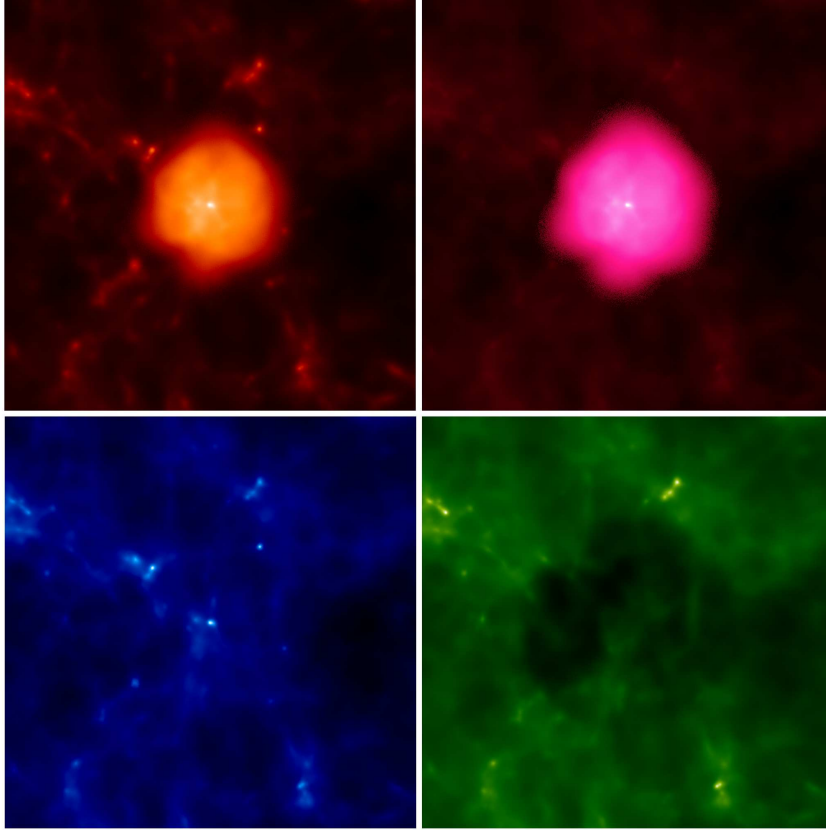


Figure 2.2: The first H II region and LW bubble. Clockwise from top-left are the temperature, electron fraction, H₂ fraction, and density, plotted in projection. While the size of our cosmological box is ~ 27 kpc in physical units at this redshift, $z \sim 23$, here we have zoomed into the inner 20 kpc, in order to see detail around the first star. The H II region extends out to ~ 4 kpc in radius, while the LW bubble extends to ~ 5 kpc, within which the molecule fraction is zero. In each panel, the lighter shades signify higher values of the quantity plotted.

the primordial gas. Figure 2.3 shows the chemical and thermal properties of the gas at a redshift $z \sim 18$, just after the death of the eighth star in our cosmological box. Here, the light-shaded particles are those which have been contained within an H II region, and so have passed through a fully ionized phase.

The ionized gas in the H II regions begins to recombine and cool once the central star dies. The dynamical expansion of these hot regions leads to the adiabatic cooling of the gas, as can be seen in the upper left panel of Figure 2.3. The plot shows relic H II regions at different evolutionary stages. The older ones are generally cooler, owing to the molecular cooling that has had more time to lower the temperature of the gas. Indeed, the first relic H II regions by this redshift, ~ 70 Myr after the first star formed, have already cooled to near the temperature of the un-ionized gas. The electron fraction of the relic H II region gas, however, is still much higher than that of the un-ionized gas, as can be seen in the upper-right panel of Figure 2.3. That the cooling of the gas occurs faster than its recombination leads to the rapid formation of molecules (e.g. Kang & Shapiro 1992; Oh & Haiman 2003; Nagakura & Omukai 2005; Johnson & Bromm 2006). This elevated fraction of both H₂ and HD molecules in the relic H II region gas is evident in the bottom panels of Figure 2.3.

The high abundance of molecules in relic H II regions can lead to efficient cooling of the gas, and this has important consequences in the first protogalaxies. In particular, a high fraction of HD in these regions could allow the gas to cool to the temperature of the cosmic microwave background

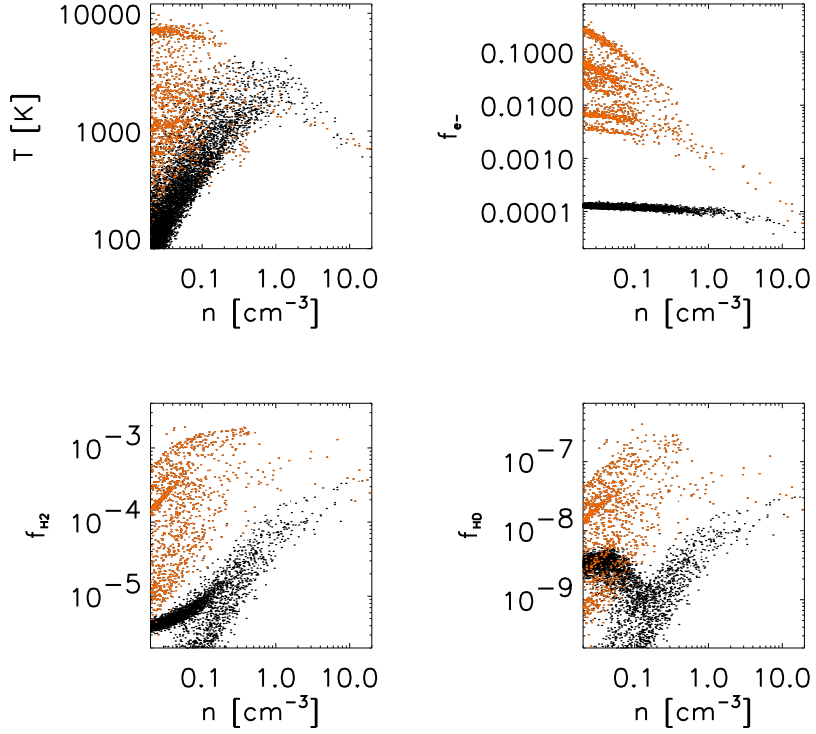


Figure 2.3: The properties of the primordial gas at redshift $z \sim 18$, at the end of the life of the eighth star. The SPH particles which have experienced an ionized phase within an H II region are colored in orange (gray), while those that have not are in black. Clockwise from the top-left, the temperature, free electron fraction, HD fraction, and H₂ fraction are plotted as functions of gas density. The relic H II region gas cools largely by adiabatic expansion, but, importantly, also by cooling facilitated by the high abundance of H₂ and HD molecules, which arises owing to the high electron fraction in this gas. The high electron fraction persists until the gas has collapsed to densities of $\geq 10 \text{ cm}^{-3}$, as can be seen in the top-right panel. The molecule fraction is highest at low densities for gas in which the molecules have not been destroyed by LW feedback, giving rise to the features seen at low densities in the bottom two panels.

(CMB), T_{CMB} , the lowest temperature attainable by radiative cooling, and this effective cooling may lead to the formation of lower mass metal-free stars (Nagakura & Omukai 2005; Johnson & Bromm 2006; Yoshida 2006). Indeed, Figure 2.3 shows that the HD fraction can greatly exceed the minimum value needed for efficient cooling to the CMB temperature floor in local thermodynamic equilibrium (LTE), $f_{\text{HD,crit}} \sim 10^{-8}$ (Johnson & Bromm 2006).

While the LW feedback from the stars that form in our box can very effectively destroy molecules within ~ 5 kpc of the stars by the end of their lives, this feedback is not continuous. Following the death of a given star, the molecules will begin to reform in the absence of LW radiation. The time required for the formation of H_2 molecules is sensitively dependent on the ionized fraction of the gas, but the formation time can be relatively short for un-ionized gas at high densities, as well. In relic H II regions the fraction of H_2 can reach 10^{-4} within ~ 1 Myr (Johnson & Bromm 2007). In collapsing minihalos, where the molecules play a key role in cooling the gas and allowing it to continue collapsing, the formation times are in general longer at the densities we consider here, $n \leq 20 \text{ cm}^{-3}$. We find that the formation timescale for un-ionized gas collapsing in minihalos is $t_{\text{form,H}_2} \sim 5 \times 10^5 \text{ yr}$ at a density of 1 cm^{-3} and a temperature of 900 K, and $t_{\text{form,H}_2} \sim 7 \times 10^6 \text{ yr}$ at a density of 0.1 cm^{-3} and a temperature of 500 K. The average time between the formation of stars in our box is ~ 10 Myr, and so the molecules inside sufficiently dense minihalos can often reform and allow the gas to continue cooling and collapsing, in spite of the intermittent LW feedback from local star forming regions.

In order to evaluate the possible effects of continuous LW feedback from sources outside of our box, we have carried out simulations in which we include a LW background which destroys H_2 molecules at a rate given by (Abel et al. 1997)

$$k_{\text{diss}} = 1.2 \times 10^{-12} J_{\text{LW}} \text{ s}^{-1} , \quad (2.14)$$

where J_{LW} is the flux of LW photons in units of $10^{-21} \text{ ergs s}^{-1} \text{ cm}^{-2} \text{ Hz}^{-1} \text{ sr}^{-1}$. We have carried out simulations in which the value of J_{LW} is taken to be zero before the formation of the first star and 0.1, 10^{-2} , and 10^{-3} afterwards, when a LW background might be expected to begin building up due to distant star formation. For each of these simulations, we found the formation redshift of the second star in the box to be $z_{2\text{nd}} = 16.3$, 20, and 20.5, respectively. In our main simulation, in which we neglect a possible background LW flux, the second star formed at $z_{2\text{nd}} = 20.6$. This demonstrates that a background LW flux of $J_{\text{LW}} \leq 10^{-2}$ would likely have little impact on our results, while a larger LW flux would simply delay the collapse of gas into minihalos and so lower the overall star formation rate in our box, consistent with previous findings (see e.g. Machacek et al. 2001; Mesinger et al. 2006). We emphasize, however, that for a substantial LW background to be established, a relatively high continuous star formation rate must be achieved, as we have shown that individual Pop III stars can only be expected to destroy molecules within ~ 5 kpc of their formation sites. In the very early stages of the first star formation, when short-lived single stars are forming in individual minihalos (see e.g. Yoshida

et al. 2006), it appears unlikely that a substantial LW background would be established, the feedback from the sources being instead largely local. It may be only later, when continuous star formation begins to occur in larger mass systems that a pervasive LW background would likely be built up (see, e.g., Haiman et al. 2000; Greif & Bromm 2006).

2.3.3 Shielding of Molecules by Relic H II Regions

As star formation continues, the volume occupied by relic H II regions increases. Because of the high molecule fraction that can develop in these regions, owing to the large electron fraction that persists for ≤ 500 Myr (Johnson & Bromm 2007), the increasing volume of the IGM occupied by relic H II regions implies an increase in the optical depth to LW photons in the vicinity of the first star formation sites. By a redshift of $z \sim 18$, eight stars have formed in our cosmological box and each has left behind a relic H II region.

As can be seen in Figures 2.3 and 2.4, the gas inside the relic H II regions that have formed contains an H_2 fraction generally higher than the primordial abundance of 10^{-6} , and up to an abundance of $\sim 10^{-3}$ in the denser regions. This elevated fraction of H_2 inside the relic H II regions leads to a high optical depth to LW photons, τ_{LW} , through the relic H II regions. The column density through a relic H II region which recombines in the absence of LW radiation can become of the order of $N_{\text{H}_2} \sim 10^{15} \text{ cm}^{-2}$ (Johnson & Bromm 2007). Because the molecules in the relic H II regions that we consider here are subject to LW feedback from neighboring star formation regions, the optical depth through

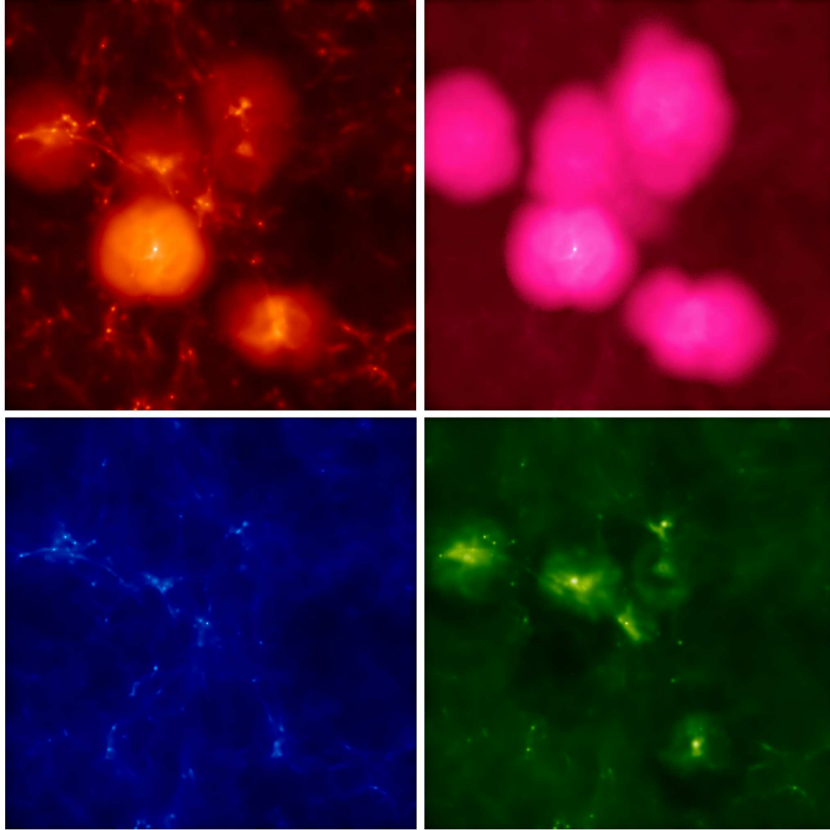


Figure 2.4: The properties of the primordial gas at the end of the life of the eighth star in our box, at redshift $z \sim 18$. Clockwise from top-left are the temperature, electron fraction, H_2 fraction, and density of the gas, in projection. Here we show the entire cosmological box, which is ~ 35 kpc in physical units. Note the high electron and H_2 fractions in the relic H II regions, where recombination is taking place. The elevated H_2 fraction in these regions raises the optical depth to LW photons through them significantly, as is illustrated in Fig. 2.5. The temperature in the older relic H II regions is not greatly elevated as compared to the temperature of the un-ionized gas, owing to the adiabatic and molecular cooling that takes place in these regions. The lighter shades denote higher values of the quantities plotted.

these regions may in general be lower. However, the rapid rate of molecule formation in these regions, even considering the LW feedback from local star forming regions in our box, allows the molecule fraction to approach 10^{-4} as late as ~ 100 Myr after the death of the central star. This elevated molecule fraction combined with the growing volume-filling fraction of relic H II regions leads to an appreciable optical depth to LW photons, which generally increases with time as more stars form and create more relic H II regions. To quantify this effect, we calculate the average column density of H_2 molecules through a cubic region of side length l as the product of the length l and the volume averaged number density of H_2 molecules, given by

$$N_{\text{H}_2} \simeq l \frac{\sum n_{\text{H}_2} V}{\sum V}, \quad (2.15)$$

where the sum is over all of the SPH particles in the volume and n_{H_2} is the number density of H_2 at each of the SPH particles. The volume associated with each individual SPH particle, V , is estimated as $V \simeq m_{\text{SPH}}/\rho$, where m_{SPH} is the mass of the SPH particle and ρ is the mass density of the gas at that particle. The optical depth to LW photons is then computed as (Draine & Bertoldi 1996; Haiman et al. 2000)

$$\tau_{\text{LW}} \simeq 0.75 \ln\left(\frac{N_{\text{H}_2}}{10^{14} \text{cm}^{-2}}\right). \quad (2.16)$$

Figure 2.5 shows the optical depth to LW photons averaged both over the central comoving $153 \text{ kpc } h^{-1}$ of our cosmological box, in which the first

star forms, and over the entire box, for which the comoving side length is $460 \text{ kpc } h^{-1}$. Before the formation of the first star, the optical depth evolves largely owing to the cosmic expansion, following the relation $\tau_{\text{LW}} \simeq n_{\text{H}_2} l \propto (1+z)^2$, because the average H_2 fraction does not change appreciably. However, with the formation of the first star in our box at $z \simeq 23$ the optical depth begins to change dramatically in the inner portion of the box, first falling to a value of $\simeq 0.1$ due to the LW feedback from the first star and then steadily climbing to values ≥ 2 as copious amounts of molecules form inside the relic H II regions that accumulate as star formation continues.

The evolution of the optical depth averaged over the entire box is not as dramatic, as the fraction of the volume of the whole box occupied by relic H II regions is much smaller than the fraction of the central region that is occupied by these molecule-rich regions. However, the optical depth averaged over the whole box, which is a better estimate of the optical depth over cosmological distances, still rises to $\tau_{\text{LW}} \geq 1.5$ across our box, an appreciable value which will serve to impede the build-up of a cosmologically pervasive LW background.

2.3.4 Black hole accretion

Accretion onto Pop III relic black holes may be inefficient for some time following the formation of these objects, owing to the fact that Pop III stars photo-heat and evaporate the gas within the minihalos which host them (Johnson & Bromm 2007; see also Yoshida 2006). Indeed, accretion onto Pop III relic black holes at close to the Eddington limit can only occur if the

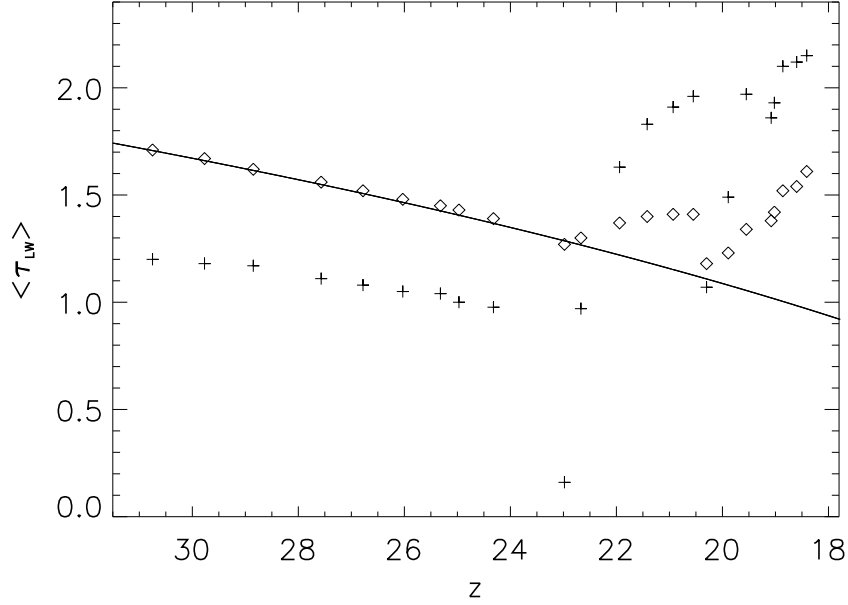


Figure 2.5: The optical depth to LW photons, τ_{LW} , averaged over two volumes in our box, as a function of redshift, z . The diamonds denote the optical depth averaged over the entire cosmological box, while the crosses denote the optical depth averaged only over a cube containing the inner comoving 153 kpc h^{-1} of the box, centered in the middle of the box with a volume one ninth that of the whole box. It is within this region that the first star forms and the star formation rate is higher than the average star formation rate over the whole box, and this is reflected in the higher local optical depth in this region as relic H II regions accumulate in the box. The average optical depth through the entire box also rises, but the increase is less dramatic. The solid line denotes the optical depth to LW photons, averaged over the whole box, that would be expected for the case that the gas maintains the average cosmological density everywhere and that the H_2 fraction does not change from the primordial value of 2×10^{-6} ; for this case, the optical depth changes owing only to cosmic expansion. Note that the optical depth averaged over the whole box matches well this idealized case up until the first star forms at a redshift of $z \sim 23$. The temporary drops in the optical depth occur due to LW feedback when individual stars form.

accreted gas has a density above $\sim 10^2 \text{ cm}^{-3}$, and it is only in collapsing halos that such densities are achieved at the high redshifts at which the first stars formed (Johnson & Bromm 2007). By assumption, all of the stars that are formed in our simulation are black hole-forming Pop III stars. If these black holes remain inside their host minihalos, then by tracking the evolution of the gas within these photo-evaporated host minihalos, we can learn when efficient accretion onto these Pop III relic black holes may occur.

The minihalo within which the first star forms at a redshift $z \sim 23$ resides within the relic H II region left by the first star. Due to the formation of a high fraction of molecules, and to the molecular cooling that ensues, the relic H II region gas cools down to temperatures $\sim 10^3 \text{ K}$, below the virial temperature of this $10^6 M_{\odot}$ minihalo. The gas then re-collapses into the minihalo, reaching a peak density of n_{res} at a redshift $z \sim 19$, or $\sim 50 \text{ Myr}$ after the formation of the first star. Figure 2.6 shows the properties of the relic H II region gas as a function of distance from the center of this minihalo, at the time when the gas has collapsed to a density of n_{res} . We cannot, with this simulation, resolve what happens once the gas collapses further and reaches higher densities. However, we can estimate the time it will take for the gas at the center of the halo to reach a density of $n \sim 10^2 \text{ cm}^{-3}$ as the free fall time of the gas, which is $t_{\text{ff}} \sim 10 \text{ Myr}$. Thus, a Pop III relic black hole at the center of this halo could be expected to begin accreting gas efficiently $\sim 60 \text{ Myr}$ after its formation. This is a significant delay, and could pose serious challenges to theories which predict that efficient accretion onto Pop III relic black holes can

lead to these black holes becoming the supermassive black holes that power the quasars observed in the *Sloan Digital Sky Survey* at redshifts $z \geq 6$ (e.g. Yoshida 2006; Johnson & Bromm 2007; Li et al. 2006).

2.3.5 HD cooling in relic H II regions

While abundant molecules can form within relic H II regions, the LW feedback from neighboring star-forming regions can suppress the effect of this elevated fraction of molecules. The electron fraction remains high in relic H II regions for up to ~ 500 Myr in the general IGM, but in higher density regions where the gas is recollapsing, the electron fraction drops much more quickly. Figures 2.3 and 2.6 show that the electron fraction drops to a value of $\leq 10^{-4}$, comparable to the electron fraction of the un-ionized gas, once the density of the relic H II region gas becomes $\geq 10 \text{ cm}^{-3}$. Thus, once the gas reaches these densities the ionized fraction will become too low to catalyze the formation of a high fraction of molecules, and of HD molecules in particular. Therefore, in order for HD to be an effective coolant of the primordial gas in relic H II regions, the abundant HD molecules that are formed at densities $\leq 10 \text{ cm}^{-3}$ must not be destroyed by LW feedback from neighboring star-forming regions before the gas collapses to high densities and forms stars. If we estimate the timescale on which the relic H II region gas would collapse to form stars as the free-fall time of the gas, we find that the molecules must be shielded from photodissociating radiation for at least $t_{\text{ff}} \geq 10$ Myr in order for the high abundance of HD molecules to persist, so that the formation of so-called

Pop III.2 (formerly Pop II.5) stars might be enabled, with their hypothesized masses of $\sim 10 M_{\odot}$ (see Johnson & Bromm 2006; see also McKee & Tan 2008).

We find that the relic H II region gas that re-collapses into the minihalo in which the first star formed, shown in Figure 2.6, carries a high fraction of HD molecules, as LW feedback from neighboring stars does not effectively dissociate the molecules in this relatively dense and self-shielded gas. The HD fraction exceeds 10^{-7} , becoming an order of magnitude higher than its value for un-ionized primordial gas collapsing in a minihalo. Thus, for this case, HD cooling will likely be effective at higher densities as the gas collapses further, and we expect that a Pop III.2 star, with a mass of the order of $10 M_{\odot}$, might form later on, if we were to run the simulation further (Nagakura & Omukai 2005; Yoshida 2006; Johnson & Bromm 2006; Yoshida et al. 2007). Had star formation taken place nearer this minihalo between the formation of the first star and the re-collapse of the gas into the host minihalo, then the molecule fraction would likely not be so elevated, and a higher mass metal-free star would be more likely to form. Thus, while in our simulation it appears that the first relic H II region that forms may give rise to Pop III.2 star formation, we emphasize that the possibility of the formation of Pop III.2 stars in relic H II regions is very dependent on the specific LW feedback that affects the gas in these regions.

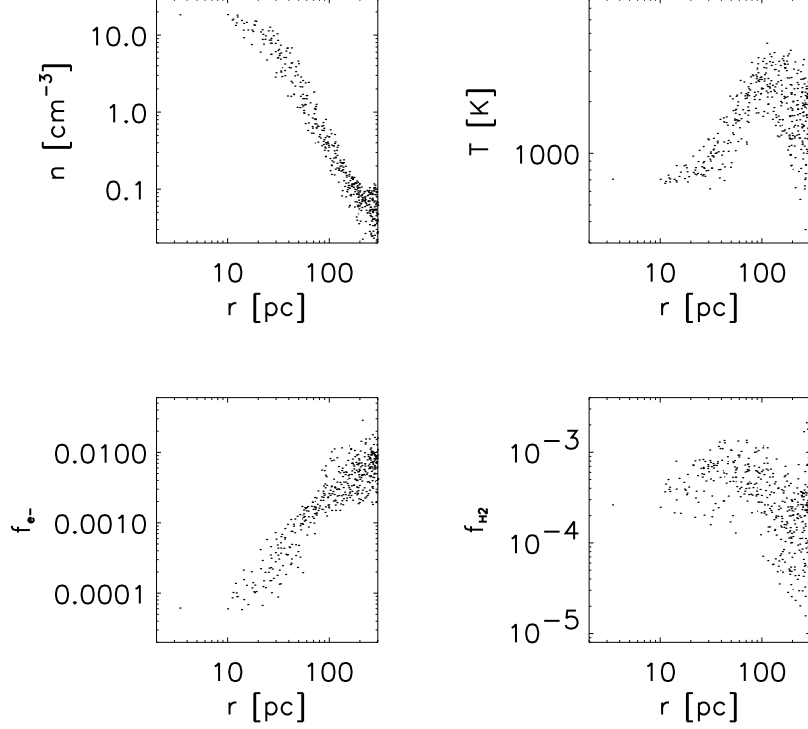


Figure 2.6: The properties of the relic H II region gas which recollapses into the minihalo which hosted the first star. Clockwise from the top-left are the density, temperature, H₂ fraction, and free electron fraction plotted as functions of distance from the center of the minihalo at the time when the density reaches n_{res} , at a redshift of $z \sim 19$. The temperature of the gas has dropped to below 10^3 K, well below the virial temperature of the minihalo, owing to molecular cooling. Owing to the high electron fraction that persists in this relic H II region, the molecule fraction in this gas is higher than in the case of un-ionized primordial gas collapsing into a minihalo. Indeed, as can be seen in Figure 2.3, the HD fraction is roughly an order of magnitude higher at these densities than in the case of un-ionized gas collapsing into a minihalo, which may allow for the efficient cooling of the gas to temperatures $T \geq T_{\text{CMB}}$ and so perhaps for the formation of metal-free stars with masses of the order of $10 M_{\odot}$.

2.3.6 Star Formation in the Presence of Radiative Feedback

To discern the effect the local radiative feedback from the first stars has on the star formation rate, we have compared the results obtained from our simulations with and without radiative feedback. By a redshift of $z \sim 18$, a total of nine star-forming regions were identified in our simulation without feedback, while at the same epoch eight stars had formed in our simulation including feedback. Thus, we find that the average star formation rate at redshifts $z \geq 18$ is diminished by a factor of perhaps only ≤ 20 percent due to local radiative feedback, although this result is subject to the small number statistics within our single cosmological box. Figure 2.7 shows the locations of the sites of star formation for both cases, plotted in comoving coordinates against the projected density field. The orange squares denote sites where Pop III stars could have formed in the case without feedback, while the green dots denote sites where Pop III stars formed in the simulation including radiative feedback. Thus, the sites where star formation is suppressed by the radiative feedback are marked by the orange squares which are not filled by a green dot.

We point out, however, that we do not include LW feedback from stars which may have formed outside of our box, and hence it is possible that the overall LW feedback may be stronger than we find here. At redshift $z \sim 18$, we end the simulation, but note that star formation will likely take place at an increasing rate as the collapse fraction increases with time. This could lead to a continuous LW background produced within our box, different from the intermittent LW feedback produced by individual stars that occurs in the

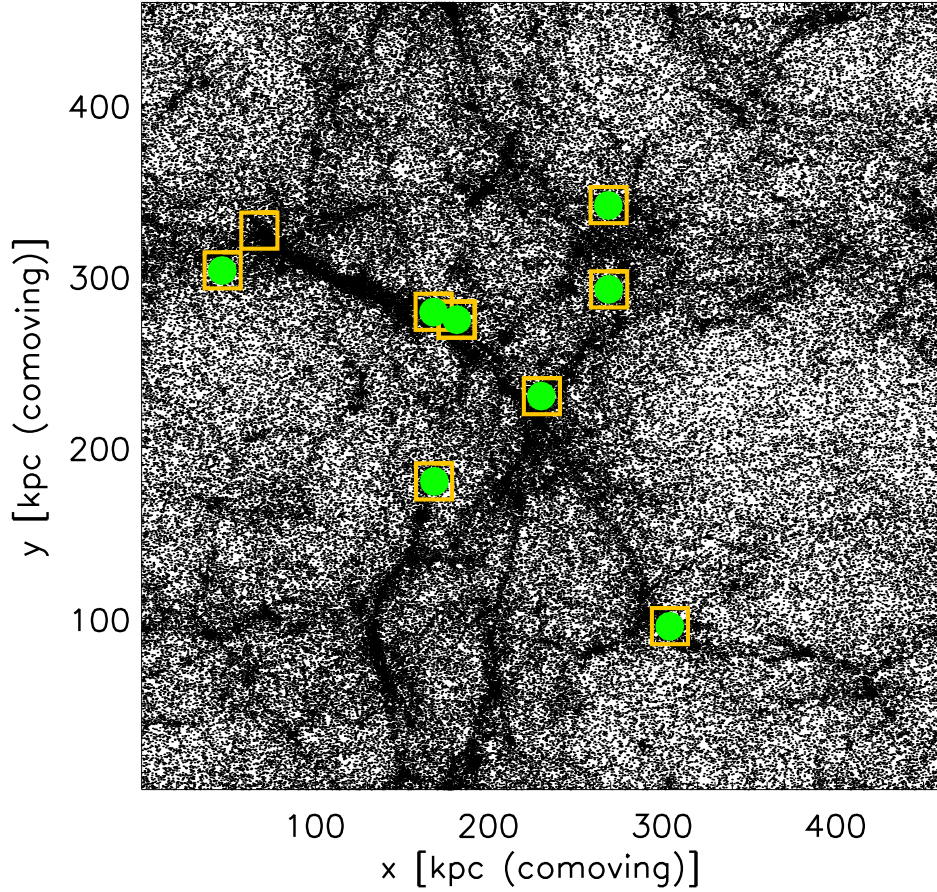


Figure 2.7: The sites of star formation with and without radiative feedback, at redshift $z \sim 18$. The black dots show the density field in our simulation box, in projection. The orange squares show the locations of minihalos in which Pop III star formation could take place, in our simulation without radiative feedback. The green dots show the sites where star formation takes place in our simulation including radiative feedback.

simulation down to $z \sim 18$.

Also, the limits of our resolution prohibit us from discerning the stronger shielding of H_2 molecules and I-front trapping that could occur within very dense collapsing minihalos (see Ahn & Shapiro 2006). However, we note that these authors find that the radiative feedback on collapsing minihalos from nearby stars generally does not greatly affect the final outcome of the collapse, as halos which collapse in the absence of radiative feedback generally also collapse when radiative feedback is applied (see also Susa & Umemura 2006), roughly consistent with our results in the present work. Thus, our limited resolution may not substantially impact the results that we find for the slight suppression of star formation due to local radiative feedback, although higher resolution simulations will be necessary to more precisely study the full impact of radiative feedback from the first stars on the first protogalaxies.

2.4 Summary and Discussion

We have performed cosmological simulations which self-consistently account for the radiative feedback from individual Pop III stars, as they form in the course of the assembly of the first protogalaxies. We have solved in detail for the H II regions, as well as for the LW bubbles of these stars, wherein molecule-dissociating radiation effectively destroys H_2 and HD molecules. The local radiative feedback from the first stars is complex, and we find a variety of novel results on the evolution of the primordial gas, on the effects of the LW radiation from the first stars, on the nature of second generation star

formation, and on black hole accretion.

While the LW radiation from the first stars can, in principle, greatly suppress Pop III star formation in the early universe, we find that a number of factors minimize the effectiveness of this negative feedback. Firstly, the LW radiation produced locally by individual stars is not uniform and constant, as LW feedback has been modeled in previous work (e.g., Ciardi & Ferrara 2005; Mesinger et al. 2006), but rather is present only during the brief lifetimes of the individual stars that produce it. Thus, even if the molecules in collapsing minihalos and relic H II regions are destroyed by the radiation from individual stars, they will, at the early stages of Pop III star formation, have time to reform and continue cooling the primordial gas in between the times of formation of local stars. Furthermore, because the LW bubbles of individual Pop III stars extend only to $R_{\text{LW}} \sim 5$ kpc from these sources, due to the short stellar lifetimes, the build up of a pervasive LW background would likely have to await the epoch of continuous star formation, which is fundamentally different from the epoch of the first stars, in which these sources shine for short periods within individual minihalos.

As star formation continues, the volume-filling fraction of relic H II regions increases as well, and this, combined with the high fraction of molecules that form in these regions, leads to an opacity to LW photons through the IGM which increases with time. This opacity can become of the order of $\tau_{\text{LW}} \geq 2$ through individual relic H II regions (Johnson & Bromm 2007; see also Ricotti et al. 2001; Machacek et al. 2001, 2003; Oh & Haiman 2002). Furthermore, as

the volume-filling fraction of relic H II regions increases with time, τ_{LW} through the general IGM may become similarly large, and this effect will have to be considered in future work which seeks to elucidate the effect of LW feedback on Pop III star formation.

We find that metal-free stars with masses of the order of $10 M_{\odot}$, the postulated Pop III.2 stars (e.g. Johnson & Bromm 2006; Greif & Bromm 2006), might form from the molecule-enriched gas within the first relic H II regions, although we note that this may not occur in general, due to LW feedback from neighboring star-forming regions. This susceptibility to LW feedback is due to the fact that the high fraction of HD molecules which forms in the electron-rich, low density regions of relic H II regions must persist until this gas has had time to collapse to high densities and form stars. If LW feedback from neighboring star-forming regions destroys the molecules after the gas has collapsed to densities $\geq 10 \text{ cm}^{-3}$, then the abundance of HD molecules will not likely be elevated when the gas forms stars and Pop III.2 star formation may be suppressed. Because this implies that the molecules must be shielded from LW radiation for, at least, the free-fall time for gas with densities $\leq 10 \text{ cm}^{-3}$, or $\geq 10 \text{ Myr}$, we conclude that Pop III.2 star formation in relic H II regions may occur only in the circumstances when local Pop III star formation is suppressed over such timescales. However, we also point out that the shielding provided by the high H_2 fraction in these relic H II regions may help to minimize the LW feedback from neighboring star-forming regions, and so may make Pop III.2 star formation in relic H II regions possible in

many cases.

We find that the ionized primordial gas surrounding the first star formed in our simulation, at a redshift of $z \sim 23$, recombines and cools by molecular cooling to temperatures below the virial temperature of the minihalo that hosted this first star. Thus, this relic H II region gas is able to re-collapse to densities $\geq 20 \text{ cm}^{-3}$ within this minihalo after ~ 50 Myr from the death of the star. It is predicted that many Pop III stars will collapse directly to form black holes with masses of the order of $100 M_{\odot}$ (e.g. Heger et al. 2003), and if such a black hole resides within this host halo, then we find that it may begin accreting dense primordial gas at close to the Eddington rate after ~ 60 Myr from the time of its formation. This is an important consideration to be incorporated into models of the growth of the $10^9 M_{\odot}$ black holes which have been observed at redshifts ≥ 6 , as it places constraints on the amount of matter that a given relic Pop III black hole could accrete by this redshift (e.g. Haiman & Loeb 2001; Volonteri & Rees 2006; Li et al. 2006).

Finally, by comparing the star formation rates which we derive from our simulation including radiative feedback with those derived from our simulation in which feedback is left out, we have seen that local radiative feedback from the first stars likely only diminishes the Pop III star formation rate by a factor of, at most, a few. In our simulation, in particular, we find that this rate is decreased by only ≤ 20 percent, although this may be less suppression than would be expected by the overall radiative feedback, as we did not include the possible effects of a global LW background. Future simulations which resolve

densities higher than those reached here, and which self-consistently track the build-up of the LW background along with the IGM opacity to LW radiation, will be necessary to more fully explore the radiative effects of the first stars on the formation of the first galaxies. However, the goal of understanding the formation of the first galaxies is now clearly getting within reach, and the pace of progress is expected to be rapid.

Acknowledgments

We would like to thank Yuexing Li and Kyungjin Ahn for helpful discussions. We are also grateful to Simon Glover and the anonymous referee for valuable comments that improved the quality of this work. The simulations used in this work were carried out at the Texas Advanced Computing Center (TACC).

Chapter 3

The Occurrence of Primordial Galaxies in the Early Universe

3.1 Introduction

How did the first galaxies in the Universe form? In the hierarchical picture of structure formation, the first galaxies, with masses of $\geq 10^8 M_\odot$, were built up from the mergers of smaller dark matter (DM) minihaloes, with virial temperatures $\leq 10^4$ K, in which the first Pop III star formation may have occurred (e.g. Bromm et al. 1999, 2002; Abel et al. 2002). The feedback effects from the first stars forming in minihaloes, likely having masses of the order of $100 M_\odot$ (e.g. Tan & McKee 2004; Yoshida et al. 2006), may thus have established the properties of the gas from which the first galaxies formed (see e.g. Ciardi & Ferrara 2005). During their brief lives of ~ 3 Myr, very massive Pop III stars emit copious UV radiation which can ionize the primordial gas and destroy H_2 molecules (e.g. Schaerer 2002), and upon their deaths they may explode as powerful supernovae, expelling the first heavy elements into their surroundings (Mori et al. 2002; Bromm et al. 2003; Kitayama et al. 2005; Greif et al. 2007).

The nature of the first galaxies may largely be determined by the metal-

licity of the gas from which they form, as the character of star formation is predicted to transition from a massive Pop III initial mass function (IMF) to a low-mass dominated IMF when the primordial gas has been enriched to a critical metallicity Z_{crit} (e.g. Bromm et al. 2001a; Schneider et al. 2003; Santoro & Shull 2006; Frebel et al. 2007; but see Jappsen et al. 2007). In turn, the metallicity of the protogalactic gas is dependent on the preceding Pop III star formation that takes place in minihaloes. While the supernova explosions of Pop III stars formed during the assembly of the first galaxies could drive the metallicity of these systems to super-critical levels (see e.g. Greif et al. 2007; Karlsson et al. 2008), Pop III star formation in minihaloes could, in principle, be largely suppressed due to radiative feedback effects (e.g. Haiman et al. 2000; Mackey et al. 2003).

Much recent work has been devoted to studying the effects of both ionizing and molecule-dissociating, Lyman-Werner (LW), radiation emitted from local star forming regions on Pop III star formation in minihaloes (Glover & Brand 2001; Shapiro et al. 2004; Alvarez et al. 2006; Abel et al. 2006; Susa & Umemura 2006; Ahn & Shapiro 2007; Yoshida et al. 2007; Johnson et al. 2007; Whalen et al. 2007), with results generally suggesting that local intermittent LW feedback does little to delay star formation, while ionizing radiation only delays star formation in minihaloes with relatively low-density gas that may not efficiently form stars even in the absence of radiative effects (e.g. Ahn & Shapiro 2007; Whalen et al. 2007). Thus, it appears likely that intermittent local radiative feedback effects may not be decisive in suppressing

the formation of Pop III stars during the assembly of the first galaxies (see also Wise & Abel 2007a).

The properties of the first galaxies are, however, more likely related to the global LW background, as it has been shown that a strong, persistent LW background can suppress star formation in the minihaloes which eventually are merged to form the first galaxies (e.g. Dekel & Rees 1987; Haiman et al. 1997; Bromm & Larson 2004). If star formation in these small systems can be suppressed effectively by the LW background, the first protogalaxies are much more likely to be kept metal-free. However, if star formation is not easily suppressed in minihaloes, either because the LW background is weak or if star formation can continue unimpeded despite strong LW feedback, then the first galaxies will likely form from already metal-enriched gas. Many studies have sought to estimate the global LW background during the epoch of the first stars (Haiman et al. 1997, 2000; Ricotti et al. 2002a,b; Glover & Brand 2003; Yoshida et al. 2003; Wise & Abel 2005; Greif & Bromm 2006). Additionally, the impact of a constant LW background on Pop III star formation has been investigated, suggesting that, while global LW feedback does not completely suppress star formation in minihaloes, it can delay such star formation (Machacek et al. 2001; Mesinger et al. 2006; O’Shea & Norman 2008; Wise & Abel 2007b).

In this paper, we investigate the impact of the build-up of a LW background on star formation in systems which later evolve into the first galaxies at redshift $z \geq 10$. In Section 3.2, we develop analytical models which self-

consistently couple the evolution of the LW background to that of the Pop III star formation rate (SFR) at $z \geq 15$. We describe our implementation of the LW background in cosmological simulations in Section 3.3. We report the outcome of simulations designed to test the hypothesis of a self-regulated LW background in Section 3.4, while in Section 3.5, we simulate the assembly of the first galaxy under the influence of such a self-regulated LW background. Finally, in Section 3.6 we discuss the implications of our findings for the galaxy formation process, and we conclude in Section 3.7.

3.2 The Lyman-Werner Background

The LW background radiation field is produced by sources, either stars or miniquasars, at cosmological distances, beginning with the formation of the first stars at the end of the cosmic dark ages. This radiation field acts to delay star formation by dissociating H_2 molecules, which are the primary coolants allowing primordial gas to collapse and form stars in minihaloes. Thus, to fully address both the production of the LW background radiation and the Pop III star formation which is sensitively coupled to it would require a cosmological simulation resolving the collapse of gas into minihaloes over enormous volumes of the Universe. As carrying out simulations over such large cosmological scales, while simultaneously resolving the collapse of gas in minihaloes, is still prohibitively expensive, we revert to simple analytical estimates for the self-consistent build-up of the LW background which draw on the results of detailed numerical simulations of Pop III star formation and radiative feedback. The

simple self-consistent analytical model that we develop in this Section may serve as a first order approximation to a more detailed self-consistent model for the build-up of the LW background and of the Pop III star formation rate in minihaloes at redshifts $z \geq 15$.

3.2.1 The Critical LW Flux

We first estimate the LW flux required to significantly delay the formation of Pop III stars in minihaloes. We note that for a typical case, following the extensive results of detailed simulations of Pop III star formation (see e.g. Bromm et al. 2002; Yoshida et al. 2003), the primordial gas first collapses adiabatically into a minihalo until it reaches a temperature $T \geq 10^3$ K and density $n \sim 1 \text{ cm}^{-3}$. As the evolution of the gas is adiabatic up to this point, the cooling properties of the gas play a role in its evolution only at higher densities. In particular, for the gas to continue collapsing on the way to forming a Pop III star, in accordance with the results of detailed simulations, a sufficient fraction of the coolant H_2 is required (Tegmark et al. 1997). In the presence of a LW radiation field, however, H_2 may be destroyed at a rate higher than it can be produced, effectively delaying the collapse of the gas.

We may estimate the flux of the radiation field required to achieve this delay by comparing the formation time of H_2 molecules, at $T \sim 10^3$ K and $n \sim 1 \text{ cm}^{-3}$, to the dissociation time of H_2 molecules as determined by the LW flux. For the dissociation time, we have (Abel et al. 1997)

$$t_{\text{diss}} \sim 3 \times 10^4 J_{\text{LW}}^{-1} \text{ yr} , \quad (3.1)$$

where J_{LW} is in units of $10^{-21} \text{ erg s}^{-1} \text{ cm}^{-2} \text{ Hz}^{-1} \text{ sr}^{-1}$. Equating to the formation time found in our simulations, $t_{\text{form}} \sim 8 \times 10^5 \text{ yr}$, yields $t_{\text{diss}} = t_{\text{form}}$ when the LW flux is $J_{\text{LW,crit}} \sim 0.04$, which we define as the critical flux necessary to significantly delay Pop III star formation in minihaloes, roughly consistent with numerous simulation results (see Machacek et al. 2001; Yoshida et al. 2003; Mesinger et al. 2006; O’Shea & Norman 2008; Wise & Abel 2007b).

3.2.2 The Maximum Background Flux

As a first step in developing our estimate of a self-consistent Pop III star formation rate and LW background flux, we calculate the maximum value for J_{LW} , as a function of redshift z , that we expect to be produced by Pop III stars forming in minihaloes at $z \geq 15$. We use the Sheth-Tormen formalism (see Sheth et al. 2001), with the cosmological parameters derived from the *Wilkinson Microwave Anisotropy Probe* (*WMAP*) third year data (Spergel et al. 2007), to find the mass fraction collapsed in minihaloes at these high redshifts. In comparison, the collapsed fraction in more massive haloes is very small, allowing us to neglect star formation that may be taking place in systems with virial temperatures $T_{\text{vir}} \geq 10^4 \text{ K}$ (see Section 3.2.3). Most studies of primordial star formation in minihaloes find that single stars with masses of the order of $100 M_{\odot}$ form in these systems (Abel et al. 2002; Bromm & Loeb 2004; Yoshida et al. 2006; Gao et al. 2007). To estimate the maximum star

formation rate we assume that each minihalo with a virial temperature $T_{\text{vir}} \geq 2 \times 10^3$ K (see e.g. Yoshida et al. 2003) hosts a $100 M_{\odot}$ Pop III star which lives for $t_* = 3$ Myr (e.g. Schaerer 2002). The comoving star formation rate of Pop III stars in minihaloes, in the absence of the negative feedback due to LW radiation, can then be estimated to be

$$\begin{aligned} \text{SFR}_{\text{III,max}} &\sim 10^{-3} \left(\frac{f_*}{10^{-3}} \right) \left(\frac{|dF/dz|}{2 \times 10^{-3}} \right) \\ &\times \left(\frac{1+z}{16} \right)^{\frac{5}{2}} M_{\odot} \text{yr}^{-1} \text{Mpc}^{-3}, \end{aligned} \quad (3.2)$$

where f_* is the fraction of collapsed baryons converted into Pop III stars, averaged over the Sheth-Tormen mass function, and $|dF/dz|$ is the change in the collapse fraction in minihaloes with redshift derived from the Sheth-Tormen formalism. We calculate f_* assuming that every minihalo with $2 \times 10^3 \text{ K} < T_{\text{vir}} < 10^4 \text{ K}$ hosts a single Pop III star with a mass of $100 M_{\odot}$, and the resulting evolution of f_* with redshift is shown in Fig. 3.1. Due to the increase of the average mass of such minihaloes with decreasing redshift, the fraction of collapsed baryons which goes into stars drops with redshift. For the following argument, it is convenient to compute a physical (proper) number density of Pop III stars in minihaloes as a function of redshift z , which we find to be

$$n_{\text{III,max}} \sim 6 \times 10^4 \left(\frac{f_*}{10^{-3}} \right) \left(\frac{|dF/dz|}{2 \times 10^{-3}} \right) \left(\frac{1+z}{16} \right)^{\frac{11}{2}} \text{Mpc}^{-3}, \quad (3.3)$$

assuming a constant Pop III mass of $100 M_{\odot}$.

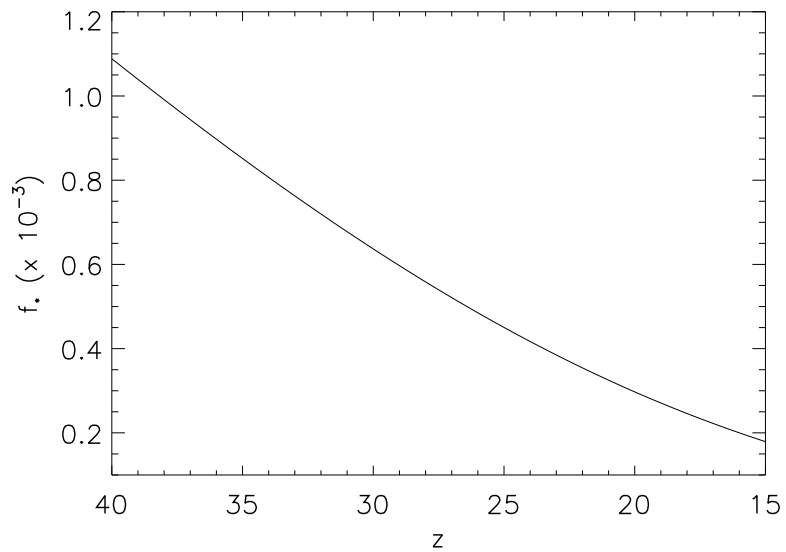


Figure 3.1: The average star formation efficiency f_* for Pop III star formation in minihaloes, assuming that a single $100 M_\odot$ star forms in each collapsed minihalo with a virial temperature $2 \times 10^3 \text{ K} < T_{\text{vir}} < 10^4 \text{ K}$. Here f_* is defined as the fraction of collapsed baryons converted into Pop III stars. The average is carried out over the Sheth-Tormen mass function.

To calculate the LW background generated in the limiting case that *every* minihalo hosts Pop III star formation, we next estimate the maximum physical distance traveled by a LW photon before being absorbed by a Lyman series transition in atomic hydrogen, which will be abundant at these epochs, when the Universe has not yet been substantially reionized (e.g. Haiman et al. 1997; Mackey et al. 2003). This distance corresponds to that of light traveling for a time needed to redshift the Ly β line of neutral hydrogen, at 12.1 eV, to the low-energy end of the LW band at 11.2 eV. At this point essentially all LW photons, with energies between 11.2 and 13.6 eV, will have been absorbed by neutral hydrogen. The distance to the LW horizon is thus

$$r_{\max} \sim 10 \left(\frac{1+z}{16} \right)^{-\frac{3}{2}} \text{ Mpc} , \quad (3.4)$$

again given in physical units. We note that this distance is an upper limit to how far a LW photon can propagate; for a more detailed calculation of the frequency-dependent propagation of LW radiation see Haiman et al. (2000). Using the number density of Pop III stars in equation (3.3), we integrate the flux from all the stars within a sphere of radius r_{\max} , obtaining the following estimate for the maximum background LW flux:

$$J_{\text{LW,max}} \sim 2 \left(\frac{f_*}{10^{-3}} \right) \left(\frac{|dF/dz|}{2 \times 10^{-3}} \right) \left(\frac{1+z}{16} \right)^4 . \quad (3.5)$$

Following Johnson et al. (2007), we here assume that the LW photons are emitted with a blackbody spectrum at 10^5 K from a $100 M_{\odot}$ Pop III star, as

modeled by Bromm et al. (2001b). In Fig. 3.2, we show the redshift evolution of $J_{\text{LW,max}}$, along with the corresponding $\text{SFR}_{\text{III,max}}$, assuming that f_* evolves as shown in Fig. 3.1.

We note that this idealized approach somewhat overestimates the LW background from $100 M_{\odot}$ primordial stars, as many of the LW photons will be absorbed over shorter distances by the higher order Lyman series transitions corresponding to higher LW photon energies (e.g. Haiman et al. 2000). Nevertheless, we expect that the above calculation gives a useful estimate for the maximum J_{LW} generated by Pop III star formation in minihaloes.

3.2.3 Self-consistent Models of the LW Background

In our calculation of the maximum LW background, we assumed that the Pop III SFR was independent of the level of the LW background generated. However, as shown in Fig. 3.2, the value of $J_{\text{LW,max}}$ can exceed that necessary to significantly delay star formation (e.g. Machacek 2001; Mesinger 2006; O’Shea & Norman 2008; Wise & Abel 2007b). Therefore, the model presented in Section 3.2.2 is inconsistent in that the SFR required to produce the maximum LW background cannot be maintained under such a strong background. Therefore, we now modify our model to more accurately couple the SFR to the LW background.

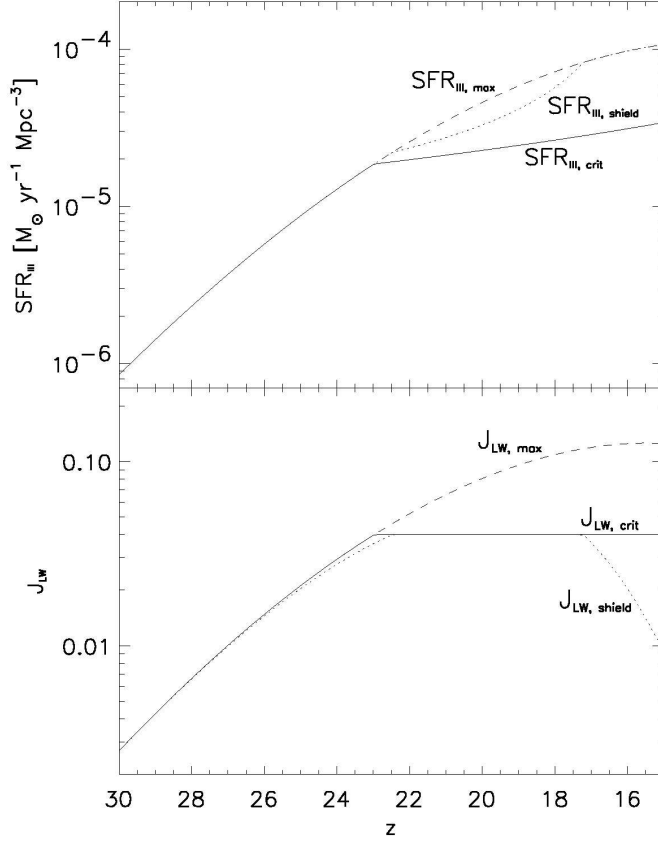


Figure 3.2: The Pop III star formation rates (*top panel*) and the corresponding LW background fluxes (*bottom panel*) for the three cases discussed in Sections 3.2.2 and 3.2.3. The maximum possible LW background, $J_{\text{LW,max}}$, is generated for the case that every minihalo with a virial temperature $T_{\text{vir}} \geq 2 \times 10^3$ K hosts a Pop III star, without the LW background in turn diminishing the SFR (dashed lines). The self-regulated model considers the coupling between the star formation rate, $\text{SFR}_{\text{III,crit}}$, and the LW background built-up by it, $J_{\text{LW,crit}}$ (solid lines). The minimum value for the LW background, $J_{\text{LW,shield}}$, is produced for the case of a high opacity through the relic H II regions left by the first stars and a corresponding star formation rate $\text{SFR}_{\text{III,shield}}$, higher than $\text{SFR}_{\text{III,crit}}$ and approaching $\text{SFR}_{\text{III,max}}$ (dotted lines). We expect that the true Pop III SFR in minihaloes has a value intermediate between $\text{SFR}_{\text{III,crit}}$ and $\text{SFR}_{\text{III,shield}}$.

3.2.3.1 Self-regulation

The sources that produce the LW flux at redshifts $z \geq 15$ may be stars or miniquasars, in principle. However, the accretion onto massive black holes resulting from the collapse of Pop III stars is not efficient in general (Johnson & Bromm 2007; Pelupessy et al. 2007), although it may be in relatively rare cases (see Li et al. 2007), and so the first miniquasars were likely not an important source of LW radiation in the early Universe. We further assume that the dominant contribution to the LW background at $z \geq 15$ is due to Pop III star formation in minihaloes, and we here neglect atomic cooling haloes as additional sources. At these redshifts, ≥ 90 percent of the collapsed mass is in minihaloes which, if they host star formation, are expected to host single massive Pop III stars (Abel et al. 2002; Yoshida et al. 2006; Gao et al. 2007). Therefore, if stars form in atomic-cooling haloes (e.g. Oh & Haiman 2002) with the same efficiency f_* with which stars form in minihaloes, the vast majority of stars will form in minihaloes at $z \geq 15$, thus justifying our assumption.

However, the star formation efficiency f_* in atomic-cooling haloes is not well-constrained at $z \geq 15$. Recently, Ricotti et al. (2008) have argued that f_* can take a range of values, from $\sim 10^{-3}$ to $\sim 10^{-1}$, roughly scaling as the square of the halo mass. Because most of the collapsed mass that goes into atomic-cooling haloes will reside in the least massive systems, we take this as evidence that the mass-weighted average of f_* is likely near the lower end of this range, which is similar to minihalo efficiencies. In Fig. 3.3 we show the fraction of LW photons, $f_{\text{LW,mini}}$, emitted by Pop III stars formed in minihaloes

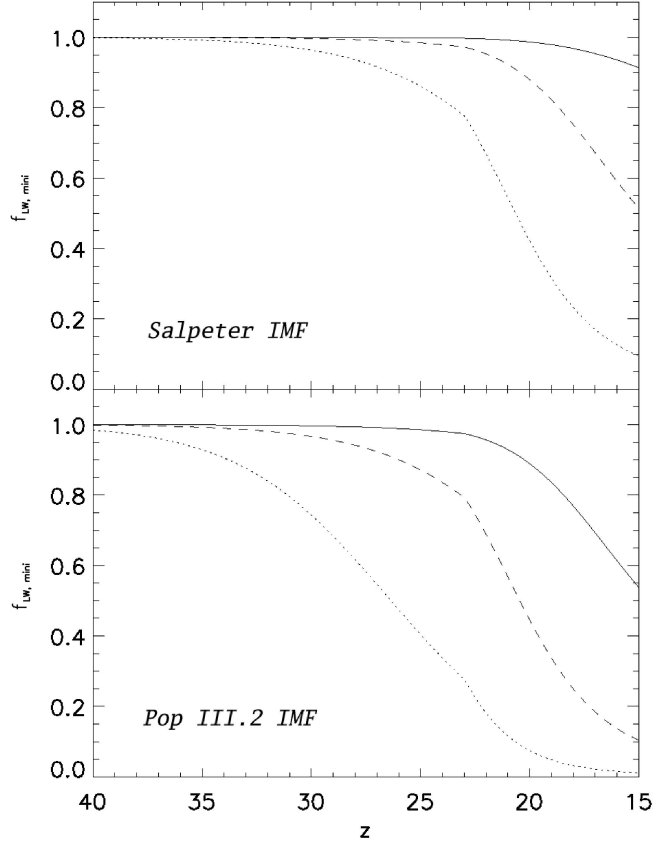


Figure 3.3: The fraction of the total LW flux contributed by Pop III stars formed in minihaloes $f_{\text{LW,mini}}$ in our self-regulated model (see Section 3.3.1), for various choices of the star formation efficiency f_* in atomic-cooling haloes, which we assume are not subject to LW feedback. Atomic-cooling haloes in which Pop II stars form with a Salpeter initial mass function (IMF) (*top panel*) produce a smaller fraction of LW photons, for a given star formation efficiency, than do atomic-cooling haloes which host Pop III.2 stars with masses of the order of $10 M_\odot$ (*bottom panel*). The solid lines correspond to a star formation efficiency of $f_* = 10^{-3}$ in atomic-cooling haloes, while the dashed and dotted lines correspond to $f_* = 10^{-2}$ and 0.1 , respectively. Our self-regulated model assumes that Pop III stars formed in minihaloes emit the dominant portion of LW photons ($f_* \geq 0.8$). For different choices of the IMF and the star formation efficiency, our model will be valid down to different redshifts.

with a star formation rate given by $\text{SFR}_{\text{III,crit}}$, for various assumptions about the efficiency of star formation and the IMF of stars formed in atomic-cooling haloes. While for minihalo star formation we assume that single $100 M_{\odot}$ stars form with an efficiency as given in Fig. 3.1, we consider values of $f_* = 10^{-1}$, 10^{-2} , and 10^{-3} for atomic cooling haloes. Furthermore, we consider two IMFs for atomic-cooling haloes: a standard Salpeter IMF for the case of an already metal-enriched (Pop II) system, and a Pop III.2 IMF postulating that metal-free stars form with masses of the order of $10 M_{\odot}$ (Johnson & Bromm 2006; see McKee & Tan 2007 for the terminology). The latter case is the predicted star formation mode in atomic cooling haloes, provided that they remain pristine (e.g. Johnson & Bromm 2006; Greif et al. 2008). For the Salpeter IMF, the number of LW photons emitted per baryon in stars is taken to be $\eta_{\text{LW}} = 4 \times 10^3$, and for the Pop III.2 case, we assume $\eta_{\text{LW}} = 2 \times 10^4$ (see Greif & Bromm 2006). Because our model of self-regulated star formation assumes that minihaloes produce the dominant portion of the LW background, it will only be valid for redshifts where $f_{\text{LW,mini}} \geq 0.8$. Assuming $f_* \geq 10^{-3}$ in atomic-cooling haloes, we thus expect that our self-regulated model of star formation in minihaloes is valid at redshifts $z \geq 15$ for a Salpeter IMF, and at redshifts $z \geq 18$ for a Pop III.2 IMF. As suggested by the results presented in Section 3.5, the IMF in such systems may transition from a Pop III IMF to a Pop II IMF after the formation of only one or a few massive Pop III stars.

With the assumption that Pop III stars in minihaloes contribute the dominant portion of the LW background, the production of the LW back-

ground becomes a purely self-regulated process: any increase in the star formation rate will translate into an increase in the LW background, which will in turn suppress the star formation rate, and vice versa. While a prohibitively expensive simulation would be required to self-consistently track the build-up of the LW background in this way (but see Yoshida et al. 2003), we suggest that a self-consistent flux would be similar to the value that we found for the critical LW flux, $J_{\text{LW,crit}}$. As explained in Section 3.2.1, a LW flux much below this value will not efficiently delay the formation of molecules in minihaloes and so will only slightly suppress the star formation rate; in turn, a LW flux much above this value will delay the star formation rate substantially (e.g. O’Shea & Norman 2008; Wise & Abel 2007b).

The star formation rate expected under the assumption that the LW background must not exceed $J_{\text{LW,crit}}$ can be derived from the Sheth-Tormen formalism. We follow our treatment for the maximum LW flux from Pop III star formation in minihaloes (Section 3.2.2), now requiring that $J_{\text{LW,crit}} = 0.04$ is not exceeded, as shown in Fig. 3.2. We then find the fraction f_{reg} of minihaloes that must form stars in order to produce this self-regulated LW flux from the simple relation

$$f_{\text{reg}}(z) \sim \frac{J_{\text{LW,crit}}(z)}{J_{\text{LW,max}}(z)}. \quad (3.6)$$

Assuming that Pop III stars form in minihaloes, if not prevented from doing so by negative feedback, as single, massive stars (e.g. O’Shea & Norman 2008; Wise & Abel 2007b), it is the number of minihaloes at a given redshift

which determines the SFR. We thus infer that this critical rate, $\text{SFR}_{\text{III,crit}}$, is suppressed, at most, by a fraction f_{reg} compared to the maximum possible Pop III rate in minihaloes, $\text{SFR}_{\text{III,max}}$. Because our value for $J_{\text{LW,max}}$ is an upper limit (see Section 3.2.2), the corresponding suppression factor, f_{reg} , is a lower limit.

The calculation presented here gives a simple estimate of the Pop III SFR at $z \geq 15$, accounting for the coupling of the SFR to the LW background generated by Pop III stars. In Section 3.4, we report on a simulation carried out to test the validity of this model as a first approximation to a more detailed self-consistent model of the Pop III star formation rate history.

3.2.3.2 Shielding from Relic H II Regions

While massive Pop III stars formed in minihaloes create large H II regions, with (proper) radii of a few kpc (Alvarez et al. 2006; Abel et al. 2006), these stars live for only ≤ 3 Myr, at which point the relic H II regions that are left behind begin to cool and recombine. The conditions in such relic H II regions are conducive to the rapid formation of H_2 and HD molecules (Nagakura & Omukai 2005; O’Shea et al. 2005; Johnson & Bromm 2006; Yoshida et al. 2007). Johnson et al. (2007) showed that the resulting opacity to LW photons, τ_{LW} , can be significant, exceeding unity across just a single relic H II region. Furthermore, these authors found that the high H_2 fraction formed in these regions generally remains high, as molecules quickly reform in between the intermittent episodes of exposure to LW radiation produced by

nearby, short-lived Pop III stars.

To evaluate the effect of the opacity through relic H II regions on the build-up of the LW background, we now repeat the calculation in Section 3.2.2, this time including a maximal optical depth to LW photons through relic H II regions, $\tau_{\text{LW,max}}$. We employ an iterative procedure in order to determine self-consistently, at each redshift, the star formation rate, the optical depth to LW photons, and the LW background flux, all of which are dependent on each other. To begin, we initialize the calculation at $z = 50$, at which time we assume that $\tau_{\text{LW,max}} = 0$, the star formation rate is equal to the maximal rate $\text{SFR}_{\text{III,max}}$, and the LW background flux is equal to the maximal value $J_{\text{LW,max}}$, and we integrate forward in time.

To calculate the cosmological average $\tau_{\text{LW,max}}$ we adopt the results of Haiman et al. (2000), who find that at $z = 15$ the average LW optical depth is $\tau_{\text{LW}} \sim 0.04$ for a uniform H_2 fraction of $f_{\text{H}_2} = 2 \times 10^{-6}$. Consistent with the results of Haiman et al., this cosmological average optical depth scales as

$$\tau_{\text{LW}} \propto r_{\text{max}} n_{\text{H}_2} \propto (1+z)^{\frac{3}{2}} \quad (3.7)$$

where n_{H_2} is the average number density of H_2 in the intergalactic medium (IGM).

As Pop III star formation in minihaloes proceeds, the volume-filling fraction of relic H II regions increases with the number of Pop III stars which form and rapidly die. Johnson & Bromm (2007) found that the high residual

free-electron fraction in relic H II regions can persist for of the order of 500 Myr, in turn driving the vigorous production of H₂ molecules. These regions are thus expected to maintain a high H₂ fraction for over a Hubble time, and their abundance is therefore assumed to be proportional to the cumulative star formation history and to only increase with time. We calculate the volume-filling fraction of relic H II regions, f_{HII} , by assuming that each Pop III star which forms in a minihalo leaves behind a relic H II region. We find

$$f_{\text{HII}} \sim \frac{4\pi}{3} \left[4\text{kpc} \left(\frac{1+z}{20} \right)^{-1} \right]^3 n_{\text{HII}} , \quad (3.8)$$

where we have assumed that each Pop III star leaves behind a relic H II region with a radius of $\sim 4 \text{ kpc} [(1+z)/20]^{-1}$ in which the recombination time is longer than the lifetime of the star (see Abel et al. 2006; Alvarez et al. 2006; Johnson et al. 2007; Yoshida et al. 2007). The (physical) number density of relic H II regions, n_{HII} , taken to be proportional to the collapse fraction in minihaloes as explained above, is given by

$$n_{\text{HII}} \sim 10^6 f_{\text{shield}} \left(\frac{f_*}{10^{-3}} \right) \left(\frac{F(z)}{6 \times 10^{-3}} \right) \left(\frac{1+z}{16} \right)^3 \text{Mpc}^{-3} . \quad (3.9)$$

Here $F(z)$ is the fraction of collapsed mass in minihaloes as a function of redshift, given by the Sheth-Tormen formalism, with the fiducial value of $F(z) \sim 6 \times 10^{-3}$ at $z \sim 15$, while $F(z) \sim 10^{-3}$ at $z \sim 20$. We account for the suppression in the SFR due to a shielded LW background by including the factor f_{shield} , defined as the ratio of the integrated SFR in the self-regulated

model including an IGM optical depth, $\text{SFR}_{\text{III,shield}}$, to be estimated below, to the integrated maximum SFR, $\text{SFR}_{\text{III,max}}$, as described in Section 3.2.1:

$$f_{\text{shield}} = \frac{\int_z^\infty \text{SFR}_{\text{III,shield}}(z') dz'}{\int_z^\infty \text{SFR}_{\text{III,max}}(z') dz'} . \quad (3.10)$$

We can then re-write the volume-filling factor of H II regions as

$$f_{\text{HII}} \sim 0.1 f_{\text{shield}} \left(\frac{f_*}{5 \times 10^{-4}} \right) \left(\frac{F(z)}{6 \times 10^{-3}} \right) . \quad (3.11)$$

For simplicity, we use a constant average value of $f_* = 5 \times 10^{-4}$ in equation (3.11), consistent with the values shown in Fig. 3.1.

To obtain the maximum average IGM optical depth to LW photons, we follow the results of Haiman et al. (2000) along with equation (3.7), this time accounting for an elevated H_2 abundance within a fraction f_{HII} of the volume of the Universe. We thus find

$$\tau_{\text{LW,max}} = 4 \left(\frac{f_{\text{HII}}}{0.5} \right) \left(\frac{f_{\text{H}_2}}{10^{-4}} \right) \left(\frac{1+z}{16} \right)^{\frac{3}{2}} \left(\frac{\delta}{10} \right) , \quad (3.12)$$

where we use $f_{\text{H}_2} = 10^{-4}$ as an upper limit for the average H_2 fraction in relic H II regions and an average overdensity in these regions of $\delta = 10$, as estimated from the simulation presented in Johnson et al. (2007).

Next, we self-consistently calculate the minihalo Pop III SFR, again assuming that the LW background flux must not exceed $J_{\text{LW,crit}}$, but this time taking into account the optical depth $\tau_{\text{LW,max}}$ through relic H II regions. The fraction of minihaloes in which Pop III stars are able to form is then given by

$$f_\tau(z) = \min \left(1, \frac{J_{\text{LW,crit}}(z)}{J_{\text{LW,max}}(z)} e^{\tau_{\text{LW,max}}} \right) , \quad (3.13)$$

analogous to the no-shielding case in equation (3.6). The intuition here is that to compensate for the loss due to the IGM opacity, a larger SFR is required to maintain a LW background at the critical level, compared to $\text{SFR}_{\text{III,max}}$; however, the SFR cannot exceed the maximum one. We thus find for the SFR of Pop III stars in minihaloes, including the effects of both a LW background and the IGM optical depth to LW photons

$$\text{SFR}_{\text{III,shield}} = f_\tau(z) \text{SFR}_{\text{III,max}} . \quad (3.14)$$

Finally, the corresponding LW background flux is

$$J_{\text{LW,shield}} = J_{\text{LW,crit}} \times \min \left(1, \frac{J_{\text{LW,max}}(z)}{J_{\text{LW,crit}}(z)} e^{-\tau_{\text{LW,max}}} \right) , \quad (3.15)$$

as plotted in Fig. 3.2. The optical depth $\tau_{\text{LW,max}}$ produced in this model is shown in Fig. 3.4. We interpret $J_{\text{LW,shield}}$ to be the minimal value for the LW background flux at $z \geq 15$. Correspondingly, we find that $\text{SFR}_{\text{III,shield}}$ is an upper limit to the Pop III SFR in minihaloes at these redshifts.

In reality, the clustering of Pop III sources, coupled with the increasing SFR towards lower redshifts, will likely lead to the efficient photodissociation of H_2 molecules in some relic H II regions even at $z \geq 15$, as well as to overlap between relic H II regions as f_{HII} grows with time. Both effects will lower the

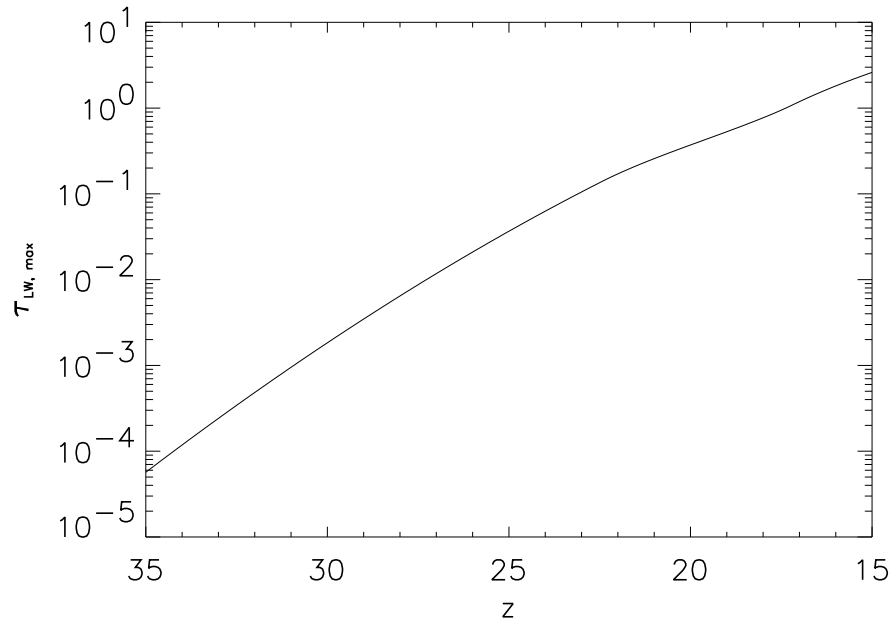


Figure 3.4: The maximum IGM optical depth to LW photons, $\tau_{LW, max}$, due to the high fraction of H_2 in the relic H II regions. This corresponds to $SFR_{III, shield}$ and a LW background flux of $J_{LW, shield}$. Note that locally the optical depth can be greater than this average, exceeding unity through a single H II region, owing to self-shielding of H_2 (see Johnson et al. 2007).

opacity to LW photons through the IGM, and the global average LW background will eventually exceed the level $J_{\text{LW}} \sim 10^{-3}$ needed for the dissociation of H_2 molecules in these regions to outpace their formation (Johnson & Bromm 2007), although we note that we have not accounted for the local optical depth to LW photons through individual relic H II regions, which can exceed unity through a single relic H II region (Johnson et al. 2007). Finally, we note that the emission of X-rays from miniquasars may, in principle, lead to a high opacity to LW photons, as it has been shown that the partial ionization from X-rays can enhance the generation of H_2 in the IGM (e.g. Kuhlen & Madau 2005). However, as noted above, it is not clear that the accretion rates onto Pop III relic black holes are sufficiently high for this mechanism to dominate the generation of LW opacity (e.g. Pelupessy et al. 2007).

3.2.4 The Expected Pop III Star Formation Rate

We expect the actual LW background at $z \geq 15$ to lie between $J_{\text{LW,shield}}$ and $J_{\text{LW,crit}}$. The corresponding Pop III SFR in minihaloes which generates this LW background likely falls between $\text{SFR}_{\text{III,crit}}$ and $\text{SFR}_{\text{III,shield}}$, since the shielding provided by relic H II regions can keep $J_{\text{LW}} \leq J_{\text{LW,crit}}$. In turn, this will allow to keep $\text{SFR}_{\text{III}} \geq \text{SFR}_{\text{III,crit}}$, owing to the diminished strength of the negative LW feedback. In the remainder of the present work we will take $J_{\text{LW,crit}}$ as a plausible maximum value for the LW background flux, and we will use this value as an input in our simulations of galaxy formation, thereby obtaining lower limits to the amount of star formation that may take place in

the assembly of these systems at $z \geq 15$. We note that, although we follow the assembly of a galaxy to $z \geq 12$, the star formation that does take place in our simulation occurs at $z \geq 15$. Thus, our simple assumption here that $J_{\text{LW}} = J_{\text{LW,crit}}$ even at $z \leq 15$ does not impact the results of our simulations significantly.

3.3 Methodology of Simulations

With the goal of estimating the degree to which Pop III star formation in minihaloes affects the properties of the gas from which the first galaxies form at $z \geq 10$, we have carried out two cosmological hydrodynamics simulations which track the detailed evolution of the primordial gas under the influence of a LW background radiation field. The first simulation is designed to test the validity of our self-regulated model for the build-up of the LW background, and is described further in Section 3.4. The second simulation follows the assembly of a galaxy virializing at $z \geq 10$, assuming a critical LW background, $J_{\text{LW,crit}}$. This simulation is described in Section 3.5.

As with previous work, for our three-dimensional numerical simulations we employ the parallel version of GADGET (version 1), which includes a tree (hierarchical) gravity solver combined with the smoothed particle hydrodynamics (SPH) method for tracking the evolution of gas (Springel et al. 2001; Springel & Hernquist 2002). Along with H_2 , H_2^+ , H , H^- , H^+ , e^- , He , He^+ , and He^{++} , we have included the five deuterium species D , D^+ , D^- , HD and HD^+ , using the same chemical network as in Johnson & Bromm (2006, 2007).

The specific initial conditions for our simulations are described separately in Sections 3.4 and 3.5.

3.3.1 Sink Particles

The primary result obtained from the present simulations is the number of Pop III stars which are able to form in minihaloes at $z \geq 15$ during the assembly of a galaxy virializing at $z \geq 10$. To track the number and location of the formation sites for Pop III stars, we allow sink particles to form when the gas has collapsed to high densities. Specifically, sinks are created when the gas has collapsed to a threshold density n_{res} , above which the mass resolution of our simulation is insufficient to reliably follow the continued collapse of the gas, as explained further in Johnson et al. (2007). We note that the time at which a sink particle forms will precede the time at which a star is able to form by roughly a free-fall time in gas with a density n_{res} ; while this can introduce an error of ≤ 10 Myr in the precise timing of star formation, the conclusions that we derive from the results presented here are not significantly impacted. Once having formed, the sink particles act as tracers of star formation sites, each sink representing the formation site of a single Pop III star. We focus our attention on when and where these sinks emerge in order to estimate the number of stars formed, and to gauge the feedback effects from these stars.

3.3.2 Implementation of Background Radiation

Motivated by the considerations presented in Section 3.2 and further justified in Section 3.4, we have included in our simulations the self-regulated model of the LW background radiation field, in the form of a global H_2 dissociation rate. The LW background is taken to be a function of redshift, its evolution given by $J_{\text{LW,crit}}(z)$, as shown in Fig. 3.2. The dissociation rate is

$$k_{\text{diss}}(z) = 10^{-12} J_{\text{LW,crit}}(z) \text{s}^{-1} . \quad (3.16)$$

In addition to the photodissociation of H_2 , the photodestruction of other species can, in principle, affect the cooling properties of the primordial gas. The main reaction producing H_2 being $\text{H}^- + \text{H} \rightarrow \text{H}_2 + \text{e}^-$ (e.g. Peebles & Dicke 1968; Lepp & Shull 1984), the photodestruction of H^- is a process that might lead to suppression of the H_2 fraction of the gas (Chuzhoy et al. 2007; see also Glover et al. 2006). However, we find the photodissociation of H^- to be unimportant for the suppression of H_2 in collapsing minihaloes. As discussed in Section 3.2.1, the gas in such minihaloes will adiabatically collapse to densities of $\geq 1 \text{ cm}^{-3}$ and temperatures of $\geq 10^3 \text{ K}$, even if the fractions of H_2 or H^- are low. Following this adiabatic collapse, the fate of the gas does depend sensitively on the abundances of these species, and it is only at this stage at which the photodissociation of H^- might begin to have an effect. We find that the chemical species at this stage, absent strong shocks or photoionization, are roughly in equilibrium when we include the effect of the LW background,

and therefore suppression of the H_2 abundance can be directly tied to the abundance of H^- at this stage. At this temperature and density, we find that the H^- formation time is of the order of years. We find that the minimal photodissociation timescale of H^- , produced for the case of the maximal LW background $J_{\text{LW,max}}$ (see Section 3.2.2), is of the order of $\geq 10^2$ yr, roughly two orders of magnitude higher than the formation timescale. Thus, the H^- fraction will not be significantly affected by a background radiation field, and in turn the abundance of H_2 will not be significantly affected, allowing us to neglect the photodissociation of H^- as a factor in delaying star formation. Furthermore, we neglect the photodissociation of H^- due to radiation from local star formation for similar reasons, as explained in Johnson et al. (2007).

We have also neglected $\text{Ly}\alpha$ heating as a suppressant of minihalo star formation (see Chuzhoy & Shapiro 2007; Ciardi & Salvaterra 2007). For the Pop III star formation rates, and corresponding production rates of UV photons, found in our simulations, $\text{Ly}\alpha$ heating will not raise the temperature of the IGM appreciably, even for the maximal SFR considered here, $\text{SFR}_{\text{III,max}}$ (see Section 3.2.2). Finally, we do not include a photoionizing background in our calculations. At these high redshifts, the IGM is still predominantly neutral. Photoionization will thus generally occur only locally, when isolated Pop III stars form, an intermittent process which is not likely to dramatically affect the overall SFR (see e.g. Ahn & Shapiro 2007; Johnson et al. 2007; Whalen et al. 2007; Wise & Abel 2007a; but see Ricotti et al. 2002a,b).

3.4 Testing the Self-Regulated Model

We have argued in Section 3.2.2 that the LW background and Pop III star formation rate at redshifts $z \geq 15$ are strongly coupled to one another, and that a self-consistent SFR is likely close to what is required to produce $J_{\text{LW,crit}}$. To test this *Ansatz*, we have carried out a fiducial simulation with no LW feedback, and one with identical initial conditions, but with the critical LW background included. Comparing the resulting suppression of star formation in our simulations to the analytical ratio $\text{SFR}_{\text{III,crit}}/\text{SFR}_{\text{III,max}}$, we can roughly gauge the validity of our simple self-regulated model.

3.4.1 Initial Conditions

We initialize these cosmological simulations according to the Λ CDM model at $z = 100$, adopting the cosmological parameters $\Omega_m = 1 - \Omega_\Lambda = 0.3$, $\Omega_B = 0.045$, $h = 0.7$, and $\sigma_8 = 0.9$, close to the values measured by *WMAP* in its first year (Spergel et al. 2003). Here we use a periodic box with a comoving size $L = 500 h^{-1}$ kpc, and particle numbers of $N_{\text{DM}} = N_{\text{SPH}} = 145^3$, where the SPH particle mass is $m_{\text{SPH}} \sim 710 M_\odot$.

As we have already noted in Section 3.2, conducting a sufficiently large cosmological simulation to thoroughly follow the build-up of the LW background is prohibitively expensive. Our choice of initial conditions for the present simulation is thus purely a practical one, so that we may follow the evolution of a sufficient number of minihaloes in our cosmological box for our purpose, which is to compare the suppression of the rate of collapse of gas in

minihaloes with the suppression of the star formation rate that is expected in our simple self-regulated model. Because this simulation is not the large-scale cosmological simulation that is necessary to fully test the self-regulated model, all we can derive from this simulation is whether or not the delay in the collapse of the few (~ 20) minihaloes that form in our small simulation box is roughly consistent with the global average suppression of the star formation rate that we predict in the self-regulated model. Therefore, the results that we derive from this test hold no statistical significance which is dependent on the specific cosmological model that we use to initialize our simulation; we only seek to compare the isolated behavior of the minihaloes in our box with the general behavior we expect in the self-regulated model. A more detailed study of the self-consistent build-up of the LW background will be the subject of future work.

The density above which resolution is lost in this simulation is $n_{\text{res}} \sim 20 \text{ cm}^{-3}$, as determined following Johnson et al. (2007). Therefore, sink particles are formed in minihaloes which reach this density threshold, and we thereafter consider these minihaloes as hosting the formation of single Pop III stars. While we are not able to resolve the process of star formation itself, we believe this is a reliable indicator of when star formation is possible, as gas collapsing in minihaloes will generally only reach these densities when cooling is efficient and the collapse has ceased to be adiabatic (e.g. Omukai et al. 2005; Yoshida et al. 2006; Johnson et al. 2007).

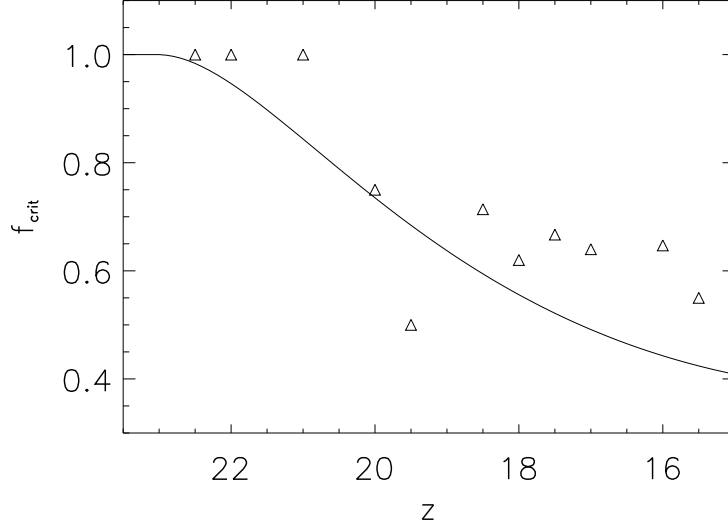


Figure 3.5: The fraction of minihaloes which form stars when exposed to the critical LW background, $J_{\text{LW,crit}}$, normalized to the total number of stars formed absent a LW background, as a function of redshift. *Solid line*: The fraction of Pop III stars expected to form in our analytical model for the critical star formation rate, $\text{SFR}_{\text{III,crit}}$, assuming the star formation efficiency f_* shown in Fig. 3.1. *Open triangles*: The results from our simulation show the same general variation with z as the analytically-derived behavior to within a factor of ~ 2 , with the points from our simulation likely being overestimates due to our choice of *WMAP* first year initial conditions for our simulation. This agreement supports the validity of our simple model for self-regulated Pop III star formation.

3.4.2 Results

In Fig. 3.5, we compare our analytical prediction, described in Section 3.3.1, to our simulation results. The line in Fig. 3.5 shows the analytically derived value for the fraction of stars, $f_{\text{crit}}(z)$, which form by a redshift z in the self-regulated model out of the total number of minihaloes which could host star formation absent any negative LW feedback. We define this fraction as the ratio of the integrated SFR in the self-regulated model to the integrated SFR in the model for maximal star formation, described in Sections 3.2.3 and 3.2.2, respectively:

$$f_{\text{crit}} = \frac{\int_z^\infty \text{SFR}_{\text{III,crit}}(z') dz'}{\int_z^\infty \text{SFR}_{\text{III,max}}(z') dz'} . \quad (3.17)$$

In this analytical treatment, we have assumed the value shown in Fig. 3.1 for the fraction of collapsed baryons in stars f_* , as a function of redshift.

The quantity f_{crit} is calculated as the number of sink particles that form by a redshift z in the simulation including the critical LW background, $J_{\text{LW,crit}}$, divided by the number that form in the simulation without any LW background included, and is plotted in Fig. 3.5. As expected, likely owing to the relatively high bias in our simulations initialized with *WMAP* first year parameters, the simulated values for f_{crit} are higher than those from our analytical derivation using *WMAP* third year parameters. Nonetheless, the agreement between our simple analytical model and the simulations is broadly consistent, given the simplicity of our model. We thus conclude that, as a

rough estimate, a self-consistent value for the LW background at redshifts $z \geq 15$ is likely close the critical value, $J_{\text{LW,crit}}$. We emphasize, however, that the effect of the opacity to LW photons through relic H II regions will be to lower J_{LW} and, simultaneously, to allow for a higher SFR than that in our simple self-regulated model shown in Fig. 3.2.

3.5 Galaxy Formation in the Early Universe

Assuming that the photodissociation of H_2 molecules by a global LW background is the dominant factor in regulating Pop III star formation in minihaloes at redshifts $z \geq 15$, we now employ our simple model for a self-regulated LW background to investigate the impact of Pop III star formation on the assembly of a galaxy at $z \geq 10$. We choose to define a galaxy as a star forming system hosted by a DM halo with a virial temperature of $\geq 10^4$ K, corresponding to a halo with total mass $\geq 10^8 M_\odot$ at $z \geq 10$ (e.g. Barkana & Loeb 2001), as gas in such a system can cool via atomic hydrogen, can likely host continuous star formation, and can retain gas against being blown out by supernovae or by photoheating (e.g. Mori et al. 2002; Kitayama & Yoshida 2005; Read et al. 2006). Here we report the results from our simulation of the formation of a galaxy which virializes at redshift $z \sim 12$, focusing on the modes and amount of star formation that may take place during its assembly. Additional aspects of the formation of such a galaxy are discussed in a companion paper (Greif et al. 2008).

3.5.1 Initial Conditions

For our simulation of the assembly of a 'first galaxy', we have employed multi-grid initial conditions which offer higher resolution in the region where the galaxy forms (e.g. Kawata & Gibson 2003; Li et al. 2007). We again initialize the simulation according to the Λ CDM model at $z = 100$, adopting the cosmological parameters $\Omega_m = 1 - \Omega_\Lambda = 0.3$, $\Omega_B = 0.045$, $h = 0.7$, and $\sigma_8 = 0.9$, close to the values measured by *WMAP* in its first year (Spergel et al. 2003). Here we use a periodic box with a comoving size $L = 1 h^{-1}$ Mpc for the parent grid. This simulation uses a number of particles $N_{\text{DM}} = N_{\text{SPH}} = 1.05 \times 10^6$, where the SPH particle mass is $m_{\text{SPH}} \sim 120 M_\odot$ in the region with the highest resolution. For further details on the technique employed to generate our multi-grid initial conditions, see the companion paper by Greif et al. (2008). The density above which resolution is lost is $n_{\text{res}} \sim 10^3 \text{ cm}^{-3}$, as determined following Johnson et al. (2007). As described in Sections 3.3 and 3.4, sink particles are formed in minihaloes which reach this density threshold, and we thereafter consider these sinks to contain single Pop III stars.

3.5.2 Formation of the First Star

The first star forms at redshift $z \sim 16.3$ inside the minihalo which is the most massive progenitor of the halo eventually hosting the galaxy. The mass of the DM halo hosting the first star is $7 \times 10^6 M_\odot$, while the virial temperature of the halo is 6×10^3 K. This is comparable to the mass of the halo when star formation begins found in other studies for the same LW background and

at similar redshift (O’Shea & Norman 2008). We note that this DM halo is approaching, but has not reached, virial equilibrium when the first star forms, having a gravitational potential energy of $\sim 1.2 \times 10^{52}$ erg and a kinetic energy of $\sim 1.1 \times 10^{52}$ erg.

The properties of the primordial gas just before the star forms are different from the canonical case of Pop III star formation in the absence of a LW background, as shown in Fig. 3.6. In the dense core of the halo, the H_2 abundance is $\leq 10^{-5}$, well below the canonical value of $\leq 10^{-3}$ at $n \sim 10^3 \text{ cm}^{-3}$, owing to the photodissociation of H_2 . In turn, the temperature of the gas in the core is ≥ 500 K, markedly higher than in the case without photodissociation, for which temperatures are generally ~ 200 K. We note that the central temperature that we find in the protostellar core is similar to what is found in the simulations of O’Shea & Norman (2008) for a comparable value of the LW background flux; however, these authors find a higher central H_2 fraction of $\geq 10^{-4}$, likely because they follow the collapse of the gas to higher densities, $n > 10^4 \text{ cm}^{-3}$, at which H_2 formation may be faster. The higher temperatures of the collapsing gas will likely translate into higher accretion rates onto the protostellar core than in the case without photodissociation (e.g. Omukai & Palla 2001, 2003; Bromm & Loeb 2004; O’Shea & Norman 2008), and so possibly into a higher final mass for the star. If the mass of the star is pushed above $\sim 260 M_\odot$, or if it remains below $\sim 140 M_\odot$, it may collapse directly to form a black hole at the end of its life without yielding a supernova explosion, thereby keeping its surroundings largely metal-free (e.g. Fryer et

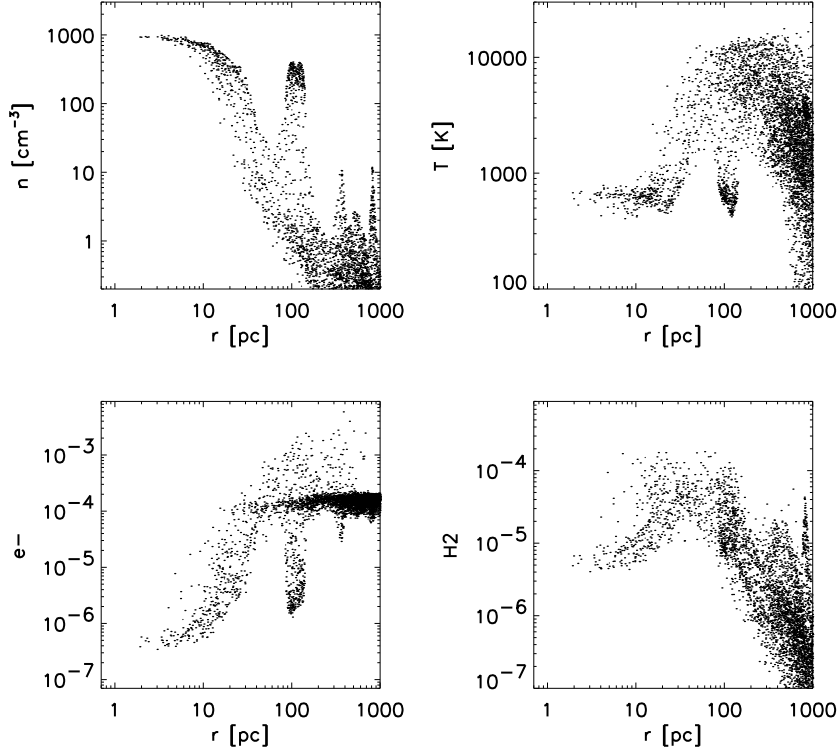


Figure 3.6: The properties of the primordial gas just before the formation of the first sink particle at $z = 16.3$, as a function of distance from the sink: density (top-left), temperature (top-right), free electron fraction f_{e^-} (bottom-left), and H_2 fraction f_{H_2} (bottom-right). Note the enhanced free electron fraction in regions heated by the virialization of the host halo. Also, note that a second star later forms at 100 pc from the first in this halo, the second halo having collapsed to densities above $n \sim 500 \text{ cm}^{-3}$ when the first star forms, densities which yield the evolution of the gas in the second halo relatively impervious to the radiative feedback from the first star (Whalen et al. 2007; Susa & Umemura 2006; Ahn & Shapiro 2007). Finally, note that the H_2 fraction is considerably lower than the values generally found for collapsing minihaloes in calculations not including a LW background. This leads to a higher temperature of the dense gas in the core of the minihalo compared to the canonical case absent a LW background (e.g. Bromm et al. 2002). This may lead to a larger mass for the Pop III star that forms from this gas. For reference, the resolution length in our simulation is $\sim 3 \text{ pc}$ (physical).

al. 2001; Heger et al. 2003).

The mass of the DM halo hosting this star is roughly an order of magnitude below that required for the virial temperature of the halo to exceed the atomic-cooling threshold of $10^{3.9}$ K, and is likewise well below the mass that we expect for the first galaxies. However, star formation is still able to take place at this relatively early time, despite the effect of the global LW background. We conclude that it is likely that at least a single Pop III star forms by $z \sim 15$ in a DM minihalo which is the most massive progenitor of an atomic-cooling halo hosting a galaxy at $z \geq 10$. The impact that such a star may have on the formation of the galaxy clearly depends sensitively on the final mass of this star.

3.5.3 Local Stellar Feedback on Minihaloes

We find that there is a second star-forming minihalo merely ~ 100 pc from the site of the formation of the first star in our simulation, as can be seen in Fig. 3.6. Because of this proximity, we expect that any radiative, mechanical, or chemical feedback from the first star may dramatically impact the evolution of this neighbouring halo. Numerous recent studies have discussed these feedback effects in detail (e.g. Ciardi & Ferrara 2005), and we here draw on them to understand how this stellar feedback may impact the formation of a galaxy in the early Universe.

Regardless of whether the first star becomes a supernova or collapses directly to form a black hole, the neighbouring halo will be subject to the ion-

izing and molecule-dissociating flux from this star (e.g. Shapiro et al. 2004; Susa & Umemura 2006; Ahn & Shapiro 2007; Johnson et al. 2007; Yoshida et al. 2007; Whalen et al. 2007). As the neighbouring halo will have already collapsed to densities $\geq 500 \text{ cm}^{-3}$ by the time the first star forms, the radiation from the first star is not likely to delay the collapse of the second halo significantly, as at these densities the core of the halo will not be photoevaporated and the molecules in the dense core may only be weakly dissociated (e.g. Susa 2007; Whalen et al. 2007). Therefore, it appears that a second star will form in the neighbouring minihalo within $\leq 10 \text{ Myr}$ after the formation of the first star (see also Wise & Abel 2007a). If the first star collapses directly to form a black hole, the formation of the second star will thus not be significantly influenced by the first star.

The type of star that forms in the neighbouring halo is not entirely clear, however, if the first star becomes a supernova, owing to the mechanical and chemical feedback that this would entail. As shown in Greif et al. (2007), the velocity of the shock produced by a Pop III supernova at a distance of 100 pc from the progenitor is $v_{\text{sh}} \leq 100 \text{ km s}^{-1}$. A shock propagating at such velocities can strongly ionize the primordial gas (e.g. Shull & McKee 1979), thereby allowing the formation of a high fraction of molecules and enhancing the cooling properties of the gas (e.g. Shapiro & Kang 1987; Mackey et al. 2003; Salvaterra et al. 2004; Machida et al. 2005). In particular, high fractions of HD can be generated behind such strong shocks, allowing the post-shock gas to cool to the temperature of the cosmic microwave background (CMB)

and perhaps to form metal-free stars with masses of the order of $10 M_{\odot}$, so-called Pop III.2 stars. We note that for this type of Pop III.2 star formation to take place the pre-shock gas must be at sufficiently high densities, unlike in the supernova simulation of Greif et al. (2007), in which this mode of star formation did not occur in the low-density IGM (see also Bromm et al. 2003). However, the neighbouring minihalo in the present case is likely to be sufficiently dense to allow for star formation to take place in the post-shock gas. We thus conclude that the halo neighbouring the first star may host a Pop III.2 star, in the case that the first star explodes as a supernova.

The mode of star formation in the neighbouring minihalo may change from Pop III to Pop II, if metal-rich supernova ejecta from the first star can efficiently mix with the primordial gas in the dense core of the minihalo (e.g. Bromm et al. 2001; Santoro & Shull 2006; Schneider et al. 2006). We can estimate the efficiency of this mixing by applying the criterion for the operation of Kelvin-Helmholtz (KH) instabilities given by Murray et al. (1993) (see also Cen & Riquelme 2008; Wyithe & Cen 2007):

$$\frac{gDr}{2\pi v_{\text{sh}}^2} \leq 1, \quad (3.18)$$

where g is the gravitational acceleration at the outer radius of the dense core of the neighbouring minihalo, and D the density ratio of gas in the halo compared to the dense shell. For the dense core of the neighbouring minihalo, we have a mass of the order of $10^5 M_{\odot}$ and a radius of $r \simeq 30$ pc. We find $D \geq 500$ and $v_{\text{sh}} \leq 100$ km s $^{-1}$, using values for the density and velocity of the shocked gas

from Greif et al. (2007). The left-hand side of equation (3.18) is thus $\geq 10^{-1}$. Following the results of Cen & Riquelme (2008), this suggests that the dense gas in the core of the neighbouring minihalo will remain largely pristine and stable for many dynamical times, while the outskirts of the halo may become more mixed. It therefore appears unlikely that the neighbouring halo will give rise to Pop II stars, but will instead probably host Pop III star formation. This will have implications for the nature of the galaxy into which these minihaloes are finally incorporated.

3.5.4 Self-shielding and Molecule Formation

While minihaloes are, in general, optically thin to LW photons, the greater gas mass in a halo hosting the formation of a first galaxy can lead to a large column density of H_2 and so to self-shielding of the molecules in the central regions of the halo (e.g. Draine & Bertoldi 1996). Taking this into account, we would like to estimate the impact of the LW background on the molecule fraction in the central regions of a first galaxy. Assuming that H_2 formation takes place through the reaction sequence



we can estimate the formation rate of H_2 as the gas collapses to high density. In our simulation, we find that the electron fraction drops due to recombinations

approximately as

$$f_e \sim 10^{-4} \left(\frac{n_{\text{H}}}{10^2 \text{cm}^{-3}} \right)^{-2}, \quad (3.21)$$

where n_{H} is the number density of hydrogen nuclei in the gas. Following Bromm et al. (2002), this results in a formation rate of H_2 at densities $n_{\text{H}} \geq 10^2 \text{cm}^{-3}$ of

$$\left(\frac{df_{\text{H}_2}}{dt} \right)_{\text{form}} \sim k_{\text{H}-} n_{\text{H}} f_e \sim k_{\text{H}-} n_{\text{H}}^{-1}, \quad (3.22)$$

where $k_{\text{H}-} \sim 10^{-15} \text{cm}^3 \text{s}^{-1}$ is the rate coefficient for reaction (19).

We can next estimate the photodissociation rate of H_2 , including the effect of self-shielding, following Bromm & Loeb (2003a). Accordingly, we estimate the column density of H_2 , using only local quantities, as $N_{\text{H}_2} \sim 0.1 f_{\text{H}_2} n_{\text{H}} L_{\text{char}}$, where the local characteristic length is given by

$$L_{\text{char}} = \left(\frac{3XM_{\text{b}}}{4\pi m_{\text{H}} n_{\text{H}}} \right)^{1/3}. \quad (3.23)$$

Here $M_{\text{b}} \sim 10^7 M_{\odot}$ is the total baryonic mass in the halo, $X = 0.76$ is the mass fraction of hydrogen, and m_{H} is the mass of the hydrogen nucleus. From our simulation of the formation of a first galaxy, which does not include the effects of self-shielding, we find a minimum average molecule fraction of $f_{\text{H}_2} \sim 10^{-5}$ at densities $n_{\text{H}} \geq 10^2 \text{cm}^{-3}$, as shown in Fig. 3.6, when $J_{\text{LW}} = J_{\text{LW,crit}}$. The photodissociation rate will be reduced due to self-shielding by a fraction

$$f_{\text{sh}} \sim \left(\frac{N_{\text{H}_2}}{10^{14} \text{cm}^{-2}} \right)^{-\frac{3}{4}} \quad (3.24)$$

when $N_{\text{H}_2} > 10^{14} \text{ cm}^{-2}$ (Draine & Bertoldi 1996). We thus find a minimum photodissociation rate of

$$\left(\frac{df_{\text{H}_2}}{dt} \right)_{\text{diss}} \sim 3 \times 10^{-17} n_{\text{H}}^{-1/2} f_{\text{H}_2}^{1/4} J_{\text{LW}} . \quad (3.25)$$

Balancing the formation rate and dissociation rates for H_2 , given by equations (3.22) and (3.25), respectively, we can solve for the density at which the dissociation rate becomes higher than the formation rate, marking the point in the collapse of the gas where H_2 dissociation begins to substantially suppress the formation of H_2 . We find this density to be

$$n_{\text{diss}} \sim 10^8 \text{cm}^{-3} \left(\frac{J_{\text{LW}}}{0.04} \right)^{-2} \left(\frac{f_{\text{H}_2}}{10^{-5}} \right)^{-1/2} . \quad (3.26)$$

For the values of $J_{\text{LW}} = 0.04$ and $f_{\text{H}_2} \sim 10^{-5}$ in our simulation, we thus find that H_2 photodissociation becomes important only at very high densities. At densities below n_{diss} , the formation rate of H_2 is higher than the photodissociation rate, owing to the higher abundance of free electrons, which catalyze the formation of H_2 according to equations (3.19) and (3.20). As the density increases, the recombination of free electrons deprives the gas of this catalyst, and the formation rate of H_2 molecules thus drops, becoming comparable to the photodissociation rate when the gas has collapsed to a density n_{diss} . We note that photodissociation may not become important at all in the evolution

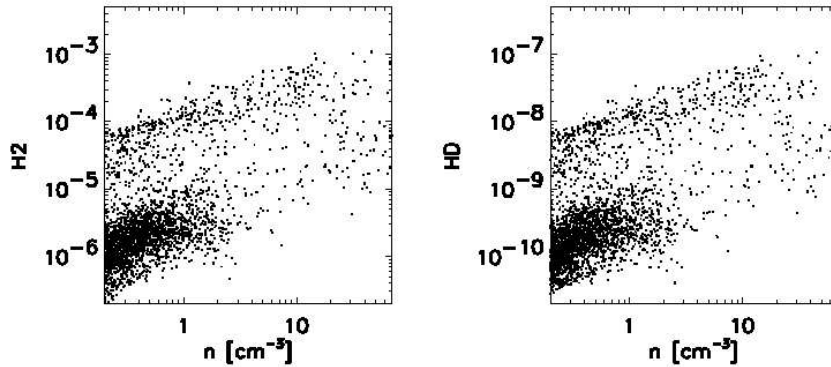


Figure 3.7: The fraction of molecules in the primordial gas of the protogalaxy at $z \sim 12.5$, as functions of density: H_2 fraction f_{H_2} (left), and HD fraction f_{HD} (right). The free electron fraction greatly exceeds the primordial value of $f_{e^-} \sim 10^{-4}$ through collisional ionization in virialization shocks, leading to enhanced fractions of both H_2 and HD, despite the presence of the LW background radiation field. Accounting for self-shielding, the molecule fraction remains elevated at high densities $n \geq 10^2 \text{ cm}^{-3}$. In the core of the halo, the HD fraction is thus expected to reach values large enough to allow the formation of Pop III.2 stars (see Greif et al. 2008).

of the gas, if $n_{\text{diss}} \geq 10^8 \text{ cm}^{-3}$, at which densities three-body reactions can efficiently produce H_2 (see e.g. Glover 2005). Furthermore, the photodissociation of H_2 is not likely to affect the evolution of the gas for cases in which the photodissociation timescale is longer than the free-fall timescale, as the gas may then cool and collapse to form a star before a significant portion of the H_2 molecules are photodissociated.

Along with the likely elevated fraction of H_2 , owing to ionization of the gas in the virialization of the galaxy, Fig. 3.7 shows that a high fraction of HD is also generated. We expect that, due to the substantial self-shielding of the

gas in the central regions of the assembling galaxy, the high HD fraction will persist in the gas as it collapses to high density, likely leading to the formation of Pop III.2 stars (see Greif et al. 2008).

3.6 Implications for the Assembly of the First Galaxies

In the preceding sections we have found that, owing in part to the self-regulation of the LW background, the Pop III star formation rate in minihaloes in the early Universe remains substantial at redshifts $z \geq 15$. In particular, we have found that the LW background is likely too weak to completely suppress star formation in the progenitor DM minihaloes that merge to form the first galaxies at $z \geq 10$. Here we discuss various implications of these results for the nature of the first galaxies.

3.6.1 The Protogalactic Star Formation Rate

While, in principle, Pop III star formation can be suppressed in minihaloes by a global LW background, we have shown that with a simple model for the self-consistent build-up of the LW background Pop III star formation is likely to take place in the assembly of a galaxy at $z \geq 10$ (see Fig. 3.8). Noting that the LW background that we used in our simulation did not take into account the effect of the opacity to LW photons through relic H II regions in the early Universe (see Section 3.2.3), the negative feedback from the global LW background may be even weaker than we found in our simulation. This, in turn, implies that the number of Pop III stars forming in protogalaxies may be

higher than we find from our simulation. A total of two minihaloes collapsed to form Pop III stars in our simulation employing the self-regulated model for the build-up of the LW background, allowing us to conclude that of the order of a few Pop III stars are likely able to form during the assembly of a galaxy at high redshift.

Additionally, we have found that conditions are prime for the formation of Pop III.2 stars, owing to the high HD fraction that is generated in the virialization shocks in such systems. Because the Pop III.2 star formation mode in atomic-cooling haloes has not been studied with simulations to the same extent as the ‘classical’, minihalo (Pop III.1) case, it is not yet possible to predict the resulting star formation rate and efficiency (but see Greif & Bromm 2006). However, we expect that, with $10^7 M_{\odot}$ of gas collapsing into such a system, Pop III.2 stars may form in clusters, given that these stars are expected to have masses of the order of $10 M_{\odot}$, compared to the $100 M_{\odot}$ predicted for Pop III.1 stars formed in minihaloes. The stellar feedback is then expected to be less severe, possibly enabling cluster formation.

3.6.2 Supernova Feedback and Metallicity

Each of the two star-forming haloes in our simulation is located within ~ 100 pc of the center of the main progenitor of the protogalaxy, allowing each star to affect the inner region of the galaxy through either radiative output or by exploding as supernovae. We can estimate the degree of metal enrichment that may take place should each of these stars explode as pair-

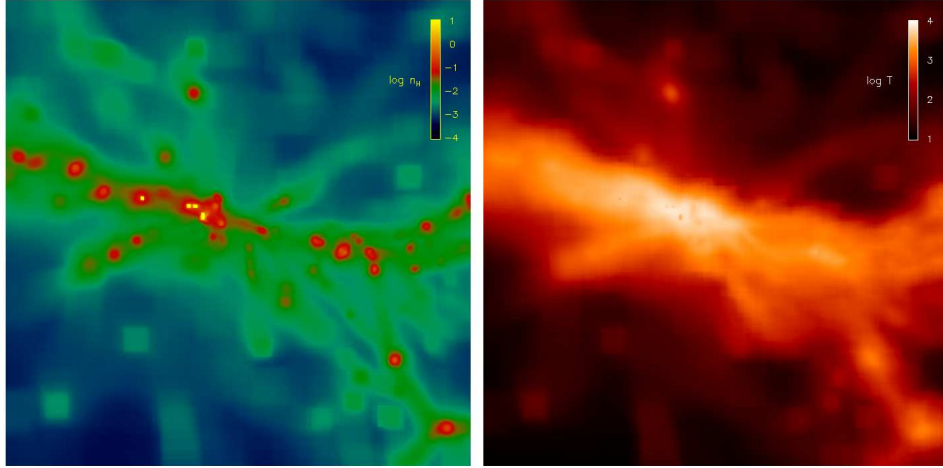


Figure 3.8: The hydrogen number density and temperature of the gas in the region of the forming galaxy at $z \sim 12.5$. The panels show the inner ~ 10.6 kpc (physical) of our cosmological box. The cluster of minihaloes harboring dense gas just left of the center in each panel is the site of the formation of the two Pop III stars which are able to form in our simulation including the effects of the self-regulated LW background. The remaining minihaloes are not able to form stars by this redshift, largely due to the photodissociation of the coolant H_2 . The main progenitor DM halo, which hosts the first star at $z \sim 16$, by $z \sim 12.5$ has accumulated a mass of $9 \times 10^7 M_\odot$ through mergers and accretion. Note that the gas in this halo has been heated to temperatures above 10^4 K, leading to a high free electron fraction and high molecule fractions in the collapsing gas (see Fig. 3.7). The high HD fraction that is generated likely leads to the formation of Pop III.2 stars in this system.

instability supernova (PISN), expected to be a common fate for massive Pop III stars (e.g. Heger et al. 2003), as follows. For a $10^8 M_\odot$ DM halo, we expect $\sim 10^7 M_\odot$ of gas to collapse into the virialized system. With $\sim 100 M_\odot$ in metals being expelled into the medium from two PISNe, we thus expect to have a mean metallicity in this system of $\sim 10^{-3} Z_\odot$.

Interestingly, this is above the value for the critical metallicity for Pop II star formation, $Z_{\text{crit}} \sim 10^{-3.5} Z_\odot$, as given by Bromm & Loeb (2003b) (see also Bromm et al. 2001a; Frebel et al. 2007; Smith & Sigurdsson 2007). This metallicity estimate assumes very efficient mixing of the metals with the virialized primordial gas. In reality, there will likely be pockets of less enriched gas in the galaxy, suggesting that in the first galaxies there may be regions in which Pop II star formation is enabled through metal cooling, as well as other, more pristine regions in which a top-heavy IMF persists (see Jimenez & Haiman 2006). Considering that the SFR may in fact be larger than what we found in our simulation, owing to weaker LW feedback, we expect that the mean metallicity in the first protogalaxies may easily exceed the critical metallicity necessary for low-mass Pop II star formation. If the mixing of these metals is efficient, the first galaxies may already host primarily Pop II star formation with a preponderance of low-mass stars, provided that the mass of the stars formed in these systems is not dictated instead by other effects, e.g. the inability of the gas to cool below the temperature of the CMB, $T_{\text{CMB}} = 2.7 \text{ K} (1 + z)$ (e.g. Larson 1998, 2005).

However, the details of the transition from a top-heavy Pop III IMF to

a low-mass Pop II IMF are not at present well understood, as it remains to understand the process by which the first metals, ejected into a hot expanding supernova remnant, are ultimately reincorporated into dense gas from which stars can form. The cooling time of the hot metal-rich ejecta from an energetic Pop III supernova is of the order of 10^8 yr (Greif et al. 2007). This is ample time for multiple Pop III stars to form from cold pockets of primordial gas and explode as supernovae, allowing to enrich the gas with the yields from multiple supernovae before it re-collapses to form the first Pop II stars. Such a mixing of SN yields would dilute any pure PISN signature from a single massive Pop III star, and may explain the lack of observed metal-poor stars exhibiting a clear PISN signature (see Karlsson et al. 2008). An additional complication might arise from the presence of cosmic rays (CRs) produced by the first supernovae. Heating and ionization due to CRs could have an important effect on the early star formation process (e.g. Jasche et al. 2007; Stacy & Bromm 2007), although these authors find that the main effect of cosmic rays is to enhance molecule formation in the central dense regions of minihaloes, which only strengthens our main conclusion that Pop III star formation in minihaloes is not easily suppressed during the assembly of the first galaxies.

3.6.3 Black Hole Formation

A fraction of the first stars likely collapsed directly to form black holes, thereby locking up the majority of the metals produced in their cores (see

e.g. Madau & Rees 2001; Fryer et al. 2001; Heger et al. 2003). In a given protogalactic system, there is thus a probability that the primordial gas will not be enriched by supernovae even if stars are able to form within this system. Without knowing the IMF of Pop III stars, however, we can only guess at what may be the fraction of Pop III stars which collapse to form black holes without ejecting appreciable amounts of metals. Heger et al. (2003) give the mass range for Pop III stars that collapse directly to black holes as ~ 40 to $\sim 140 M_{\odot}$ and $\geq 260 M_{\odot}$, while that over which a PISN takes place is given as ~ 140 to $\sim 260 M_{\odot}$, for stellar models which neglect the effects of rotation.

Given that Pop III stars formed in minihaloes are characterized by a top-heavy IMF with typical masses of the order of $100 M_{\odot}$, it seems reasonable to assume that the probability for a Pop III star to collapse directly into a black hole, and thus locking up its metal-rich core, is of the order of 0.5. We note that this is consistent with the constraints on the fraction of PISNe from Pop III stars reported by Karlsson et al. (2008). If we then take it that our simulation of the assembly of a $\sim 10^8 M_{\odot}$ galaxy is typical and use the fact that we find of the order of a few stars forming during this assembly process, we obtain a probability of the order of ≤ 0.1 that the first galaxy may be metal-free at the time of its formation. While this is only a rough estimate, the fact that we find little chance that star formation can be completely suppressed during the assembly of a galaxy at redshifts $z \geq 10$ suggests that metal-free galaxies are probably a minority population of the first galaxies, with a majority of galaxies already hosting some amount of Pop II star formation. We

emphasize, however, that Pop III star formation may continue to occur, even after the first supernovae, in regions of a galaxy which are not enriched with metals or in which the mixing of metal-rich supernova ejecta with primordial gas is inefficient.

Finally, as discussed in Section 3.5.2, given that the LW background can suppress H_2 cooling even in gas that does collapse to form Pop III stars, the high accretion rates in the formation of these objects may allow for a large fraction of such Pop III stars to have masses above $\sim 260 M_\odot$, allowing them to directly collapse into black holes and thus eject few metals. The LW background radiation may therefore act to keep galaxies metal-free even in cases where Pop III star formation is not prevented.

3.7 Summary and Conclusions

We have investigated the impact of the H_2 -dissociating LW background radiation on the formation of Pop III stars during the assembly of the first galaxies at $z \geq 12$. To this end, we have constructed simple models of the build-up of this radiation field which are self-consistent, accounting for the coupling of the star formation rate to the generation of the LW background. We have motivated and, to the extent possible, checked the self-consistency of a model in which the LW background does not exceed the critical value $J_{\text{LW,crit}} \sim 0.04$ at redshifts $z \geq 15$. Furthermore, we have elucidated the effect of a high opacity to LW photons through the first relic H II regions on the LW background, finding that the LW background flux may take values $\leq J_{\text{LW,crit}}$

at $15 \leq z \leq 18$, if the cosmological average optical depth to LW photons becomes sufficiently high. While our models are idealized, they are informed by detailed cosmological simulations of Pop III star formation and are consistent with previous results. We suggest that the actual LW background most likely assumes values intermediate between $J_{\text{LW,shield}}$ and $J_{\text{LW,crit}}$. However, detailed large scale simulations tracking star formation and accounting for the opacity of the IGM to LW photons will be required to better understand the true nature of the LW background at high redshifts. In addition, observations of the cosmic near-infrared background could conceivably be used to place conservative upper limits on the level of the LW background at high redshifts, as LW photons would be reprocessed into Ly α photons as they are redshifted with the expansion of the Universe, thus allowing them to contribute to the total Ly α flux emitted at high z that may be observed today (e.g. Santos, Bromm & Kamionkowski 2002; Fernandez & Komatsu 2006). Taking into account the LW background, we find that the comoving rate of Pop III star formation in minihaloes at $25 \geq z \geq 15$ is likely $\leq 10^{-4} \text{ M}_{\odot} \text{ yr}^{-1} \text{ Mpc}^{-3}$, with the upper limit corresponding to the case of a maximal opacity to LW photons through relic H II regions at these redshifts. Overall, we find that the global Pop III SFR is likely decreased from the maximum SFR rate possible by a factor of, at most, ~ 3 due to the LW background at $z \geq 15$.

We have simulated the assembly of a galaxy at $z \geq 12$, assuming the critical LW background in our self-regulated model of global Pop III star formation. We find that of the order of a few Pop III stars are likely to form

in the minihaloes that later merge to form the galaxy. Due to the chemical feedback that accompanies the explosions of Pop III stars as supernovae, possibly as PISNe, we conclude that most galaxies may already be enriched to a metallicity of the order of $\sim 10^{-3} Z_{\odot}$ when they are formed. If this is the case, then Pop II star formation may be widespread in these systems even at these early times. Alternatively, if the IMF of Pop III stars is such that a large fraction of them collapse directly to form black holes, thereby locking up the metals produced in their cores, then the interstellar medium of the first galaxies is more likely to remain metal-free. We find that a high fraction of the coolant HD is produced in the primordial gas during the virialization of the galaxy, despite the presence of the LW background, which likely leads to the formation of metal-free stars with masses of the order of $10 M_{\odot}$ in these systems. If metal-free galaxies do exist, they may therefore be dominated by such a population of stars, perhaps the first stellar clusters (see also Clark et al. 2008). More detailed simulations tracking the collapse and fragmentation of the gas, along with feedback from Pop III stars, will be necessary in order to test this scenario.

The character of star formation clearly becomes more complicated in the first galaxies compared to the canonical picture of Pop III star formation in minihaloes, with the chemical feedback from the first stars, turbulence driven by rapid mergers and accretion of gas from the IGM (see Wise & Abel 2007c; Greif et al. 2008), HD cooling, CR heating and possibly magnetic fields all playing important roles. Future missions, such as the *James Webb Space*

Telescope may thus be expected to observe some variety in the first galaxies. The majority is likely already enriched with heavy elements, hosting Pop II star formation, while a small fraction might still be largely metal-free, possibly hosting clusters of Pop III.2 stars. The veil is about to be lifted, giving us access to the time when galaxy formation first began.

Acknowledgments

We would like to thank Simon Glover for valuable comments that have improved the presentation of this work. VB acknowledges support from NSF grant AST-0708795 and NASA *Swift* grant NNX07AJ636. The simulations presented here were carried out at the Texas Advanced Computing Center (TACC).

Chapter 4

The First Galaxies: Signatures of the Initial Starburst

4.1 Introduction

The epoch of the first galaxies marked a fundamental transition in the Universe, ending the Cosmic Dark Ages, beginning the process of reionization, and witnessing the rapid proliferation of star formation and black hole growth (e.g. Barkana & Loeb 2001; Bromm & Larson 2004). While the theory of primordial star formation and early galaxy formation has rapidly developed (see Ciardi & Ferrara 2005; Glover 2005; Barkana & Loeb 2007), observations of the first galaxies at redshifts $z > 10$ have so far been out of reach (but see Stark et al. 2007). In the coming decade, the *James Webb Space Telescope* (JWST) promises to provide direct observations of this critical period in cosmic history, allowing to place new constraints on the stellar initial mass function (IMF) at high redshift, on the luminosity function of the first galaxies, and on the progress of the early stages of reionization (e.g. Barton et al. 2004; Gardner et al. 2006; Windhorst et al. 2006; Ricotti et al. 2008; Haiman 2008).

The IMF of the stellar populations which form in the first galaxies is of central importance in determining their properties and impact on early cosmic

evolution. The current theoretical consensus posits that the first stars, which formed in isolation in dark matter (DM) minihaloes, likely had masses of the order of $100 M_{\odot}$ (Bromm et al. 1999, 2002; Abel et al. 2002; Yoshida et al. 2006, 2008; McKee & Tan 2008). In the first galaxies, which form in DM haloes with masses $\sim 10^8 M_{\odot}$ (Greif et al. 2008; Wise et al. 2008), there is no such theoretical consensus on the IMF, as the initial conditions of the star-forming gas are uncertain (see Jappsen et al. 2009a,b). A large fraction of these first galaxies are likely to already host Population II (Pop II) star formation, due to previous metal enrichment (Johnson et al. 2008; see also Trenti & Stiavelli 2009; Clark et al. 2008). However, clusters of primordial stars likely form in some fraction of the first galaxies, owing to either inhomogeneities in the Lyman-Werner (LW) background which can suppress star formation where galaxies are strongly clustered (Dijkstra et al. 2008; see also Ahn et al. 2008) or to the direct collapse of the first stars to black holes, thereby locking up the metals produced in their cores (e.g. Heger et al. 2003).

Due to the hard spectra of massive metal-free stars, strong nebular emission in helium recombination lines has been suggested as an observable indicator of a population of such stars (e.g. Bromm et al. 2001; Oh et al. 2001; Tumlinson et al. 2001; Schaerer 2002). In particular, a high ratio of the luminosity emitted in He II $\lambda 1640$ to that emitted in Ly α or H α may be a signature of a galaxy hosting massive Pop III star formation, and has already served as the basis for searches for such galaxies (e.g. Dawson et al. 2004; Nagao et al. 2005, 2008). In addition, high equivalent widths (EWs) of Ly α

and He II $\lambda 1640$ are expected to characterize galaxies undergoing a Pop III starburst (e.g. Schaerer 2003). While no definitive detections of such galaxies have been achieved to date, observations of galaxies at $3 \lesssim z \lesssim 6.5$ with large Ly α EW and strong He II $\lambda 1640$ emission may indicate that some galaxies host Pop III star formation even at such relatively low redshift (see Jimenez & Haiman 2006; Dijkstra & Wyithe 2007).

Previous analytical calculations of the recombination radiation expected from the first galaxies have been carried out under a number of idealized assumptions, namely of a static, uniform density field, and of the formation of a static Strömgen sphere. Taking a complementary approach, we study here the properties of the recombination radiation emitted by the first galaxies with a focus on how the dynamical evolution of the galaxy affects the properties of this radiation. We present high-resolution cosmological radiation hydrodynamics simulations of the production of nebular emission from a cluster of primordial stars formed within the first galaxies. We resolve the H II and He III regions generated by the stellar cluster, thereby arriving at improved predictions for the emission properties of the first galaxies, which will be tested by the JWST.

Our paper is organized as follows. In Section 4.2, we describe our simulations and the methods used in their analysis; in Section 4.3 our results are presented, along with the implications for both IMF and star formation rate (SFR) indicators; in the final Section 4.4, we summarize and give our conclusions.

4.2 Methodology

We carry out radiation hydrodynamics simulations which track the impact of the radiation from Pop III stellar clusters forming promptly within a dwarf galaxy at $z \sim 12.5$. In this section we describe the simulations and the calculations carried out in analyzing their outcomes.

4.2.1 The simulations

As with previous work, for our three-dimensional numerical simulations we employ the parallel version of GADGET (version 1), which includes a tree (hierarchical) gravity solver combined with the smoothed particle hydrodynamics (SPH) method for tracking the evolution of gas (Springel et al. 2001; Springel & Hernquist 2002). Along with H_2 , H_2^+ , H , H^- , H^+ , e^- , He , He^+ , and He^{++} , we have included the five deuterium species D , D^+ , D^- , HD and HD^+ , using the same chemical network as in Johnson & Bromm (2006, 2007).

For our simulation of the assembly of a dwarf galaxy at $z \sim 12.5$, we have employed multi-grid initial conditions which offer higher resolution in the region where the galaxy forms (e.g. Kawata & Gibson 2003). We initialize the simulation according to the Λ CDM power spectrum at $z = 100$, adopting the cosmological parameters $\Omega_m = 1 - \Omega_\Lambda = 0.3$, $\Omega_B = 0.045$, $h = 0.7$, and $\sigma_8 = 0.9$, close to the values measured by the *Wilkinson Microwave Anisotropy Probe* in its first year (Spergel et al. 2003). Here we use a periodic box with a comoving size $L = 1 h^{-1}$ Mpc for the parent grid. Our simulations use $N_{\text{DM}} = N_{\text{SPH}} = 1.05 \times 10^6$ particles for DM and gas, where the SPH particle mass is

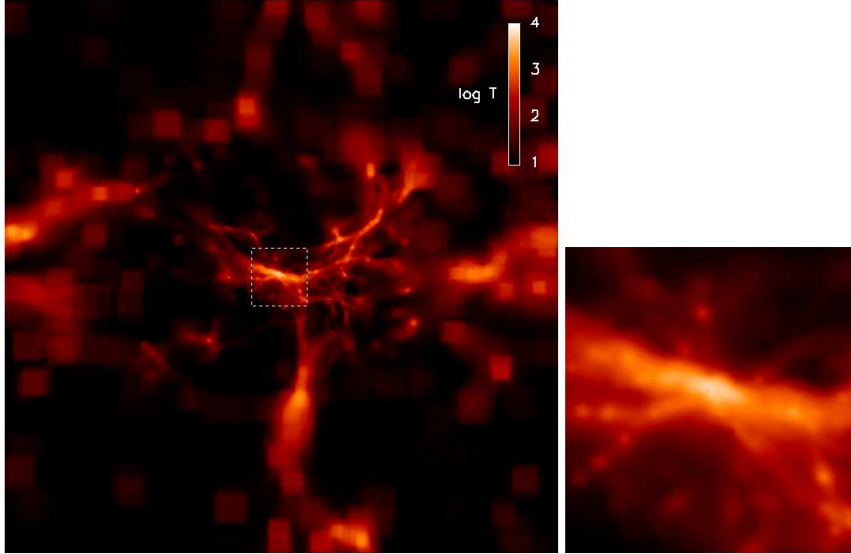


Figure 4.1: The projected gas temperature at $z = 12.7$, just before the stellar cluster turns on. Shown at left is the entire 1.4 Mpc (comoving) simulation box. The region of highest resolution is in the center of our multi-grid simulation box; magnified at right is the central ~ 10 kpc (physical), where the $\sim 10^8 M_\odot$ dark matter halo hosting the stellar cluster is located. Note that the gas is heated to $\geq 10^4$ K when passing through the virialization shock.

$m_{\text{SPH}} \sim 120 M_\odot$ in the region with the highest resolution. For further details on the technique employed to generate our multi-grid initial conditions, see Greif et al. (2008). The maximum gas density that we resolve is $n_{\text{res}} \sim 10^3 \text{ cm}^{-3}$, while gas at higher densities is accreted onto sink particles, as described in Johnson et al. (2007). We have also included the effect of a LW background radiation field, at a level of $J_{\text{LW}} = 0.04 \times 10^{-21} \text{ erg s}^{-1} \text{ cm}^{-2} \text{ Hz}^{-1} \text{ sr}^{-1}$, just as in Johnson et al. (2008).

To capture the effects of the ionizing radiation emitted by a single

Pop III stellar cluster within the dwarf galaxy, we approximate the cluster as a point source located at the center of the most massive DM halo in our simulation box at $z = 12.7$. The projected gas temperature in the entire simulation box at this redshift is shown in Fig. 4.1 (left panel); the right panel shows the temperature in the region of the host halo at the center of the box, which has a virial mass of $9 \times 10^7 M_{\odot}$, characteristic of the first galaxies. At each timestep, we find the boundaries of both the H II and He III regions generated by the stellar cluster using a ray-tracing technique that improves our earlier implementation (Johnson et al. 2007).

The procedure used to calculate the Strömgren sphere around the stellar cluster for a given time-step Δt is similar to the ray-tracing scheme used in Johnson et al. (2007). We create a spherical grid centered at the location of the cluster, consisting of $\sim 1.2 \times 10^4$ rays and 1000 linearly spaced radial bins. We resolve the central kiloparsec around the source, roughly the virial radius of the host halo, with 250 radial bins, while the remaining 750 bins are linearly spaced out to ~ 20 kpc.

In a single, parallelized loop, the Cartesian coordinates of all particles are converted to spherical coordinates, such that their density and chemical abundances may be mapped to the bins corresponding to their radius, azimuth and zenith, denoted by r , θ and ϕ , respectively. To avoid missing dense clumps, particles contribute to bins independent of distance, but proportional to their density squared. Once this preliminary step is complete, it is straightforward to solve the ionization front equation along each ray:

$$n_n r_I^2 \frac{dr_I}{dt} = \frac{Q_{\text{ion}}}{4\pi} - \alpha_B \int_0^{r_I} n_e n_+ r^2 dr , \quad (4.1)$$

where r_I denotes the position of the ionization front, Q_{ion} the number of ionizing photons emitted per second by the stellar cluster, α_B the case B recombination coefficient, and n_n , n_e and n_+ the number densities of nonionized particles, electrons and ionized particles, respectively. The numbers of H I-, He I- and He II-ionizing photons are $Q_{\text{ion}} = N_* q_{\text{ion}}$, where N_* is the number of stars in the cluster (here we assume that all have the same mass) and q_{ion} is the number of ionizing photons emitted by a single star, given by

$$q_{\text{ion}} = \frac{\pi L_*}{\sigma T_{\text{eff}}^4} \int_{\nu_{\text{min}}}^{\infty} \frac{B_\nu}{h\nu} d\nu , \quad (4.2)$$

where σ is the Stefan-Boltzmann constant, ν_{min} denotes the minimum frequency corresponding to the ionization thresholds of H I, He I and He II, and we assume that massive Pop III stars emit a blackbody spectrum B_ν (in $\text{erg s}^{-1} \text{cm}^{-2} \text{Hz}^{-1} \text{sr}^{-1}$) with an effective temperature T_{eff} and a luminosity L_* (e.g. Schaerer 2002).

To obtain a discretization of the ionization front equation, we replace the integral on the right-hand side of equation (1) by a discrete sum:

$$\int_0^{r_I} n_e n_+ r^2 dr = \sum_i n_{e,i} n_{+,i} r_i^2 \Delta r , \quad (4.3)$$

where Δr is the radial extent of the individual bins. Similarly, the left-hand side of equation (4.1), which models the propagation of the ionization front

into neutral gas, is discretized by

$$n_n r_I^2 \frac{dr_I}{dt} = \frac{1}{\Delta t} \sum_i n_{n,i} r_i^2 \Delta r_i, \quad (4.4)$$

where Δt is the current time-step and the summation is over radial bins starting with the bin lying immediately outside of $r_{I,\text{old}}$, the position of the ionization front at the end of the previous time-step, and ending with the bin lying at the new position of the ionization front. We perform the above steps separately for the H II and He III regions, since they require distinct heating and ionization rates.

We have chosen the size of the bins that are used in our ray-tracing routine to roughly match the volume of gas represented by a single SPH particle within the ~ 1 kpc virial radius of the halo hosting the stellar cluster, such that the boundaries of the photoionized regions are maximally resolved while also reliably conserving ionizing photons. However, in some cases it may occur that the mass contained in a bin is smaller than that of the SPH particle contained within it, such that ionizing the entire SPH particle involves ionizing more gas than is contained in the bin. In turn, this can lead to an overestimate of the number of recombinations. While this effect is minor in our simulations, in the calculations presented below we enforce that the total number of recombinations does not exceed the total number of ionizing photons available.

We carry out four simulations, each with a different combination of IMF and total cluster mass. For the IMF, we assume for simplicity, and in light

of the still complete uncertainty regarding its detailed shape, that the cluster consists either entirely of $25 M_{\odot}$ or $100 M_{\odot}$ Pop III stars. These choices are meant to bracket the expected characteristic mass for Pop III stars formed in the first galaxies, which depending on the cooling properties of the gas may be Pop III.2 stars with masses of order $10 M_{\odot}$ or, possibly, Pop III.1 stars with masses perhaps an order of magnitude higher (Johnson & Bromm 2006; Greif et al. 2008; McKee & Tan 2008; but see Jappsen et al. 2009a). For each of these IMFs, we vary the total stellar mass in the cluster, choosing either $2.5 \times 10^3 M_{\odot}$ or $2.5 \times 10^4 M_{\odot}$ for the total mass in stars. These choices correspond to ~ 1 and ~ 10 percent, respectively, of the cold gas available for star formation within the central few parsecs of such a primordial dwarf galaxy (see Wise et al. 2008; Regan & Haehnelt 2009). We calculate the ionizing flux from each of these clusters, assuming blackbody stellar spectra at 7×10^4 and 10^5 K and bolometric luminosities of 6×10^4 and $10^6 L_{\odot}$, for the 25 and $100 M_{\odot}$ stars, respectively, appropriate for metal-free stars on the main sequence (Marigo et al. 2001).

For simplicity, we have chosen to keep the input stellar spectra constant in time over the course of the simulations. Accordingly, we run the simulations only for 3 Myr, which is roughly the hydrogen-burning timescale of a $100 M_{\odot}$ primordial star, and about half that of a $25 M_{\odot}$ primordial star. We note that while the H I-ionizing flux from $100 M_{\odot}$ primordial stars is roughly constant over this timescale, the He II-ionizing flux decreases by a factor of ~ 2 by a stellar age of 2 Myr, and by a much larger factor near the end of

hydrogen-burning as the star evolves to the red (e.g. Marigo et al. 2001; Schaerer 2002). We note, however, that stellar models accounting for the effects of rotation yield less precipitous drops in the emitted ionizing flux with time, as fast rotation, especially of low-metallicity stars, can keep the stars on bluer evolutionary tracks (e.g. Yoon & Langer 2005; Woosley & Heger 2006; Vázquez et al. 2007); indeed, Pop III stars may have been fast rotators (see Chiappini et al. 2008). Nonetheless, the results that we derive pertaining to He II recombination emission from clusters of $100 M_{\odot}$ stars may be, strictly speaking, only reliable for stellar ages $\lesssim 2$ Myr. An in-depth study of the impact that stellar evolution has on the emission properties of primordial galaxies is given in Schaerer (2002); in the present work, we take a complementary approach and instead focus on how the emission properties are affected by the hydrodynamic evolution of the gas in the first galaxies.

We make the related simplifying assumption that the stellar cluster forms instantaneously. This is valid if the timescale for star formation t_{SF} is much shorter than the lifetime of the stars that we consider, or $t_{\text{SF}} \ll 3$ Myr. If we assume that stars form on the order of the free-fall time t_{ff} , and take it that the star cluster forms within the central ~ 1 pc of the halo (see e.g. Wise et al. 2008; Regan & Haehnelt 2009), then we find $t_{\text{SF}} \sim 5 \times 10^5$ yr, for which our assumption is marginally valid. We note that more work is needed to accurately determine the star formation timescale in the first galaxies, as the works cited here neglect, in particular, the important effect of molecular cooling on the evolution of the primordial gas.

4.2.2 Deriving the observational signature

The simulations described above allow us to calculate the luminosities and equivalent widths of the recombination lines emitted from high-redshift dwarf galaxies during a primordial starburst. A related quantity we obtain is the escape fraction of ionizing photons from such a galaxy. Here we describe each of these calculations.

4.2.2.1 Escape fraction of ionizing photons

Photons which escape the host halo from which they are emitted proceed to reionize the intergalactic medium (IGM), where densities are generally very low, yielding long recombination times. Ionizing photons which do not escape the host halo are, however, available to ionize dense gas which recombines quickly, leading to appreciable emission in recombination lines. Therefore, the luminosity of a galaxy in recombination radiation is intimately related to the escape fraction of ionizing photons. The escape fraction of ionizing photons from the halo hosting the stellar cluster is given by subtracting the number of recombinations Q_{rec} per second within the virial radius from the total number of ionizing photons emitted by the cluster:

$$f_{\text{esc}} = (Q_{\text{ion}} - Q_{\text{rec}}) (Q_{\text{ion}})^{-1} , \quad (4.5)$$

again with $Q_{\text{ion}} = N_* q_{\text{ion}}$. This equation is valid under the assumption that within the host halo the number of ionizing photons which fail to escape is balanced by the number of recombinations within the halo. This is a reasonable

assumption, since the number of atoms which become ionized within the host halo is far less than the total number of recombinations that occur in the halo, the ionization of previously neutral gas being the only other sink for ionizing photons within the halo. The number of recombinations is given as

$$Q_{\text{rec}} = \sum_i \alpha_{\text{B}} \frac{m_i}{\rho_i} \left[\frac{\rho_i}{\mu_i m_{\text{H}}} \right]^2 f_e f_{\text{HII}} , \quad (4.6)$$

where α_{B} is the case B recombination coefficient for hydrogen, m_{H} the mass of a hydrogen atom, while m_i , μ_i and ρ_i are the total mass, mean molecular weight, and mass density of the i th SPH particle, respectively. For each SPH particle, f_{HII} and f_e denote the fraction of nuclei in H II and the fraction of free electrons, respectively.

Here the summation is over all SPH particles within the virial radius of the host halo, or within a physical distance of ~ 1 kpc from the central stellar cluster. We calculate the escape fractions of both H I-ionizing and He II-ionizing photons. These quantities are generally not equal, and they each contribute to determining the radiative signature of the initial starbursts in the first galaxies.

4.2.2.2 Luminosity in recombination lines

For each of our simulations, we compute the luminosity emitted from photoionized regions in each of three recombination lines: H α , Ly α , and He II $\lambda 1640$. These luminosities are calculated by again summing up the contributions from all SPH particles within the virial radius, where virtually all of the

recombination line luminosity emerges, as follows:

$$L_{\text{H}\alpha} = \sum_{\text{i}} j_{\text{H}\alpha} \frac{m_{\text{i}}}{\rho_{\text{i}}} \left[\frac{\rho_{\text{i}}}{\mu_{\text{i}} m_{\text{H}}} \right]^2 f_{\text{e}} f_{\text{HeIII}} , \quad (4.7)$$

$$L_{\text{Ly}\alpha} = \sum_{\text{i}} j_{\text{Ly}\alpha} \frac{m_{\text{i}}}{\rho_{\text{i}}} \left[\frac{\rho_{\text{i}}}{\mu_{\text{i}} m_{\text{H}}} \right]^2 f_{\text{e}} f_{\text{HeIII}} \quad (4.8)$$

$$L_{\lambda 1640} = \sum_{\text{i}} j_{\lambda 1640} \frac{m_{\text{i}}}{\rho_{\text{i}}} \left[\frac{\rho_{\text{i}}}{\mu_{\text{i}} m_{\text{H}}} \right]^2 f_{\text{e}} f_{\text{HeIII}} , \quad (4.9)$$

where the j are the temperature-dependent emission coefficients for the lines (Osterbrock & Ferland 2006), and f_{HeIII} is the fraction of helium nuclei in He III for each SPH particle.

Given the luminosity in a recombination line over an area of the sky, we may compute the flux in that line, as observed at $z = 0$ with a spectral resolution $R = \lambda/\Delta\lambda$, where λ is the wavelength at which the emission line is observed (e.g. Oh et al. 2001). While Ly α photons are scattered out of the line of sight in the IGM prior to reionization (Loeb & Rybicki 1999), a process which we do treat in the present calculations, H α and He II $\lambda 1640$ photons will not suffer such severe attenuation. Assuming that the line is unresolved, the monochromatic flux in H α , for example, is

$$\begin{aligned} f_{\text{H}\alpha} &= \frac{l_{\text{H}\alpha} \lambda_{\text{H}\alpha} (1+z) R}{4\pi c D_{\text{L}}^2(z)} \\ &\sim 20 \text{ nJy} \left(\frac{l_{\text{H}\alpha}}{10^{40} \text{ erg s}^{-1}} \right) \left(\frac{1+z}{10} \right)^{-1} \left(\frac{R}{1000} \right) , \end{aligned} \quad (4.10)$$

where $l_{\text{H}\alpha}$ is the luminosity in H α along the line of sight through the emitting galaxy, $D_{\text{L}}(z)$ is the luminosity distance at redshift z ($\sim 10^2$ Gpc at $z = 10$), and $\lambda_{\text{H}\alpha}$ is the rest frame wavelength of the line, 656.3 nm. If the galaxy is spatially unresolved, appearing as a point source, we may simply substitute $L_{\text{H}\alpha}$ for $l_{\text{H}\alpha}$ in equation (4.10), to compute the total flux from the galaxy. In terms of total (integrated) line flux, we have the equivalent expression:

$$F_{\text{H}\alpha} = \frac{L_{\text{H}\alpha}}{4\pi D_{\text{L}}^2(z)} \\ \sim 10^{-20} \text{erg s}^{-1} \text{cm}^{-2} \left(\frac{L_{\text{H}\alpha}}{10^{40} \text{erg s}^{-1}} \right) \left(\frac{1+z}{10} \right)^{-2}.$$

4.2.2.3 Recombination line equivalent widths

Another observable quantity obtained from our simulations is the rest-frame equivalent width (EW) of recombination lines. We calculate the EWs of the three recombination lines considered, following Schaerer (2002):

$$W_{\text{H}\alpha}^0 = \frac{L_{\text{H}\alpha}}{L_{\lambda, \text{neb}} + L_{\lambda, *}} \quad (4.11)$$

$$W_{\text{Ly}\alpha}^0 = \frac{L_{\text{Ly}\alpha}}{L_{\lambda, \text{neb}} + L_{\lambda, *}} \quad (4.12)$$

$$W_{\lambda 1640}^0 = \frac{L_{\lambda 1640}}{L_{\lambda, \text{neb}} + L_{\lambda, *}}, \quad (4.13)$$

where the monochromatic continuum luminosity, evaluated at the wavelength of the line, is the sum of the nebular emission $L_{\lambda,\text{neb}}$ and the stellar emission $L_{\lambda,*}$. The nebular continuum luminosity is given by

$$L_{\lambda,\text{neb}} = \frac{c}{\lambda^2} \frac{\gamma_{\text{tot}}}{\alpha_{\text{B}}} Q_{\text{rec}} , \quad (4.14)$$

where λ is the wavelength in question, and Q_{rec} is again the total number of recombinations per second in the halo. The continuous emission coefficient γ_{tot} accounts for free-free, free-bound, and two-photon continuum emission, as described in Schaerer (2002). The stellar continuum luminosity is calculated assuming a blackbody stellar spectrum and is given by

$$L_{\lambda,*} = \frac{N_*}{\lambda^5} \frac{8\pi^2 hc^2 R_*^2}{\exp(hc/\lambda k_{\text{B}} T_{\text{eff}}) - 1} , \quad (4.15)$$

where N_* is the number of stars in the cluster, T_{eff} is the effective surface temperature of a star, and R_* is the stellar radius.

4.3 Results and Implications

We next discuss the observable characteristics of primordial dwarf galaxies. In particular, we evaluate the utility of indicators for the SFR and the stellar IMF in such galaxies.

4.3.1 Evolution of gas inside the galaxy

With the ignition of a stellar cluster at the center of the host halo, the gas surrounding the cluster is photoheated, raising its pressure and leading to

its outward expansion. In turn, the overall recombination rate in the host halo drops, allowing the expansion of the H II region to continue for a constant rate of ionizing photon production. Fig. 4.2 shows the growth of the H II region and the concomitant expansion of the gas in the center of the host halo for the more massive $100 M_{\odot}$ cluster. The H II region breaks out of the host halo within the first ~ 1 Myr, and after 3 Myr it extends to ~ 7 physical kpc, only slightly larger than the size of the H II region created by a single massive Pop III star in a minihalo (e.g. Alvarez et al. 2006).

While the gas surrounding the formation sites of the first stars in minihaloes is easily photoevacuated by a single massive Pop III star (e.g. Kitayama et al. 2004; Whalen et al. 2004), the deeper gravitational potential well of the DM haloes hosting the first galaxies allows for the retention of gas even under intense photoheating; indeed, this is one criterion used to define the first galaxies (e.g. Read 2006; Johnson et al. 2008; Greif et al. 2008).

As shown in Fig. 4.3, a substantial portion of the gas in the galaxy, even within ~ 100 pc of the stellar cluster, remains neutral after 3 Myr. This gas is shielded from the ionizing radiation, causing the ionization front (I-front) to propagate outward anisotropically in the inhomogeneous cosmological density field (see also e.g. Shapiro et al. 2004; Abel et al. 2006; Alvarez et al. 2006). Even for the case of the highest ionizing flux, the fraction of ionized gas within the central ~ 100 pc is ~ 0.4 , leaving the majority of the high density gas neutral. While the photodissociating radiation from the initial stellar cluster will slow the collapse of this primordial gas (e.g. Susa & Umemura 2006; Ahn & Shapiro

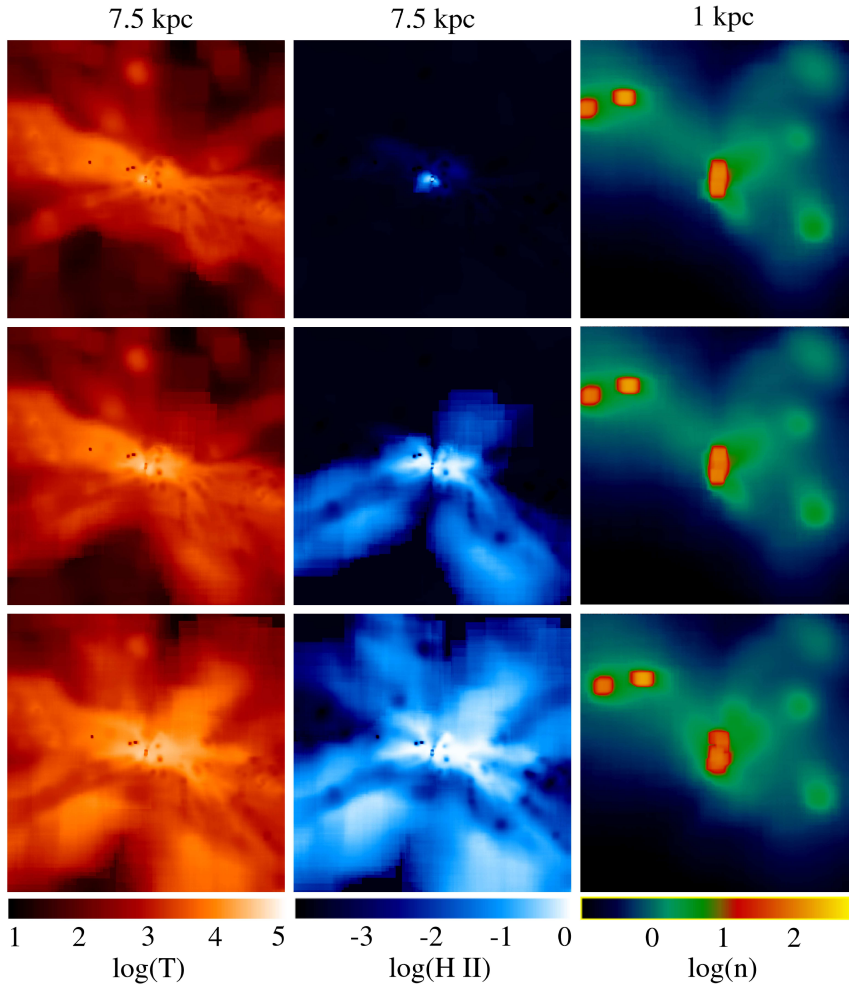


Figure 4.2: The density-weighted temperature (*left column*), density-weighted H II fraction (*middle column*), and number density (*right column*), each averaged along the line of sight, of the gas surrounding the more massive $100 M_{\odot}$ star cluster, shown at three different times from the prompt formation of the cluster: 500,000 yr (*top row*), 1 Myr (*middle row*), and 3 Myr (*bottom row*). The H II region grows as the density of the gas in the center of the host halo gradually drops in response to the intense photoheating. Note the different length scale of each column, given at the top in physical units; the density is shown only within the central region of the host halo.

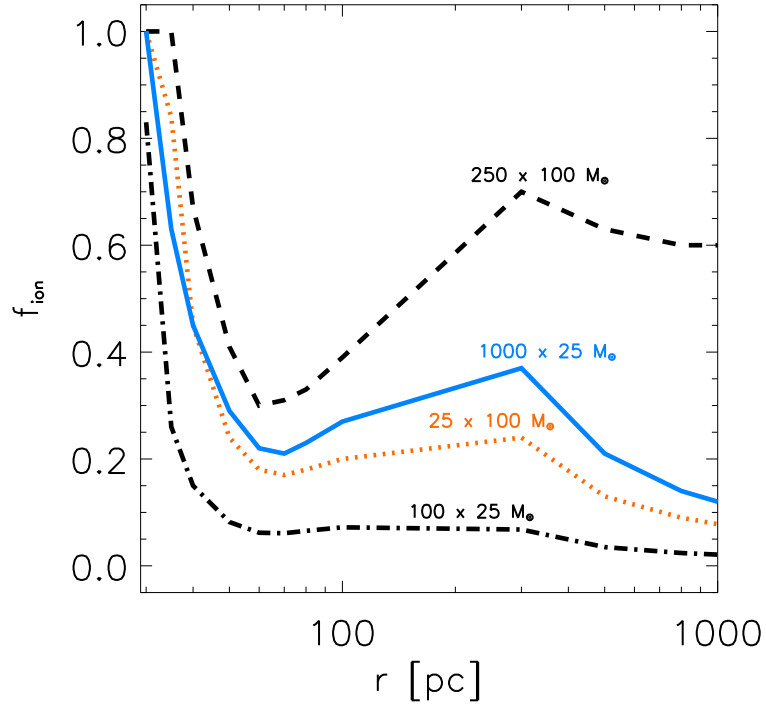


Figure 4.3: The mass fraction of enclosed gas which is photoionized, f_{ion} , as a function of the distance from the central star cluster, after 3 Myr of photoheating. Each line corresponds to a different choice of IMF and total mass in stars, as labeled. The ionized fraction begins to drop at ≥ 300 pc mostly due to two minihaloes at ~ 400 and ~ 500 pc, shown in Fig. 4.2 (right panels), which remain shielded from the ionizing radiation and are thus largely neutral. Within ~ 100 pc, there is a large fraction of gas which remains un-ionized at densities $\geq 100 \text{ cm}^{-3}$. This gas will likely collapse to form stars, despite the strong radiative feedback from the central stellar cluster.

2007; Whalen et al. 2008), some fraction of it will likely be converted into stars once the most massive stars in the cluster have died out. Indeed, the shocks engendered by the supernovae that mark the end of their lives may expedite the collapse of the gas (e.g. Mackey et al. 2003; Salvaterra et al. 2004; Machida et al. 2005; Greif et al. 2007; Sakuma & Susa 2009). The incomplete ionization of the central gas confirms that the masses that we have chosen for the clusters are not overly large, as there is still some neutral gas available for subsequent star formation regardless of the radiative feedback.

The gas that is photoionized, however, is gradually expelled from the center of the halo, and after 3 Myr of photoheating the density of the photoionized gas within ~ 20 pc of the cluster drops to 10 cm^{-3} for the more massive cluster of $100 M_{\odot}$ stars shown in Fig. 4.2. For our other choices of IMF and total cluster mass the dynamical response is less dramatic, as the ionizing flux is weaker; for example, after 3 Myr the density of the central photoionized gas is 50 cm^{-3} for the less massive cluster of $25 M_{\odot}$ stars. The varying degree to which photoheating dynamically impacts the host halo leads to important differences in the properties of the emitted radiation.

Although the limited resolution of our simulations allows only to track the expansion of the H II region from an initial physical size of 10 pc, we expect that after roughly a sound-crossing time of the central unresolved ~ 10 pc, or after the first few 10^5 yr, the evolution of the H II region is reliably resolved. It should thus be noted that the breakout of the H II region may be delayed by order this timescale compared to our simulations. We note that in the Milky

Way the expansion of the photoheated gas in an H II region may be slowed due to turbulent pressure confinement (e.g. Xie et al. 1996; Mac Low et al. 2007), resulting in ultra-compact H II regions persisting for 10^5 yr (Wood & Churchwell 1989), much longer than the sound-crossing timescale for such regions. As turbulence begins to play an important role in the formation of the first galaxies (Wise et al. 2008; Greif et al. 2008), the initial evolution of H II regions therein may be similarly confined. This possibility notwithstanding, we expect that the spatial resolution that we do achieve suffices to track changes in the luminosity emitted in recombination lines and in the escape fraction of ionizing radiation, which we discuss in the remainder of this Section.

4.3.2 Star formation rate indicators

The luminosity emitted in recombination lines, such as $H\alpha$, has been found to scale remarkably well with the SFR of galaxies at low redshift (e.g. Kennicutt 1983; but see Pflamm-Altenburg et al. 2007). The SFR obtained using such relations relies on some knowledge of the IMF of the stars which are forming, as well as on the escape fraction of ionizing radiation. Fig. 4.4 shows our calculations of the escape fraction f_{escHII} of H I-ionizing photons for each of our choices of IMF and total mass in stars, and Fig. 4.5 shows the escape fraction f_{escHeIII} of He II-ionizing photons. The corresponding luminosities emitted in $H\alpha$, $Ly\alpha$, and He II $\lambda 1640$ are presented in Fig. 4.6.

As shown in Fig. 4.4, there is a clear trend toward higher H I-ionizing photon escape fractions for more massive stellar clusters, with the majority

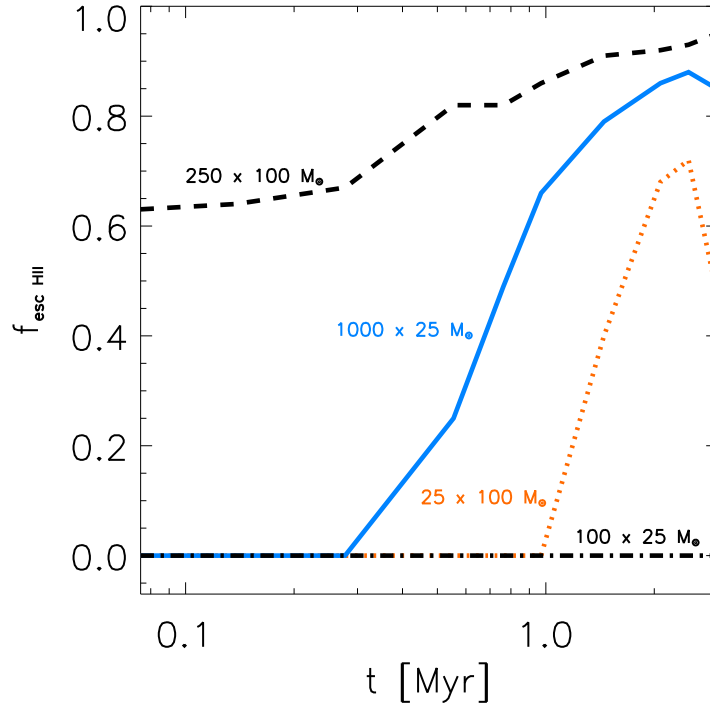


Figure 4.4: The escape fraction of hydrogen-ionizing photons, $f_{\text{esc HII}}$, from the host galaxy, each line corresponding to a different choice of IMF and total mass in stars, as labeled. Note the tight anticorrelation between the escape fraction plotted here and the luminosity in the hydrogen recombination lines shown in Fig. 4.6, demonstrating that the vast majority of the energy emitted in hydrogen recombination lines emanates from the dense ionized gas within the host halo, as is shown in detail in Fig. 4.10.

of the ionizing photons escaping from clusters with the larger total stellar mass. The escape fraction is not, however, independent of IMF; for a given total mass in stars, the escape fraction can differ by a wide margin. Both the variability in the escape fraction with time and the range of values that we find are in rough agreement with other recent calculations of the escape fraction of ionizing photons from dwarf galaxies at $z \sim 10$ (Wise & Cen 2009; Razoumov & Sommer-Larsen 2009). For a recent calculation of the escape fraction of ionizing photons from more massive galaxies, see Gnedin et al. (2008).

The breakout of the H II region generated by the less massive $100 M_{\odot}$ star cluster occurs after ~ 1 Myr, leading to an escape fraction ~ 0.5 after 2 Myr. In contrast, the H II region of the equally massive $25 M_{\odot}$ star cluster remains confined to the host halo for ≥ 3 Myr, contributing no ionizing photons to the IGM. The progress of the initial stages of hydrogen reionization, likely driven by star formation in the first galaxies (e.g. Loeb 2008), may thus depend on whether these galaxies hosted massive ($\sim 10 M_{\odot}$) or very massive stars ($\sim 100 M_{\odot}$) (see also Choudhury & Ferrara 2007).

The evolution of the H I-ionizing photon escape fraction is reflected in the evolution of the luminosity of hydrogen recombination lines, as shown in Fig. 4.6. Comparing the panels on the left to those on the right, the luminosity in the Ly α and H α lines, while generally higher for larger total mass in stars, does not scale with the total mass in stars. Indeed, owing to the increase in the escape fraction of ionizing photons, after ~ 1 Myr the luminosity in hydrogen recombination lines from the clusters with greater total

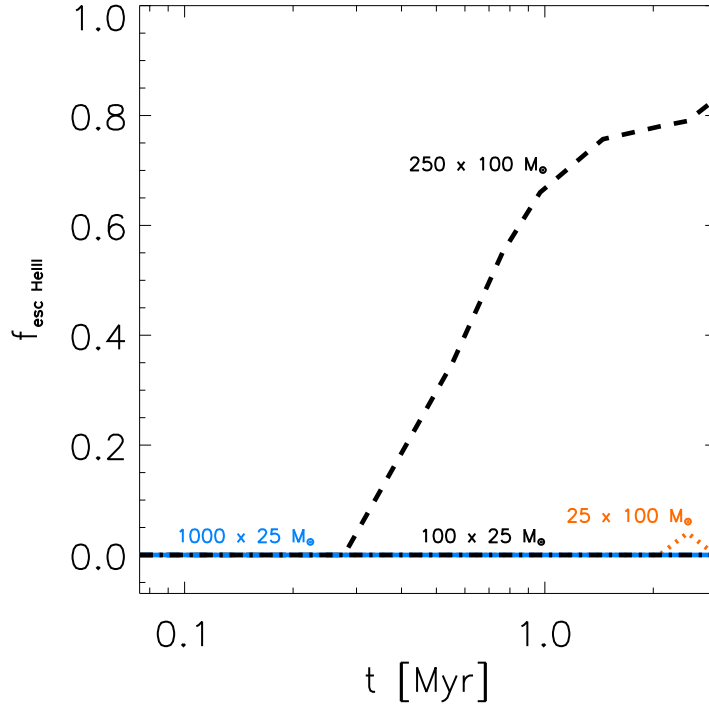


Figure 4.5: The escape fraction of He II-ionizing photons, f_{escHeIII} , from the host galaxy, each line labeled as in Fig. 4.4. For most cases, the negligible escape fraction leads to a tight correlation between the luminosity emitted in the He II $\lambda 1640$ line and the total mass contained in stars, in contrast to the weaker correlation for hydrogen recombination lines, as discussed in Section 4.3.2.

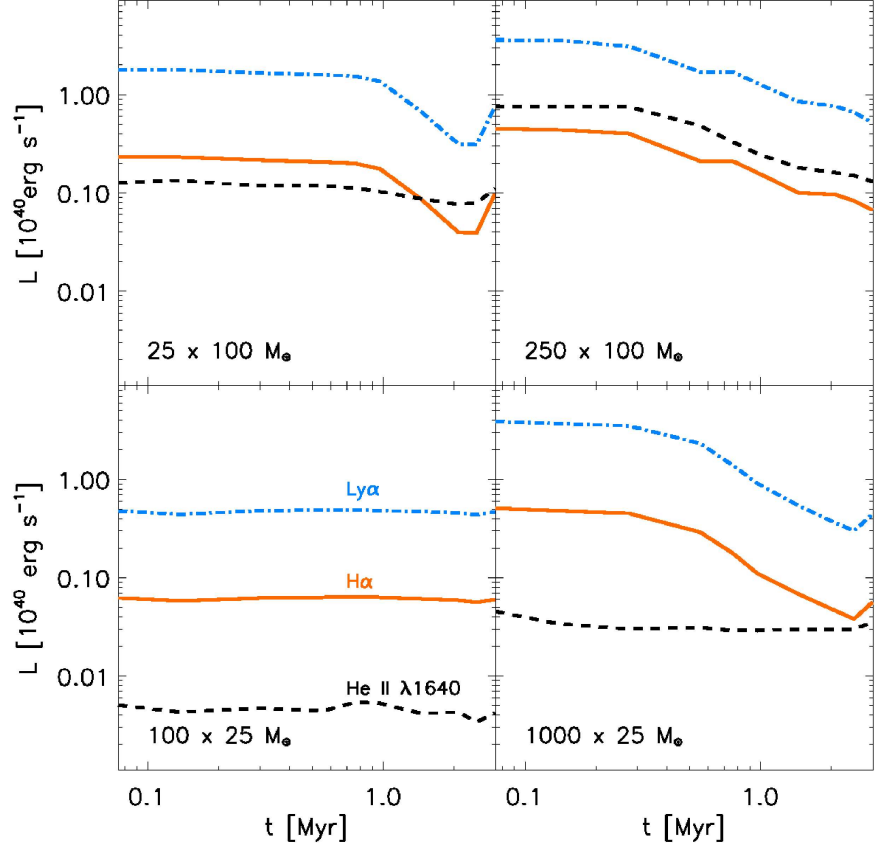


Figure 4.6: The luminosity of the galaxy, as a function of the time from the prompt formation of the cluster, in three recombination lines: $\text{Ly}\alpha$ (*dot-dashed blue*), $\text{H}\alpha$ (*solid red*), and $\text{He II } \lambda 1640$ (*dashed black*). The four panels correspond to our four different choices of IMF and total mass in stars; these are, clockwise from top-left: twenty-five $100 M_{\odot}$ stars, two hundred fifty $100 M_{\odot}$ stars, one thousand $25 M_{\odot}$ stars, and one hundred $25 M_{\odot}$ stars. The luminosities generally decrease with time, as the photoheating acts to decrease the density of the ionized gas, lowering the recombination rate. Note the different evolution of the $\text{He II } \lambda 1640$ luminosity as compared to that of the hydrogen recombination lines, owing to the lower escape fraction of He II -ionizing photons (see Fig. 4.5).

stellar mass drops below that of the clusters with lower total stellar mass, for a given IMF. Overall, because of the temporal evolution of the luminosity in a given line, there is no one-to-one relationship between the total mass in stars and the luminosity in a given recombination line. There is thus likely to be a relatively weak correlation between the SFR and the luminosity in the hydrogen recombination lines emitted from the first dwarf galaxies, owing to the dynamical evolution of the photoionized gas and the escape of ionizing radiation into the IGM.

Similar to the case of the hydrogen recombination lines, the luminosity in the He II $\lambda 1640$ line is anticorrelated with the escape fraction of He II-ionizing photons, shown in Fig. 4.5. However, different from the case of the hydrogen lines, the luminosity emitted in He II $\lambda 1640$ line is generally much more strongly correlated with the total mass in stars, for a given IMF. This is due to the low escape fraction of He II-ionizing photons, which is essentially zero for every case studied here, except for the case of the more massive cluster of $100 M_{\odot}$ stars. With such a high fraction of He II-ionizing photons being balanced by recombinations within the host halo, there is a near linear relation between the total mass in stars and the luminosity emitted in He II $\lambda 1640$, making this line a potentially much more reliable SFR indicator than hydrogen lines such as H α . There are slight departures from linearity due to the temperature dependence of the emission coefficient $j_{\lambda 1640}$, which varies by a factor of ~ 2 over the temperature range of the ionized gas in our simulations and is generally lower for the hotter H II regions generated by the

more massive stellar clusters (Osterbrock & Ferland 2006).

4.3.3 Initial mass function indicators

The luminosity emitted from a galaxy in recombination lines depends not only on the stellar IMF, but also on the density field of the galaxy and the escape fraction of ionizing photons. Therefore, the utility of recombination line strengths as IMF indicators hinges on an understanding of the dynamical evolution of the photoionized gas, especially for the case of starbursts in the first dwarf galaxies, in which such dynamical effects can be most pronounced.

For the starbursts that we simulate here, the luminosity of the He II $\lambda 1640$ emission line relative to the hydrogen recombination lines can be read from Fig. 4.6, while the equivalent widths of these lines are presented in Fig. 4.7. Comparing the top panels of Fig. 4.6 to the bottom panels, it is evident that the ratio of the luminosity emitted in He II $\lambda 1640$ to that in $H\alpha$ (or $Ly\alpha$) can be very different depending on the IMF. Fig. 4.7 shows that there is a similar distinction in the ratios of the EWs. For the $100 M_{\odot}$ star clusters the luminosity in He II $\lambda 1640$ is comparable to that in $H\alpha$, while for the $25 M_{\odot}$ star clusters the luminosity in He II $\lambda 1640$ is up to an order of magnitude lower than that in $H\alpha$. However, as the escape fraction of H I-ionizing photons increases with time for the more massive $25 M_{\odot}$ stellar cluster, the luminosities in these two lines become comparable, revealing that there is some ambiguity in the use of this ratio of line luminosities as an indicator of the IMF of young (~ 3 Myr) stellar clusters. Thus, in some cases dynamical effects may compromise

the use of this line ratio in distinguishing between clusters of Pop III.1 and Pop III.2 stars, with typical masses of order $100 M_{\odot}$ and $10 M_{\odot}$, respectively.

The ratio of the observed fluxes in He II $\lambda 1640$ and $H\alpha$, as calculated using equation (4.10), is displayed in Fig. 4.8. In this Figure, it is clear that this line ratio is sensitive to the IMF, although it is not a constant for each cluster. Instead, for clusters in which the escape fraction of H I-ionizing photons increases with time dramatically, while the escape fraction of He II-ionizing photons remains roughly constant, this line ratio varies with the flux observed in $H\alpha$. While the ratio of the fluxes is a somewhat ambiguous IMF indicator, the clusters with the more top-heavy IMF do consistently exhibit larger ratios of He II $\lambda 1640$ to $H\alpha$. Nagao et al. (2005) present a search for He II $\lambda 1640$ emission from a strong Ly α emitter at $z = 6.33$, finding an upper limit for the ratio of He II $\lambda 1640$ to Ly α . Assuming a standard value of 0.07 for the ratio of luminosity in $H\alpha$ to that in Ly α (Osterbrock & Ferland 2006), we show in Fig. 4.8 the upper limit that these authors report (see also Dawson et al. 2004). Although a weak upper limit, it is clear that observations with only slightly greater sensitivity will allow to differentiate between the flux ratios predicted here for massive and very massive Pop III IMFs.

Comparing the EW of $H\alpha$ in the four panels of Fig. 4.7, it is clear that it is not strongly dependent on the IMF or on the total mass in stars, varying by at most a factor of three between each of the cases. While showing more variation between the four cases, the EW of Ly α also shows considerable ambiguity as an IMF indicator, its maximum value varying by about a factor

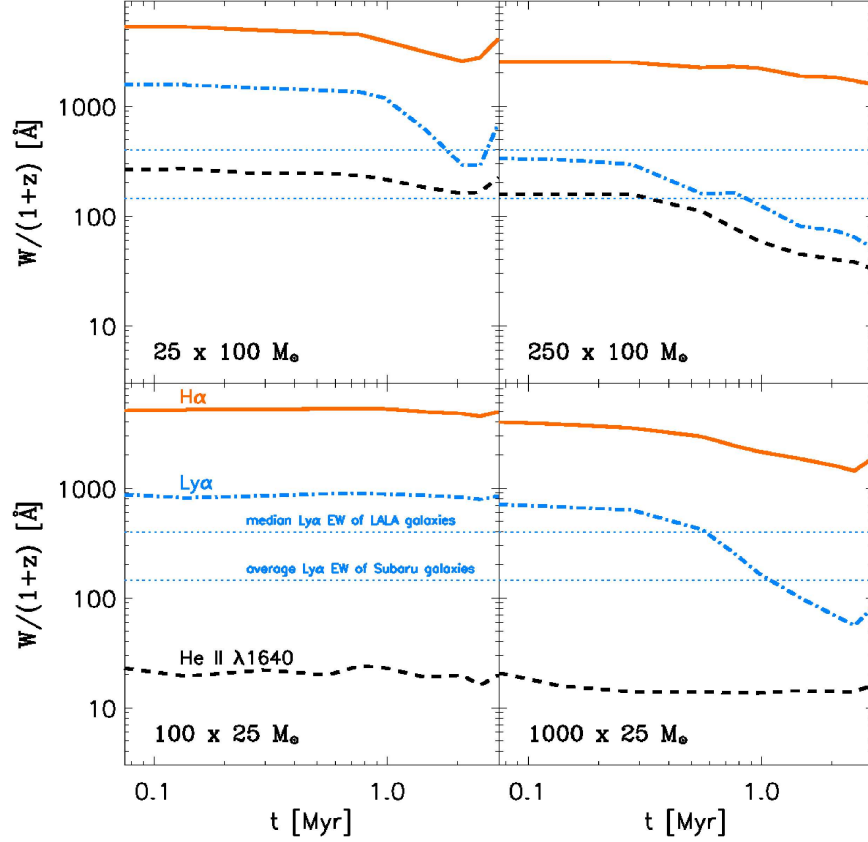


Figure 4.7: The rest frame equivalent widths, $W^0 = W / (1+z)$, where W is the observed EW, as a function of time, of the same three recombination lines shown in Fig. 4.6. For comparison, in each panel we plot the observed EWs of galaxies from two different surveys: the *dotted line* at 400 \AA denotes the median EW of $\text{Ly}\alpha$ emitters detected at $z = 4.5$ in the LALA survey (Malhotra & Rhoads 2002), while the *dotted line* at 145 \AA denotes the average EW of the six $\text{Ly}\alpha$ emitters at $z \geq 6$ detected in the Subaru deep field (Nagao et al. 2007). Note that the $\text{Ly}\alpha$ EWs that we compute are upper limits, as scattering in a neutral IGM has not been taken into account.

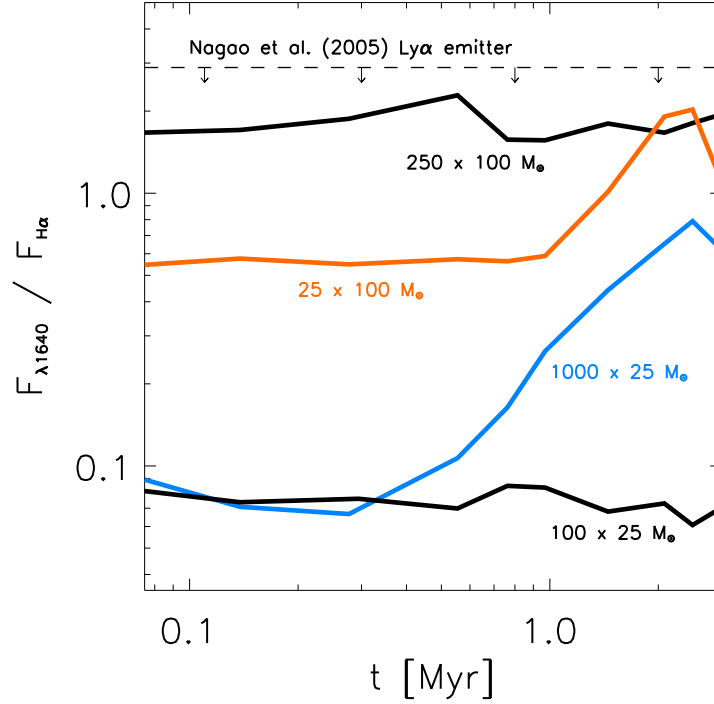


Figure 4.8: The ratio of the integrated fluxes in He II $\lambda 1640$ and H α , $F_{\lambda 1640}/F_{H\alpha}$, as a function of time, for each of the four clusters simulated here, as labeled. The dashed horizontal line denotes the upper limit of this ratio for the strong Ly α emitter SDF J132440.6+273607 at $z = 6.33$, as reported by Nagao et al. (2005). Similar upper limits for Ly α emitters at $z = 4.5$ have been reported by Dawson et al. 2004.

of three between each of the four cases. This insensitivity of the Ly α EW to the IMF arises from two effects. Firstly, the stellar continuum luminosity $L_{\lambda,*}$ increases in a similar manner as the number of ionizing photons from the massive ($25 M_{\odot}$) IMF to the very massive IMF ($100 M_{\odot}$). This acts to keep the EW, roughly the ratio of the two, relatively constant. Secondly, while the luminosity in Ly α decreases with the increasing escape fraction of ionizing photons for the more massive clusters, the continuum luminosity remains largely unchanged, leading to a decrease in the EW with time for these clusters. We note that the Ly α EWs presented here are only upper limits, as we have not accounted for scattering of Ly α photons in the IGM (see e.g. Dijkstra et al. 2007).

The EW of He II $\lambda 1640$ is a more definitive indicator of IMF, being higher for the clusters of $100 M_{\odot}$ stars than for the clusters of $25 M_{\odot}$ stars, regardless of the total mass in stars or of the age of the cluster (up to 3 Myr). As with the utility of He II $\lambda 1640$ as a SFR indicator, this largely follows from the generally low escape fraction of He II-ionizing photons.

For comparison with observed galaxies, we plot in Fig. 4.7 the two observational results: the median Ly α EW of galaxies detected in the Large Area Lyman Alpha (LALA) survey, $W^0 \sim 400\text{\AA}$, and the average EW of six galaxies observed at $z \geq 6$ in the Subaru deep field, $\sim 145\text{\AA}$ (Nagao et al. 2007). The large LALA EWs are comparable to what we find for primordial dwarf galaxies, although the LALA galaxies likely do not host Pop III star formation (but see Jimenez & Haiman 2006). The detection of an EW of

the He II $\lambda 1640$ line 10\AA would be a stronger indication of a galaxy hosting primordial star formation, as shown in Fig. 4.7, although none has been found as of yet. We note that observed Lyman break galaxies at $z \sim 3$ have been found to have He II $\lambda 1640$ EWs of $\sim 2\text{\AA}$ (Shapley et al. 2003), consistent with what is expected for Wolf-Rayet stars formed in starbursts (see Schaerer & Vacca 1998; Brinchmann et al. 2008).

4.3.4 Detectability of Recombination Radiation

In Fig. 4.9, we present our predictions for the observable recombination line fluxes, for each of the stellar clusters that we simulate. Fig. 4.10 shows the surface brightness in $H\alpha$ as observed on the sky, for the two more massive stellar clusters, which each have a total mass in stars of $2.5 \times 10^4 M_{\odot}$. The fluxes in each plot, largely determined by our choices for the total stellar mass, are calculated using equation (4.10). While the larger H II region generated by the more massive stars encompasses more dense gas, creating more widely distributed emission in $H\alpha$, as shown in Fig. 4.10, the highest flux per square arcsecond is in the central region of the halo hosting the less massive stars. This is due again to the less dramatic dynamical response of the gas to photoheating, leading to higher densities, and thus higher recombination rates. Due to this effect, the highest fluxes are generated just after the birth of a stellar cluster, as shown in Figure 4.9, when the density of the photoionized gas is still high, not having had time to expand in response to the concomitant heating. Indeed, Fig. 4.9 shows that the flux in $H\alpha$ from the more massive $25 M_{\odot}$ star cluster

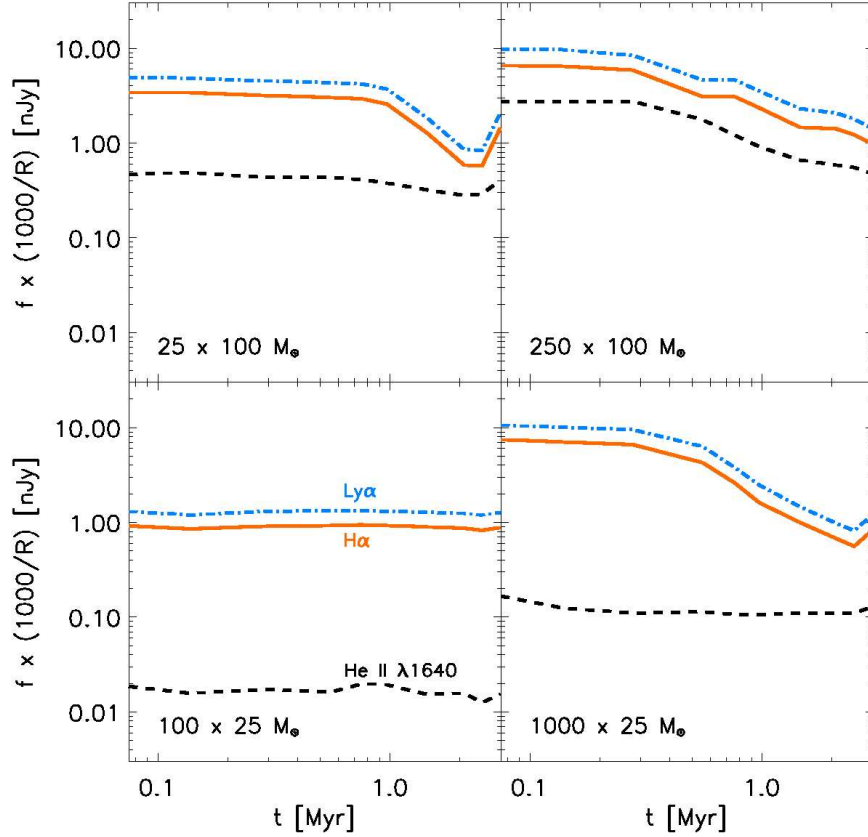


Figure 4.9: The observed fluxes, f , as a function of time, of the same three recombination lines shown in Fig. 4.6, for the galaxy we simulate at $z \sim 12.5$. The fluxes are normalized to what would be observed with a spectroscopic resolution of $R = 1000$, and are computed using equation (4.10) assuming that the galaxy appears as an unresolved point source. Note that the flux in $\text{Ly}\alpha$ is an upper limit, as the present calculation does not take into account scattering in a neutral IGM.

may reach $10 \times (R/1000)$ nJy before the breakout of the H II region. Catching the first galaxies when still in the earliest stages of their initial starbursts, within the first few 10^5 yr, is thus likely to provide one of the best chances for observations of purely primordial stellar populations in the early Universe.

Aboard the JWST, the H α line would be observed with the Mid-Infrared Instrument (MIRI). Its pixel size of 0.1 arcsec would not resolve the brightest portions of the galaxies that we simulate, which, as shown in Fig. 4.10, are of order 0.01 arcsec. With a resolution capability of $R = 3000$ the MIRI has a sensitivity of 200 nJy for a signal-to-noise of 10, in exposures of $\sim 10^6$ s (see Panagia 2004), making it unable to detect even the brightest galaxies that we simulate, the flux in H α of these being 20 nJy for $R = 3000$.

With a greater sensitivity of 100 nJy (Panagia 2004), the Near Infrared Spectrograph (NIRSpec) operates in the wavelength range 0.7 to 5 μm , allowing it to possibly detect Ly α out to $z \sim 40$ and He II $\lambda 1640$ out to $z \sim 30$. However, the flux in He II $\lambda 1640$ is always below that in H α and, hence, is too low to be detected. The Ly α line, with the highest flux of the three recombination lines shown in Fig. 4.9, is also not directly detectable, with a flux falling well below the ~ 100 nJy sensitivity limit of NIRSpec. Furthermore, although the luminosity in Ly α is always intrinsically higher than that in H α , before reionization the observable flux in Ly α may be dramatically decreased due to scattering in the neutral IGM (e.g. Dijkstra et al. 2007). Because we do not account for this effect in the present calculations, the Ly α fluxes presented here are only upper limits.

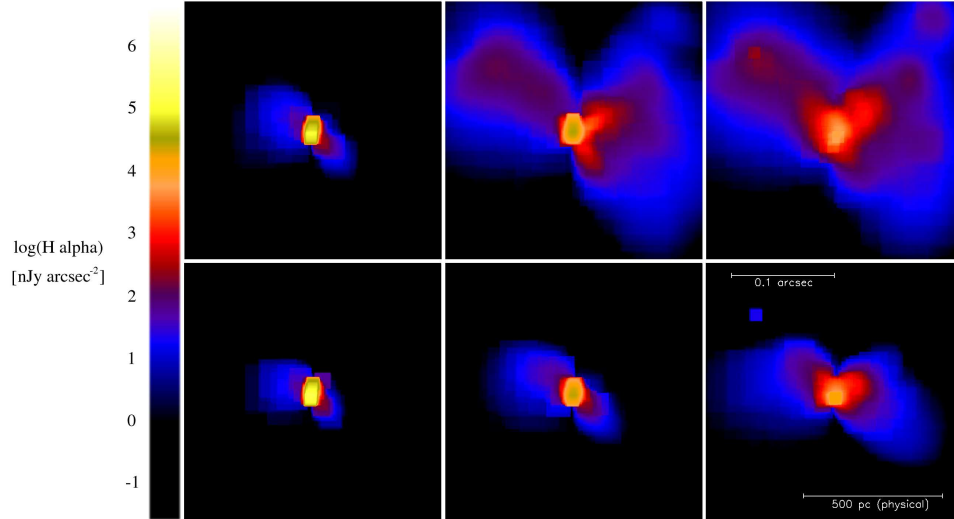


Figure 4.10: The flux in $H\alpha$, $f_{H\alpha}$, per square arcsecond, emitted from a primordial dwarf galaxy, as observed on the sky at $z = 0$, assuming a spectroscopic resolution of $R = 1000$. Shown here are the two most massive of the four stellar clusters that we simulate, one containing $25 M_{\odot}$ stars (*bottom panels*), the other containing $100 M_{\odot}$ stars (*top panels*). From left to right, the clusters are shown at 10^5 yr, 1 Myr, and 3 Myr after formation. Note that the emission is concentrated in the densest photoionized regions, the filaments around the galaxy (compare the top panels to Fig. 4.2) and especially the dense gas within the inner ~ 100 pc of the galaxy. The highest total fluxes occur at the earliest times, before the H II region has broken out; hence, the youngest stellar clusters are the most readily observed.

The Near Infrared Camera (NIRCam) aboard the JWST, which will be used to conduct deep surveys designed to detect the first galaxies, will be capable of detecting point source fluxes as low as ~ 3.5 nJy at a signal-to-noise of 10 for a 10^5 second exposure (e.g. Gardner et al. 2006). With a resolution of 0.03 arcsec per pixel, the NIRCam would also not quite resolve the galaxies that we simulate. We can evaluate the possibility that NIRCam may detect them as point sources, however, by estimating the continuum flux of the galaxies as observed at $\sim 2 \mu\text{m}$. As can be read from Figs. 4.6 and 4.7, the continuum flux, $\propto L_{\lambda 1640} / W_{\lambda 1640}$, varies only by a factor of a few between Ly α and He II $\lambda 1640$. Thus, for simplicity we assume that the continuum is roughly flat and calculate the specific continuum flux, as observed at $z = 0$, as

$$\begin{aligned}
 f_{\text{cont}} &\sim \frac{L_{\lambda 1640}}{4\pi c D_L^2(z)} \frac{\lambda_{\lambda 1640}^2 (1+z)}{W_{\lambda 1640}^0} \\
 &\sim 0.03 \text{nJy} ,
 \end{aligned}
 \tag{4.16}$$

where $W_{\lambda 1640}^0$ is the equivalent width in the rest frame of the galaxy, as defined in equation (4.9). This flux is well below the sensitivity limit of the NIRCam, and so we conclude that detection of the continuum radiation from the galaxies we simulate would also be undetectable. We note, however, that under favorable circumstances, gravitationally lensed emission from a primordial galaxy undergoing an only slightly more luminous starburst may be detectable with the JWST, given that lensing can boost the flux by a factor of order 10 (e.g.

Refsdal 1964; Stark et al. 2007).

The first dwarf galaxies could be more luminous than we find here if the efficiency of star formation ϵ_{SF} , defined as the fraction of the total baryonic mass in the galaxy contained in stars, is larger than what we have assumed in our simulations, where our choices for the total mass in stars correspond to modest values of $\epsilon_{\text{SF}} \sim 10^{-3} - 10^{-4}$. A larger efficiency ($\epsilon_{\text{SF}} \sim 10^{-1}$), for the top-heavy IMFs considered here, would yield a cluster observable by NIRCam (e.g. Gardner et al. 2006). However, as we have demonstrated, the much higher ionizing flux from a $\sim 10^6 M_{\odot}$ cluster of massive primordial stars would induce a strong hydrodynamic response which would lead to a rapid decline in the luminosity emitted in recombination radiation. Thus, even if such clusters can be identified by their continuum emission, the detection of recombination radiation, and with it information about the stellar IMF, may be beyond the capabilities of the JWST. Furthermore, the formation of such a massive cluster of primordial stars may face an impediment due to the strong radiative feedback within the cluster itself. Recent simulations of clustered star formation in the present-day Universe suggest that radiative feedback influences the fragmentation behavior of the gas and possibly lowers the overall star formation efficiency (see Krumholz et al. 2007; Bate 2009). However, the situation is by no means clear (e.g. Dale et al. 2005, 2007).

It is possible that more massive ($10^9 - 10^{10} M_{\odot}$) primordial galaxies form at $z \sim 12$, or form at lower redshift, making their detection feasible. However, such more massive, and therefore more luminous, galaxies are likely to also

be more chemically evolved, and so may already be dominated by Pop II star formation. Thus, it may be that the galaxies which host pure Pop III starbursts, such as those we study here, will remain out of reach of even the JWST, although this critically depends on the poorly constrained process of metal enrichment in the early Universe (see e.g. Pan & Scalo 2007; Tornatore et al. 2007; Cen & Riquelme 2008; Johnson et al. 2008). We emphasize, however, that the dynamical effects studied here are likely to play a role even in the more luminous galaxies that will be detected, and are important to take into account in evaluating observations meant to constrain the SFR or the IMF.

4.4 Summary and Conclusions

We have presented calculations of the properties of the recombination radiation emitted from a primordial dwarf galaxy at $z \sim 12.5$, during the initial stages of a starburst. Our cosmological radiation-hydrodynamical simulations allow us to track the detailed dynamical evolution of the emitting gas in the central regions of the galaxy, and thus to study its effect on the emerging radiation. The goal of this study has been to determine the observable signatures of the initial starbursts in the first galaxies. In particular, we have aimed to find reliable indicators of the star formation rate and of the stellar IMF.

Owing to the escape of H I-ionizing photons into the IGM, we find only a weak correlation between the total mass in stars and the luminosity in hydrogen recombination lines. This suggests that $\text{Ly}\alpha$ and $\text{H}\alpha$, despite the

high luminosity in these lines, may not serve as strong indicators of the SFR, unlike in the low-redshift Universe (e.g. Kennicutt 1983). The He II $\lambda 1640$ line may be a more effective SFR indicator, as the luminosity in this line scales more closely with the total mass in stars, due to the lower escape fraction of He II-ionizing photons.

We confirm that the ratio of He II $\lambda 1640$ to either Ly α or H α can be used as an IMF indicator, although its utility is compromised in some cases by the unequal escape fractions of H I- and He II-ionizing photons. The most robust IMF indicator, in terms of distinguishing between populations of massive ($10 M_{\odot}$) and very massive ($100 M_{\odot}$) Pop III stars, is the EW of He II $\lambda 1640$, as it is consistently higher for the more massive stars regardless of the total mass in stars. We note that while in principle the radiation emitted by a central accreting black hole (BH) in a primordial dwarf galaxy could introduce complications for using He II $\lambda 1640$ as IMF indicator (e.g. Tumlinson et al. 2001), recent work suggests that BH accretion is inefficient in the early Universe (e.g. Johnson et al. 2007; Pelupessy et al. 2007; Alvarez et al. 2008; Milosavljević et al. 2008, 2009). Such miniquasar activity may thus not result in appreciable observable radiation for the first $\sim 10^8$ yr.

In terms of the detectability of the recombination radiation from the first galaxies, we have shown that due to the dynamical response of the gas to photoheating, a top-heavy IMF or a high star formation efficiency can be self-defeating, leading to a decrease in the line luminosity of the galaxy. We conclude that the detection of purely primordial dwarf galaxies at $z \sim 10$ is

likely to be beyond the capabilities of the JWST, although their detection may be just possible if the galaxies are strongly lensed. More luminous, $10^9 - 10^{10} M_{\odot}$ (total mass), galaxies may thus be detected by the JWST; however, such more massive galaxies are likely to be already chemically enriched due to previous episodes of star formation in their progenitors. These systems are then expected to host Pop II star formation, or a composite of Pop II and Pop III, depending on the still poorly understood mixing of heavy elements in the first galaxies (e.g. Karlsson et al. 2008).

Our results demonstrate how the radiation emitted from the first galaxies depends on the hydrodynamic effects of the photoionization from clusters of massive stars. This is complementary to the results of previous studies (e.g. Schaerer 2002, 2003), which highlight the evolution of the emitted radiation owing to the aging of a stellar population. Clearly, both effects must be considered in future work.

The initial starbursts of the first galaxies may constitute the formation sites of the only metal-free stellar clusters in the Universe, since after the first several Myr supernova feedback can quickly enrich the galaxy with metals (e.g. Mori et al. 2002; Kitayama & Yoshida 2005; but see Tornatore et al. 2007, Cen & Riquelme 2008). Also, a large fraction of the first dwarf galaxies, with masses of order $10^8 M_{\odot}$, may already form from metal-enriched gas (Johnson et al. 2008; see also Omukai et al. 2008); it is an important open question what fraction of dwarf galaxies forming at $z \sim 10$ are primordial when they begin forming stars. Future observations of those first dwarf galaxies that do host

primordial star formation offer one of the few opportunities for constraining the primordial IMF.

Acknowledgments

We would like to thank Josh Adams, Marcelo Alvarez, and Mark Dijkstra for helpful discussions. We are also grateful to Lars Hernquist for his comments on a previous version of this paper, as well as to the anonymous referee whose suggestions greatly improved the presentation of this work. VB acknowledges support from NSF grant AST-0708795 and NASA ATRP grant NNX08AL43G. THG thanks for travel support from the Heidelberg Graduate School of Fundamental Physics, funded by the Excellence Initiative of the German Government (grant number GSC 129/1). RSK thanks the German Science Foundation (DFG) for support via the Emmy Noether grant KL 1358/1 and also acknowledges subsidies from the DFG SFB 439 Galaxies in the Early Universe as well as from the FRONTIER program of Heidelberg University. The simulations presented here were carried out at the Texas Advanced Computing Center (TACC).

Chapter 5

Stellar Archaeology

In the previous Chapter, detailed calculations of the radiation emitted from the first galaxies were presented, with the aim of providing some insight into how future direct observations of the radiation emitted from Pop III stellar clusters can be used to constrain the IMF of the first stars. In this Chapter, we now turn to a more indirect means of obtaining constraints on the primordial IMF, but one which is available to us today: stellar archaeology.

5.1 The Minimum Observable Metallicity of Stars in the Galaxy

5.1.1 Introduction

The first stars, the so-called Population III (Pop III), were the key drivers of early cosmic evolution. Their copious production of hydrogen-ionizing radiation initiated the reionization of the Universe, and the first supernova (SN) explosions seeded the pristine intergalactic medium (IGM) with the first heavy elements (Ciardi & Ferrara 2005; Barkana & Loeb 2007). The character of this stellar feedback sensitively depends on the initial mass function (IMF) of the first stars. The current theoretical model of their formation, based on numerical simulations, suggests that the Pop III IMF was top-heavy

(Bromm & Larson 2004). In the context of modern cold dark matter (CDM) cosmology, there are two physically distinct sites of early star formation. The very first stars are predicted to have formed in so-called minihaloes at redshift $z \sim 30 - 20$. The subsequent SNe dispersed the first heavy elements into the surrounding gas, thus setting the initial conditions for the formation of the second-generation of already slightly metal-enriched (Pop II) stars. If the prediction of a top-heavy IMF is correct, of order one Pop III star would form per minihalo, whereas a small cluster of predominantly low-mass Pop III stars would arise in the alternative case of a normal, Salpeter-like IMF. The second site for the formation of stars at high redshift are the atomic cooling haloes, with of order a 100 times the mass of the minihaloes. Their dark matter potential wells are sufficiently deep to induce the collapse of the material that was affected by the SN feedback from the Pop III stars in minihaloes. These systems are therefore the sites for the formation of the second generation (Pop II) stars. Due to their predominantly low masses they may still be found today as the most metal-poor stars.

Each galaxy thus exhibits a certain minimum metallicity, reflecting the pre-enrichment from Pop III stars. We here explore the fundamental question of the minimum Fe and Mg abundances observable in the Milky Way to derive constraints on early galaxy formation and on the Pop III IMF. We pursue a “near-field cosmology” approach (Freeman & Bland-Hawthorn 2002), established over the past decade by large objective-prism surveys (Beers & Christlieb 2005) of metal-poor stars as vital tracers of Galactic chemical evo-

lution and the early Universe. These stars carry the fossil record of the physical conditions in the first star forming systems (“stellar archaeology”). To successfully retrieve any such signatures, it is crucial that the atmospheric composition of the observed stars has not been altered either intrinsically by the products of nuclear burning in the stellar interior, or externally by accretion of interstellar material during their long lifetimes. Mass transfer across a binary system may also change the abundances of certain elements (e.g. C), but not the ones that are of interest in this study (Fe, Mg). The first effect can be accounted for by selecting relatively unevolved main-sequence and giant stars. Regarding the second issue, only a few approximate calculations are available (Talbot & Newman 1977; Yoshii 1981; Iben 1983), based on the idealized assumption that all stars have the same velocity. We therefore revisit the issue of accretion with a full stellar kinematic analysis of a large sample of metal-poor stars, so that we can assign individual velocities to them. A more realistic modeling of accretion is crucial because stellar archaeology pre-supposes a negligible contribution to the observed abundances from such pollution, so that it is possible to derive constraints on the early Universe and the Pop III IMF. Testing the prediction of a top-heavy IMF is one of the main goals of the upcoming *James Webb Space Telescope (JWST)*, but it is important to also utilize complementary probes that are already accessible now, such as the most metal-poor stars.

5.1.2 Minimum Stellar Metallicity

A fundamental characteristic of the Milky Way is the minimum observable metal-enrichment in its stars. The existence and level of such a “metallicity floor” is governed by the Pop III IMF. If the first stars were formed with a normal, Salpeter-like IMF, contrary to the current consensus view, there would be no minimum stellar metallicity, and truly metal-free, low-mass stars would exist. In this case, significant interstellar accretion could masquerade such putative primordial abundances in those stars. Without detailed knowledge of their accretion history, this would prevent us from identifying them as such low-mass Pop III stars. Hence, any information about the IMF would be irretrievably lost.

For a top-heavy IMF, the situation is very different. Recent numerical simulations of the assembly process of atomic cooling haloes, which are often thought to constitute the first galaxies, have shown that Pop III star formation only occurs in a few of the progenitor minihaloes that eventually merge into the atomic cooling halo (Johnson et al. 2008). For simplicity, we here assume that only one minihalo hosted a Pop III star that ended its life in a SN explosion. This accommodates the possibility that a fraction of the minihalo Pop III stars formed massive black holes by direct collapse, without any concomitant metal enrichment. Under this assumption, we can now derive an estimate for the “bedrock enrichment” from Pop III stars with a top-heavy IMF, which would in turn set the minimum stellar metallicity observable in the Galaxy’s oldest Pop II stars. Current simulations predict the typical Pop III mass to only

within a factor of 10. Consequently, within the general top-heavy paradigm, a number of qualitatively very different SN pathways for the first stars are still possible (Heger & Woosley 2002; Iwamoto et al. 2005), and it is important to consider these. If the progenitor Pop III star had a mass in the range $140 - 260 M_{\odot}$, an energetic pair-instability SN (PISN) would occur, which is characterized by extremely large metal yields (Heger & Woosley 2002). The Mg yield is almost constant over the entire PISN mass range; assuming that the Mg yield from a single PISN is well-mixed in an atomic cooling halo containing a total gas mass of $10^7 M_{\odot}$ leads to the narrowly confined prediction of $[\text{Mg}/\text{H}]_{\text{min}} \simeq -3.2$.¹ Since this overlaps with the range of observed stellar Mg abundances, a fraction of Pop II stars could carry the signature of PISN nucleosynthesis. However, this fraction is likely very small since no clear PISN “odd-even” effect has thus far been found among metal-poor stars. No useful PISN prediction can be made in the case of Fe, since the corresponding yields range from zero to very high values, depending on the precise progenitor mass (Heger & Woosley 2002). Alternatively, if the Pop III progenitor had a less extreme mass, but still in the black hole forming range of $M_{*} \geq 25M_{\odot}$, a peculiar class of “faint”, core-collapse (CC) SNe becomes possible. The class of such low explosion-energy SNe, experiencing mixing and fallback onto a nascent black hole, was introduced to produce very low Fe yields (Umeda & Nomoto 2003; Iwamoto et al. 2005) in order to explain the two hyper Fe-poor stars with $[\text{Fe}/\text{H}] < -5.0$. Higher explosion energies are required to explain

¹ $[\text{A}/\text{B}] = \log_{10}(N_{\text{A}}/N_{\text{B}}) - \log_{10}(N_{\text{A}}/N_{\text{B}})_{\odot}$, for elements A, B.

the abundance pattern of metal-poor stars with $[\text{Fe}/\text{H}] \geq -4.5$. We use these observationally calibrated nucleosynthesis calculations to constrain the likely range in Fe and Mg abundances that would result if the first stars died as such faint CC SNe. The different pre-enrichment levels are indicated in Fig. 5.1, for comparison with the observational data.

Based on these SN yield considerations, we have derived typical values for the Pop III pre-enrichment. We now wish to place extreme lower limits on the observable stellar Mg and Fe abundances in the Galaxy that result from assuming a top-heavy Pop III IMF. It is often argued that the transition from a top-heavy to a normal, Salpeter-like IMF for the subsequent generations of Pop II/I stars (including those considered here) is governed by a “critical metallicity” (Bromm & Larson 2004). Its value is still rather uncertain, depending on whether fine-structure line cooling is dominant (Bromm & Loeb 2003; Frebel et al. 2007), or dust cooling (Schneider et al. 2006). To arrive at a robust estimate that does not depend on the detailed nature of the critical metallicity, we consider a range that extends from typical fine-structure to dust predictions. Within the fine-structure model (Bromm & Loeb 2003), carbon is the most important coolant, leading to a critical abundance of $[\text{C}/\text{H}]_{\text{min}} = -3.5$. Combining this with the empirically determined maximum carbon-to-magnesium and carbon-to-iron ratios found in metal-poor stars, i.e. in HE 0107–5240 ($[\text{C}/\text{Mg}]_{\text{max}} = 2.5$; Collet et al. 2006) and HE 1327–2326 ($[\text{C}/\text{Fe}]_{\text{max}} = 3.8$; Frebel et al. 2008), we estimate the minimum Mg and Fe abundances to be $[\text{Mg}/\text{H}]_{\text{min}} = -6.0$ and $[\text{Fe}/\text{H}]_{\text{min}} = -7.3$. Dust cooling

models typically result in lower critical abundances, $[C/H]_{\min} = -4.5$, and the minimum observable Fe and Mg abundances are reduced accordingly. Our predictions for the minimum Fe and Mg values are shown in Fig. 5.1 (*yellow regions*).

The level of our predicted metallicity floor is particularly interesting for the goals of current and future surveys with regard to identifying the most metal-poor stars. Some of the recently discovered metal-poor stars have extremely low Mg and Fe abundances that begin to approach our theoretical predictions for the metallicity floor. These objects suggest that additional examples of such stars can be found with current observational techniques, potentially even with abundances below the current record holders. Based on spectrum synthesis calculations, we estimate that suitably cool giants should have at least one detectable Mg and Fe line at abundances as low as $[Mg/H] \sim -6.5$ and $[Fe/H] \sim -8.0$, respectively. Technological limitations should therefore not prevent us from reaching abundances that are within our predicted minimum metallicity ranges.

5.1.3 Data on Metal-Poor Stars

In order to explore whether the most metal-poor stars used here to constrain the minimum stellar abundances, or other metal-poor halo stars in general, are possibly affected by accretion, we reconstruct their individual accretion histories by carrying out a detailed kinematical analysis. Our sample stars are selected from the Sloan Digital Sky Survey (SDSS), which provides

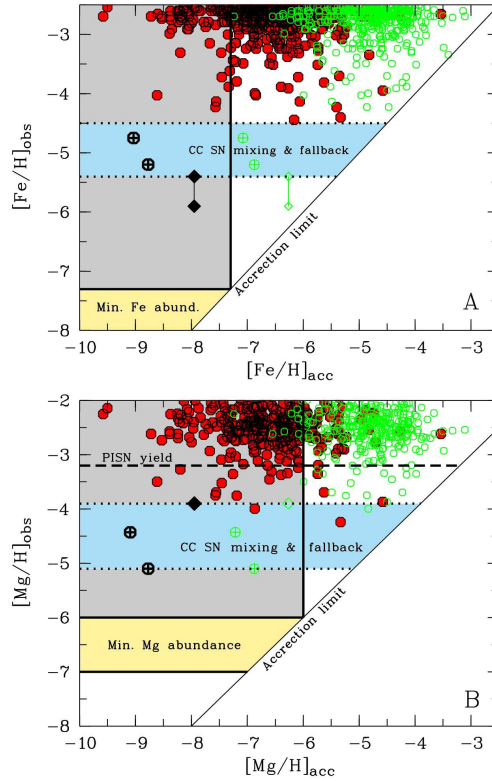


Figure 5.1: Observed vs. “accreted” Fe (*panel A*) and Mg (*panel B*) abundances for the sample of metal-poor stars (*red circles*). The case where all stars pass through a dense cloud once is also presented (*green open circles*). The three most Fe-poor stars are indicated (*crossed circles, diamond*). For HE 1327–2326, both the 1D non-LTE and 3D LTE Fe values are shown. All stars have accreted fewer metals than what is observed, thus demonstrating the validity of the basic assumption underlying stellar archaeology. The minimum Fe and Mg abundance ranges, calculated under the assumption of a top-heavy Pop III IMF, are given (*yellow region*). The approximate Mg abundance arising from a PISN event in an atomic cooling halo is indicated (*dashed line, panel B*), as well as the Fe and Mg levels of enrichment from a $25 M_{\odot}$ mixing and fallback SN (*dotted lines, blue regions*). We highlight those stars (*gray regions*) that can be used to place constraints on the Pop III IMF, where accretion does not affect whether they lie above or below the theoretical “bedrock abundances”, predicted for a top-heavy IMF. Since all observed Mg abundances within the IMF-sensitive (*gray*) region to date fall above this bedrock range, we conclude that a top-heavy IMF is favored for the first stars.

the necessary input data (radial velocities, distances, proper motions, abundances) for such an analysis.² Studies based on the kinematics from SDSS have already led to groundbreaking results (e.g. Carollo et al. 2007). A full description of the data products used here can be found elsewhere (Munn et al. 2004; Lee et al. 2008; Adelman-McCarthy et al. 2008). We note though that we employed $[\text{Fe}/\text{H}]$ abundances derived from the CaK line and selected 565 stars with $[\text{Fe}/\text{H}] < -2.5$. The spectra of all stars with $[\text{Fe}/\text{H}] < -3.4$ were inspected because the majority of them turned out to be spectral artifacts or misclassified objects, and not real metal-poor stars. This leaves 474 stars in the sample. To obtain $[\text{Mg}/\text{H}]$, we set the available $[\alpha/\text{Fe}]$ equal to $[\text{Mg}/\text{Fe}]$. Based on temperature estimates from the $\text{H}\delta$ line, we find that the sample contains 472 turnoff (dwarf) stars with known proper motions; the remaining two appear to have unrealistically low temperatures so we exclude them from the sample. Reliable proper motions are not available for most of the well-studied metal-poor giants since their distances are very large, and hence uncertain. Future missions such as GAIA will enable us to extend this work by providing accurate proper motions, especially for all the metal-poor giants. Since our diagnostic is based on readily obtainable medium-resolution spectra, it will be straightforward to apply it to the extensive data sets from future large-scale surveys.

²See <http://www.sdss.org/dr6/>.

5.1.4 Role of Accretion

We assume that a given star moves in a rigid, three-component Milky Way potential, adopted from Johnston (1998), for 10 Gyr. Using a standard orbit integrator (D. Lin, priv. comm. 2008; see Fulbright 2000 for further details), we determine the orbital parameters, such as U, V, W velocities and eccentricity, for all sample stars. For simplicity, accretion is assumed to take place only during disk crossings. The density structure in the disk interstellar medium (ISM) is highly inhomogeneous, such that every star will encounter regions of different density at each disk crossing. Since the accretion rate depends only linearly on density (see Sec. 4), as opposed to the inverse-cubed scaling with velocity, we here for simplicity work with an average ISM density. Using the empirically determined volume filling fraction as a function of density (Talbot & Newman 1977), we find for the average disk density, $n \simeq 5 \text{ cm}^{-3}$ and assume a disk height of $\sim 100 \text{ pc}$.

We estimate the amount of accreted gas onto a low-mass star that passes through interstellar gas assuming Bondi-Hoyle accretion (Bondi 1952):

$$\dot{M} \simeq 2\pi(GM)^2\rho/(v_{\text{rel}}^2 + c_s^2)^{3/2}, \quad (5.1)$$

where M is the mass of the star, $\rho \simeq m_{\text{H}}n$ the gas density, v_{rel} the stellar velocity relative to the gas, and $c_s \simeq 5 \text{ km s}^{-1}$ the sound speed in the general Milky Way ISM. We calculate the relative velocity of a star during each disk crossing according to $v_{\text{rel}} = \sqrt{(U, V - V_0, W)^2}$, where $V_0 \simeq 200 \text{ km s}^{-1}$ is the average rotation speed of the disk. For the ISM abundances, we assume a solar

distribution with the overall metallicity evolving according to:

$$Z_{\text{ISM}}(t) = (1 + t/t_{\text{H}})^{-4} [10^{-3} + 0.67 * \{(1 + t/t_{\text{H}})^5 - 1\}] Z_{\odot}, \quad (5.2)$$

where $t_{\text{H}} = 13.7 \text{ Gyr}$ is the Hubble time, such that $Z_{\text{ISM}} \sim Z_{\odot}$ at the time of the formation of the Sun $\sim 5 \text{ Gyr}$ ago. This relation follows from detailed homogeneous chemical enrichment models (Pagel 1997). As halo stars will pass through the Milky way disk between 50 and 80 times, the average density and metallicity of the accreted gas is likely to be similar for all stars. However, the stellar velocities at disk crossing can vary widely, thus dominating the accretion rate because of the strong dependence on relative velocity in equ. (1). Stars with the highest velocity relative to the disk will experience the least pollution by the Milky Way ISM, and are therefore most likely to display a surface metallicity endowed at the earliest epochs of star formation.

We specifically choose to investigate the accretion history of Mg and Fe, which are easily measurable abundances in metal-poor stars. Also, these abundances are not affected by potential mass transfer across a binary system. We calculate the total amount of accreted Mg and Fe by summing up the contributions from every disk crossing. To finally arrive at surface abundances, we assume that $\sim 10^{-3}$ of the stellar mass is contained in the convective outer layer for dwarfs. For giants this fraction would rise to ~ 0.1 (Yoshii 1981).

In Fig. 5.1, we compare the resulting accreted Mg and Fe abundances for every star (all dwarfs) with its observed values. All stars have lower “accreted abundances” than their observed abundances. This generally confirms

that accretion does not dominate the abundance pattern of old metal-poor stars, thus rendering the overall concept of “stellar archaeology” viable. It also suggests that if the first stars were characterized by a Salpeter-like IMF, and if they traveled at sufficiently high velocity, it should be possible to find surviving stars with arbitrarily low abundances. At these low metallicities, even traces of accreted material may have an impact on the surface abundances, making detailed knowledge of any potential accretion indispensable.

For the three most Fe-poor stars currently known, the subgiant HE 1327–2326 ($[\text{Fe}/\text{H}] = -5.9$; Frebel et al. 2005, 2008), together with the giants HE 0107–5240 ($[\text{Fe}/\text{H}] = -5.2$; Christlieb et al. 2002) and HE 0558–4840 ($[\text{Fe}/\text{H}] = -4.8$; Norris et al. 2007) we find the same result. Their accretion levels are somewhat uncertain (by ~ 1 dex) due to poorly determined distances and proper motions, but still indicate an approximate level of accretion that is well below their observed abundances. Regarding distance and proper motion uncertainties for the other stars, we verified that the derived amounts of accreted material are not significantly affected when the input parameters are changed by up to 30%.

We also consider the special case where each star passes once through an extremely dense cloud of 100 pc diameter and $n \sim 10^3 \text{ cm}^{-3}$, comparable to the inner region of a giant molecular cloud (GMC). We further assume that this occurs when the star has its smallest v_{rel} , to maximize the potential for accretion. In this case, the observed abundance pattern may be dominated by the signature of the ISM. It is not known whether every star encounters a

GMC, but even in the case it does, the accretion process will strongly depend on the space velocity of the star. In Fig. 5.1, we show the total accreted Mg and Fe for all stars in this extreme case (*green circles*). We find that the stars still have slightly lower “accreted abundances” than the observed values. If a star were to have an accreted abundance larger than the currently observed one, it might indicate that such a star never entered a dense GMC during its lifetime. Our GMC “maximum accretion” scenario thus provides a robust upper limit to the total accreted abundance for each star. We note that in our accretion estimates the potential role of stellar winds has been neglected. The presence of a wind would likely balance any accretion or prevent it altogether (Talbot & Newman 1977). Since wind strength scales with stellar mass and metallicity, the low-mass, metal-poor stars considered here should have little or no wind. Hence, the accreted $[\text{Fe}/\text{H}]$ and $[\text{Mg}/\text{H}]$ abundances are likely an upper limit. We thus conclude that stellar archaeology is not hampered by interstellar accretion, even for our maximum accretion scenario. Furthermore, we demonstrate that kinematic information is vital for the identification of the lowest-metallicity stars.

Finally, we compare our results with the “pollution limit” derived previously by Iben (1983). This limit was calculated in an attempt to explain the paucity of low-metallicity stars (G-dwarf problem), within the framework of a normal, Salpeter-like IMF for the first stars. The estimated Fe pollution of $[\text{Fe}/\text{H}]_{\text{acc}} = -5.7$ (one value for all stars) would in this interpretation naturally prevent the discovery of any stars with lower metallicities. However, we show

that the “accretion limit” is a strong function of stellar kinematics, and that there is therefore no such universal limit. Our result thus suggests that the traditional, pollution-based, explanation for the absence of surviving low-mass Pop III stars needs to be revisited. Furthermore, with the latest Fe abundance measurement for HE 1327–2326 of $[\text{Fe}/\text{H}] = -5.9$ (Frebel et al. 2008), the Iben pollution limit has already been reached. This star, however, is currently thought to be a second generation object displaying the nucleosynthetic yields of a metal-free CC SN with a mass $\sim 25 M_{\odot}$ (Iwamoto et al. 2005), and not a masqueraded, low-mass Pop III star. In addition, HE 1327–2326 does not exhibit scaled-down solar abundances, contrary to the expectation that a star with an accretion-dominated signature should show a solar abundance pattern.

5.1.5 Implications

As an interesting consequence from the preceding analysis, we can derive some observational constraints on the underlying Pop III IMF that determined the level of pre-enrichment. From Fig. 5.1, we infer that select stars with high velocities and correspondingly low accreted abundances (*gray region*) are useful probes of the Pop III IMF. Accretion alone would not have been able to push them above the minimum levels predicted for a top-heavy IMF. If these stars had formed from extremely low-metallicity gas, their observed present-day surface abundances should still have reflected this. The fact that these low-accretion stars all have abundances above the minimum floor predicted for a top-heavy Pop III IMF supports the notion that the first

stars were very massive (see also Tumlinson 2006; Salvadori et al. 2007). We here would like to repeat that such tests can only be carried out if proper attention is given to the individual accretion history of each star.

To make this test fully convincing, we need to address possible observational biases. In particular, the apparent lack of IMF-sensitive stars below the top-heavy prediction could simply reflect their small numbers. However, current survey sizes reach levels of completeness that render such an interpretation increasingly unlikely. To gauge the putative number of low-mass Pop III stars in the Galaxy, assuming a Salpeter-like primordial IMF, we begin with the approximate number of minihaloes that formed before the redshift of reionization, and that eventually merged to become part of the Milky Way. Using standard extended Press-Schechter (EPS) theory (Lacey & Cole 1993), we estimate that $\sim 10^4$ Milky Way progenitor minihaloes hosted Pop III star formation. The $\sim 100M_{\odot}$ in cold, dense gas available to form stars, as found in numerical simulations, would then result in ~ 100 low-mass Pop III stars. The total number of such hypothetical Pop III fossils in the Galaxy would be $\sim 10^6$. Given that the Galactic halo today contains $\sim 10^9$ stars, one low-mass Pop III star should be found per $\sim 10^3$ stars surveyed (Oey 2003). In the Hamburg/ESO survey, each of the two stars with $[\text{Fe}/\text{H}] < -5$ was found in a sample of ~ 2000 selected metal-poor stars, which in turn comprise $\sim 10\%$ of a subset of halo stars with no metallicity selection. To first order, it thus seems unlikely that a selection effect would significantly affect our results. This argument is further strengthened by SDSS, which has spectroscopically measured

metallicities for several hundred thousand stars.

Our results (see Fig. 5.1, *panel B*) finally also suggest that only a small fraction of the first stars died as PISNe because a number of stars have observed [Mg/H] ratios below the abundance floor predicted for PISN enrichment. We thus conclude that the majority of the first stars were very massive, but had masses below $\sim 140 M_{\odot}$. Current data and simulations are not yet precise enough to determine the PISN fraction with any certainty, but our diagnostic can in principle be extended to constrain this important quantity (see also Karlsson et al. 2008).

We have thus shown that stellar archaeology can provide crucial observational constraints on the primordial IMF, given that the metal-poor stars of interest have sufficiently high space velocities to avoid significant accretion. Together with our prediction that stars with abundances below the currently known lowest values can be found in ongoing and future discovery efforts, stellar archaeology becomes directly relevant for the science goals of the next generation of 30 m-class optical telescopes such as the Giant Magellan Telescope (GMT) and the Thirty Meter Telescope (TMT). Future surveys will continue to provide us with local constraints on star formation at the edge of the observable Universe. Selecting suitable candidates for this task will increasingly rely on our ability to combine chemical abundance analyses with kinematic information.

Acknowledgments

We thank A. Weiss, S. Cassisi and H. Bluhm for helpful discussions. A. F. acknowledges support through the W. J. McDonald Fellowship of the McDonald Observatory. V. B. is supported by NSF grant AST-0708795. Funding for the SDSS and SDSS-II has been provided by the Alfred P. Sloan Foundation, the Participating Institutions, NSF, the U.S. DoE, NASA, the Japanese Monbukagakusho, and the Max Planck Society, and the Higher Education Funding Council for England. Further details can be found at <http://www.sdss.org/collaboration/credits.html>.

5.2 The Chemical Signature of the First Stars in the Universe

5.2.1 Introduction

Little is known about the first stars in the universe, the so-called Population III (Pop III henceforth). Over which range of masses were they formed? And what was their relative distribution by mass, i.e., their initial mass function (IMF)? The apparent lack of metal-free stars in the Galactic halo suggests that star formation in metal-free gas should be skewed towards relatively high masses, as compared to the mass scale of $\leq 1 M_{\odot}$ found in the solar neighborhood (e.g., Bond 1981; Oey 2003; Karlsson 2005; Tumlinson 2006). This finding is corroborated both by theoretical arguments (e.g., Larson & Starfield 1971) and by numerical simulations (Bromm et al. 1999; Bromm et al. 2002; Abel et al. 2002; Yoshida et al. 2006) following the collapse of

primordial baryonic matter inside the very first non-linear structures, virialized dark matter halos of $\sim 10^6 M_\odot$, so-called minihalos. As a consequence of the inefficiency of primordial gas to cool to temperatures below $\sim 10^2$ K, these simulations indicate that the first stars were predominantly very massive objects with masses $\geq 100 M_\odot$.

It can be argued that star formation in minihalos, apart from being regulated by H_2 cooling, occurred under simplified conditions where the absence of magnetic fields, ultraviolet radiation, and a pre-established turbulent velocity field resulted in a unique metal-free stellar population (e.g., Bromm & Larson 2004; Glover 2005). For instance, in shock-compressed or photoionized primordial gas, the formation of the coolant HD is boosted, leading to a decrease in the typical mass of metal-free stars down to $\sim 10 M_\odot$ (Johnson & Bromm 2006). Similarly, lower mass stars may also be formed in turbulent molecular clouds with a negligible magnetic field (Padoan et al. 2007). The presence of a magnetic field could also, in the case of magnetized accretion disks, lead to smaller stellar masses as the accretion onto the proto-stellar core may be reduced by magnetically driven outflows (Silk & Langer 2006).

In spite of their peculiarity and apparent rarity, the first, very massive stars ultimately set the stage for subsequent star and galaxy formation. If mass-loss through rotationally induced stellar winds was limited (Ekström et al. 2006), a significant fraction of these stars was likely to explode as pair-instability supernovae (PISNe), leaving no remnant behind (Heger & Woosley 2002). Interestingly, η Carinae and the Pistol Star, both in the mass range

$\sim 100 - 200 M_{\odot}$, are two examples of such very massive stars in our own Galaxy. Moreover, the recent detection of a particularly energetic supernova (SN) explosion, SN 2006gy (progenitor mass estimated to $m \sim 150M_{\odot}$) in NGC 1260, indicates that stars may explode as PISNe, even at low redshift (Smith et al. 2007).

Since very massive stars are extremely shortlived (≤ 3 Myr), primordial PISNe ($140 \leq m/M_{\odot} \leq 260$, Heger & Woosley 2002) would supposedly be the first stellar objects to enrich the interstellar medium (ISM) with metals. As predicted by homogeneous chemical evolution models (e.g., Ballero et al. 2006), such an initial enrichment would establish a metallicity floor and imprint the chemical signature of PISNe in the early ISM, from which the first low-mass ($m \leq 1 M_{\odot}$) stars later formed. The unique chemical signature of the primordial PISNe should thus predominantly be retained in the oldest and, in particular, the most metal-poor stars belonging to the Galactic halo population. To date, no such signature has been found (e.g., Christlieb et al. 2002; Cayrel et al. 2004; Cohen et al. 2004; Barklem et al. 2005; Frebel et al. 2005). This has been regarded as an indication that stars in the early universe with masses in excess of $100 M_{\odot}$ were extremely rare (e.g., Tumlinson et al. 2004; Ballero et al. 2006), if not altogether absent. However, we shall argue that true second generation stars which were formed from material predominantly enriched by primordial PISNe have metallicities significantly above those of the stars in the metal-poor tail of the Galactic halo metallicity distribution function (MDF), at variance with the classical picture described above. Fur-

thermore, although the mass fraction of Pop III stars ending up as PISNe may be significant, the fraction of low-mass stars bearing their chemical signature is small, which explains the absence of such stars in previous surveys.

The organization of the paper is as follows. In §5.2.2 we consider the chemical enrichment by the first stars in its cosmological context, while the detailed chemical enrichment model and parameters are discussed in §5.2.3. The results are presented in §5.2.4, and we conclude with a discussion of the implications in §5.2.5.

5.2.2 The Cosmological Context

The end of the epoch known as the cosmic dark ages, when our universe witnessed the first sources of stellar light, is one of the final frontiers in modern cosmology. One indirect way to search for the first, Pop III stars is to detect their contribution to the cosmic infrared background. Although tantalizing progress has been made (e.g., Kashlinsky et al. 2007), we have to await the advent of next generation telescopes, such as the *James Webb Space Telescope (JWST)* and the *Atacama Large Millimeter/submillimeter Array (ALMA)* (e.g., Walter & Carilli 2007), to be able to resolve individual sources and their birth sites, and to place stronger constraints on the IMF and the star formation rate (SFR) in primordial galaxies.

A complementary approach is to search for Pop III signatures in the local fossil record, i.e., to look for specific chemical abundance ratios in the atmospheres of old, low-mass stars in the Milky Way which may have formed

from gas enriched with the ejecta from the first SNe. This general strategy is termed near-field cosmology, and this particular approach is a powerful way to learn about the first generations of stars. Unlike stars exploding as core collapse SNe, stars in the PISN mass range (i.e., $140 \leq m/M_{\odot} \leq 260$) exhibit only a very small neutron excess in their interiors (Heger & Woosley 2002). As a consequence, there is a pronounced odd-even effect, i.e., particularly low abundance ratios of odd- Z elements to even- Z elements, in the ejecta of PISNe. Furthermore, due to the lack of excess neutrons in addition to less-rapid expansion timescales during the explosion, the rapid n-capture process presumably does not take place in PISNe (Heger & Woosley 2002; Umeda & Nomoto 2002). These and other chemical characteristics observable in low-metallicity stars, such as low values for Fe/Ca, could, in principle, be used to identify a possible pre-enrichment by PISNe. However, despite considerable efforts made to identify and analyze the metal-poor tail of the Galactic halo MDF (see the in-depth review by Beers & Christlieb 2005), no observational evidence for a population of very massive stars exploding as PISNe has yet been found. It may appear, therefore, that only a negligible fraction of metal-free stars had masses in excess of $100 M_{\odot}$. We will here argue, however, that this apparent absence of PISN progenitors might arise from a subtle observational selection effect.

Classical, homogeneous chemical evolution models (see e.g., Prantzos 2005; Ballero et al. 2006) predict that signatures of primordial PISNe, if they ever existed, by necessity must dominate the chemical abundance patterns

found in the most metal-poor stars for two reasons: the very short lifetimes of the PISN progenitors and the assumption that SN ejecta are mixed instantaneously within the entire system. Evidently, such calculations would suggest that all true second generation stars, i.e., stars enriched by a single primordial SN, will have the lowest metallicities of the observed metal-poor stars. This, however, may not be the case. As we will show, the chemical signature of primordial PISNe may only be found in stars of somewhat higher metallicity, possibly explaining why searches for the most metal-poor stars have not turned up any stars showing the PISN signature.

Although atomic diffusion in general is boosted by turbulence, giving rise to turbulent diffusion, the mixing of mass in the ISM is not instantaneous. This fact becomes increasingly important in lower metallicity systems, as it implies that there should exist coeval regions in the ISM enriched by different types of SNe with distinctly different abundance patterns. In particular, the amount of, e.g., calcium produced in a PISN can be several orders of magnitude higher than what is synthesized in a normal core collapse SN, with ratios such as Fe/Ca that are only $\sim 1/10$ of those in core collapse SNe. A second generation star formed out of gas enriched by a single primordial PISN may therefore have a metal content which is atypical *and* significantly higher than a star formed from gas enriched by one, or even several core collapse SNe (see Bromm et al. 2003; Greif et al. 2007). This effect is illustrated in Figure 5.2 which shows, in a statistical sense, the spatial variation in the level of chemical enrichment that may be expected in the early universe. Also

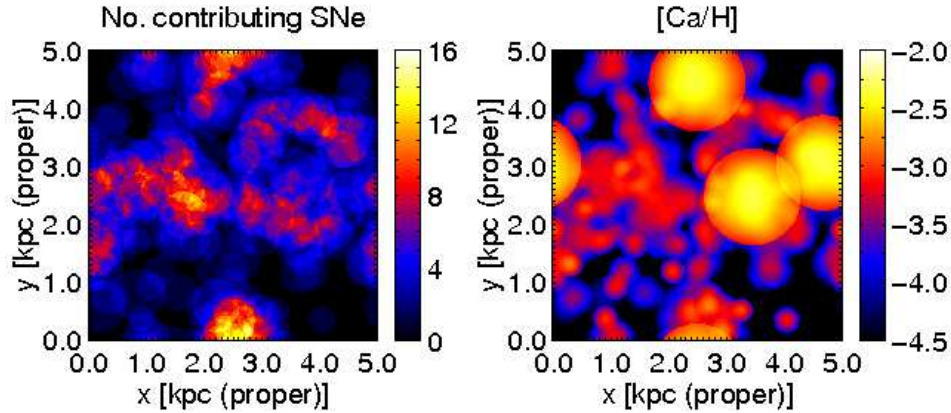


Figure 5.2: Illustration of the inhomogeneous chemical enrichment model. SNe of different types enrich space during the assembly of a $10^8 M_{\odot}$ halo. *Left panel:* The number of contributing SNe in the interstellar medium at some early time. *Right panel:* The corresponding Ca abundance. Although the ejecta of PISNe are spread over very large volumes, the Ca abundance in regions enriched by a single PISN is significantly higher than in regions enriched even by numerous core collapse SNe.

shown is the corresponding variation in the number of SNe contributing to the enrichment. Notice the poor correlation in certain regions between this number and the actual level of enrichment. As a result of the non-instantaneous mixing of metals, which, by construction, is not handled in homogeneous chemical evolution models, the chemical relics of the very first stars in the universe (i.e., the primordial PISNe) could predominantly be “hidden” in a population of relatively metal-rich stars.

Since we are unable to follow the hierarchical build-up of the Milky Way halo in detail, we shall focus on the chemical enrichment of individual so-called ‘atomic cooling halos’ of mass $\sim 10^8 M_{\odot}$, which are able to cool

due to lines of atomic hydrogen. These halos are probably massive enough to harbor continuous star formation while small enough to be dispersed during the subsequent assembly of the Galactic halo, either one-by-one or by first being incorporated into larger halos (see Robertson et al. 2005). Likely, a significant fraction of the metal-poor stars in the Galactic halo originate from such atomic cooling halos, in which the first SN-enriched gas may have re-collapsed and formed Pop II stars (e.g., Greif et al. 2007), including the second generation stars that we seek to identify. In accordance with this picture, Scannapieco et al. (2006) demonstrated that second generation stars should be expected over a wide range of Galactocentric radii. We shall assume that the star formation history of the atomic cooling halos begins with the first stars formed in collapsed minihalos. This picture is in agreement with hierarchical structure formation, where smaller systems merge to form larger ones. In the following, star formation will be divided into two modes: Pop III star formation, which only occurs in metal-free gas, and Pop II star formation, occurring in gas already enriched with metals.

5.2.3 Modeling Early Chemical Enrichment

In order to discern the chemical signature of the first massive Pop III stars, we have constructed a model for how the early universe was enriched with heavy elements ejected by the first SNe. Our model accounts, self-consistently, for the formation of both Pop III and Pop II stars, and allows us to study in some detail how SNe from each of these populations contributed to the abun-

dances that can be observed today in Galactic metal-poor stars. In this section, we describe our chemical evolution model, emphasizing how it incorporates the distinct characteristics of Pop III star formation in a cosmological setting.

5.2.3.1 The Basic Model

Although the details of the inhomogeneous chemical enrichment model are described elsewhere (see Karlsson 2005, 2006; Karlsson & Gustafsson 2005), we will provide a general outline and discuss relevant improvements below. The model is based on the mixing volume picture, where the metal-rich ejecta of individual SNe are spread within finite but continuously growing volumes $V_{\text{mix}}(t)$. In this picture, the mixing volume growth is modeled as a random-walk process, predominantly driven by turbulent gas motions. At any given time t , we may thus define the size of V_{mix} as

$$V_{\text{mix}}(t) = \frac{4\pi}{3}(6D_t t + \sigma_E)^{3/2}, \quad (5.3)$$

where $D_t = \langle v_t \rangle l_t / 3$ is the turbulent diffusion coefficient and σ_E is the minimal mixing area, introduced to account for the initial expansion of the ejected material, before it merges with the ambient medium. Furthermore, in accordance with the diffusion approximation, the concentration of metals within V_{mix} is assumed to be non-uniform, following a Gaussian density profile. This was not taken into account in earlier versions of the model. The turbulent diffusion coefficient is estimated to be $D_t \simeq 3.3 \times 10^{-4} \text{ kpc}^2 \text{ Myr}^{-1}$, assuming a typical turbulent velocity of $\langle v_t \rangle \simeq v_{\text{vir}} \simeq 10 \text{ km s}^{-1}$, where v_{vir} is the virial velocity of

$\sim 10^8 M_\odot$ atomic cooling halos, and a turbulent correlation length of $l_t = 100$ pc, a typical value for the virial radius of a minihalo, on which scale mergers may be expected to drive turbulent mixing.

During the early expansion of the SN remnant itself, no star formation is expected to occur within V_{mix} . This is taken into account by assuming an initial, instantaneous growth of V_{mix} set by σ_E . The value of σ_E depends on how much mass of gas is swept up by the remnant, which is chiefly determined by the explosion energy of the SN and only very weakly dependent on the density and metallicity of the ambient medium (Cioffi et al. 1988). For core collapse SNe, this initial dilution mass is estimated to be $M_{\text{dil}} \simeq 10^5 M_\odot$ assuming an explosion energy of $E = 10^{51}$ ergs, an average ISM metallicity of $Z/Z_\odot = 10^{-3}$, and a density of $n \simeq 0.1 \text{ cm}^{-3}$ (the weak dependences on Z and n are neglected, see Ryan et al. 1996 and references therein), while for PISNe, $M_{\text{dil}} \simeq 5 \times 10^5 (E/10^{51} \text{ ergs})^{0.6} M_\odot$ at $z \sim 20$ (Bromm & Loeb 2003). Depending on the PISN explosion energy, the associated initial dilution mass may be nearly two orders of magnitude larger than the corresponding dilution mass for core collapse SNe. Clearly, the inclusion of this effect is important as it may strongly influence the abundance of chemical elements in regions where subsequent stars eventually are allowed to form (see Fig. 5.2).

The present model is modified to handle the statistics of the metal-free Pop III and the metal-enriched Pop II separately. Pop II star formation is assumed to be spatially uncorrelated. This means that the probability, $w_{\text{II}}(k, t)$, of finding a region in space enriched by the ejecta of k Pop II SNe at

time t can be approximated by the Poisson distribution, i.e.,

$$w_{\text{II}}(k, t) = \text{Po}(k, \mu_{\text{II}}(t)) = e^{-\mu_{\text{II}}(t)} \mu_{\text{II}}(t)^k / k!, \quad (5.4)$$

where $\mu_{\text{II}}(t)$ denotes the space-averaged number of Pop II SNe contributing to the enrichment at time t . For Pop III star formation, however, the situation is somewhat different. If Pop III stars would have been randomly distributed in those areas where star formation occurred, i.e., in the higher density filaments, the probability of finding a region in such a filament enriched by a given number k of Pop III SNe would have been described by equation (5.4). However, the fact that no metal-free star is allowed to form in a region previously enriched by metals (but see Wyithe & Cen 2007; Cen & Riquelme 2007) introduces a type of anti-clustering effect. The fraction of enriched gas will thus be larger than that described by the Poisson statistics, for any given value of $\mu_{\text{III}}(t) > 0$, the space-averaged number of contributing Pop III stars at time t (see §5.2.3.4). To approximately account for this “no overlapping”-effect, the Poisson distribution is empirically modified by a Gaussian. Thus, the probability w_{III} of finding a region enriched by k Pop III stars is given by

$$w_{\text{III}}(k, t) = c_k e^{-(\mu_{\text{III}}(t)-k)^2/4} \times \text{Po}(k, \mu_{\text{III}}(t)), \quad (5.5)$$

where c_k is a normalization factor. In contrast to w_{II} , the probability density function described by equation (5.5) is more narrowly peaked towards $\mu_{\text{III}} = k$. In particular, w_{III} predicts a faster-than-exponential decrease of the fraction of

primordial gas available to Pop III star formation, as a function of μ_{III} . With time, $w_{\text{III}}(k=0, t)$ will still decrease slower than predicted by the corresponding Poisson equation since the Pop III SN rate, in fact, is proportional to the available fraction of primordial gas, as will be further discussed in §5.2.3.4.

Given the expressions in equation (5.4) and (5.5), we may calculate the probability $f_{\text{III}}(k', k)$ that a low-mass star (here defined to be a star which has survived to the present, i.e., with a mass $\leq 0.8 M_{\odot}$) is formed out of gas enriched by a total number k of SNe (i.e., Pop III + Pop II), k' of which are Pop III SNe. This probability is given by the integral

$$f_{\text{III}}(k', k) = \tilde{c}_k \int_0^{\tau_{\text{H}}} a_{\star}(t) w_{\text{III}}(k', t) w_{\text{II}}(k - k', t) u_{\text{II}}(t) dt. \quad (5.6)$$

Here, u_{II} denotes the formation rate of Pop II stars expressed in terms of the resulting SN rate (see §5.2.3.4), while $a_{\star}(t)$ is the fraction of still surviving stars in a stellar generation formed at time t and \tilde{c}_k is a normalization factor (note that $\tilde{c}_k \neq c_k$). The age of the system is set to $\tau_{\text{H}} \simeq 10^{10}$ yr to account for late-time star formation in the Milky Way halo. Equation (5.6) is used to predict the Pop III contribution to the amount of metals in the gas from which the low-mass stars were formed. Following Karlsson (2005, 2006), we make use of Equations (5.3)–(5.6) to calculate the predicted relative number density of still surviving ($m \leq 0.8 M_{\odot}$) metal-poor stars with any given chemical composition. These density functions are then analyzed and compared to observations. In the remainder of this section, we will define and discuss the

other model parameters.

5.2.3.2 Density Evolution

Due to the inability of our chemical enrichment model to account for spatial variations, except in a statistical sense, we will adopt the average density evolution $n = n(t)$ of a spherically collapsing $10^8 M_\odot$ halo embedded in an expanding universe. We assume that the density of the halo follows the top-hat model for its collapse and virialization (e.g., Padmanabhan 2002; Bromm et al. 2002). After virialization at $z_{\text{vir}} \simeq 10$, a constant density of $n = n_{\text{vir}} = 0.1 \text{ cm}^{-3}$ is assumed, where n_{vir} denotes the average density at virialization.

5.2.3.3 Initial Mass Functions and Stellar Yields

The relative distribution by mass for metal-free and extremely metal-poor stars is largely unknown. This is especially true for the high-mass end of the IMF since all metal-free, massive stars in our part of the universe are long gone. We must therefore resort to theoretical predictions. We shall assume that the IMF of the metal-enriched Pop II follows that of the solar neighborhood, which can be approximated with a broken power-law, i.e., $dN/dm \equiv \phi(m) \propto m^\alpha$, with a Salpeter-like exponent of $\alpha = -2.3$ above $m = 0.5 M_\odot$ and a shallower slope of $\alpha = -1.3$ below this mass (Kroupa 2001). Very massive stars exploding as PISNe are assumed to form exclusively in metal-free gas and are therefore not formed in the Pop II mode (but see

Langer et al. 2007). Conversely, low-mass stars are only allowed to form in the Pop II mode. In addition, following Bromm & Loeb (2003), low-mass star formation is restricted to occur in regions with efficient cooling, i.e., where the abundance of carbon and/or oxygen is high enough. To include this effect, we adopt the metallicity criterion D_{trans} , introduced by Frebel et al. (2007), which takes into account the simultaneous cooling by O I and C II. Hence, low-mass stars are only able to form in gas with C and O abundances such that

$$D_{\text{trans}} = \log_{10} (10^{[\text{C}/\text{H}]} + 0.3 \times 10^{[\text{O}/\text{H}]}) > -3.5 .$$

The special initial conditions in the first collapsing minihalos presumably favored the formation of a population of very massive stars. Although these conditions are not always met in metal-free gas in general (see, e.g., Johnson & Bromm 2006; Padoan et al. 2007), the top-heaviness of the primordial IMF seems to persist. In particular, the apparent lack of metal-free stars in the present Galactic halo indicates that primordial low-mass star formation was highly suppressed (e.g., Karlsson 2005; Tumlinson 2006). For the Pop III IMF, we shall assume that stars below $10 M_{\odot}$ were not able to form. Above this limit, stars in the mass range of core collapse SNe are assumed to be distributed in the same way as for Pop II, i.e., as a power-law with a slope of $\alpha = -2.3$. Note that although Padoan et al. (2007) derive a primordial/metal-poor IMF with a slope which asymptotically approaches $\alpha = -3.5$ at the high-mass end, the slope in the core collapse range is significantly shallower.

As regards the shape of the unknown, metal-free very-high-mass IMF, we take a conservative approach and assume that stars in the mass range of PISNe are all formed with equal probability, independent of their individual masses. As a measure of the fraction of very massive Pop III stars, we introduce the parameter β . This parameter is defined as the ratio between the number of PISNe and the total number of exploding stars in a Pop III generation. With this definition, β is a lower limit to the original fraction of very massive Pop III stars, as a fraction of these stars will become black holes by direct collapse instead of exploding as PISNe (e.g., Heger et al. 2003).

In the following, β will be considered as a free model parameter, and, as we shall see, it is also one of the parameters to which the result is most sensitive. If $\beta = 1$, all Pop III stars were formed as very massive stars ending their lives as PISNe, while if $\beta = 0$, no PISN ever occurred in the early universe. In later sections, we shall constrain β by comparing observations with model results. It is, however, possible to estimate the plausible range for β from a theoretical point of view. By extrapolating the Galactic IMF (Kroupa 2001) to very high masses, β is estimated to be 0.032. Alternatively, using the more realistic primordial IMF by Padoan et al. (2007), a β of 0.017 is obtained. Greif & Bromm (2006) estimated the mass fraction of metal-free stars that went into very massive stars by considering the relative number of minihalos and atomic-cooling halos in the early universe. They derived a value of 5 – 10% by mass, which translates into a $\beta \simeq 0.005 - 0.01$, based on the idea that the PISNe and core collapse SNe were formed in different types of

halos, the former in minihalos and the latter in atomic halos.

We consider here only those chemical elements which are predominantly synthesized in massive stars, e.g., calcium and iron. We will not take into account the limited enrichment by intermediate-mass stars and thermonuclear (Type Ia) SNe, whose main contributions to the chemical enrichment occur at a considerably later stage in the history of the Milky Way. The ejection of newly synthesized material will be restricted to two mass ranges: that of core collapse SNe and that of PISNe (Heger & Woosley 2002). The stellar yields of core collapse SNe, with progenitor masses in the range $13 \leq m/M_{\odot} \leq 40$, are taken from the new calculations by Nomoto et al. (2006), while the yields of the PISNe ($140 \leq m/M_{\odot} \leq 260$) are taken from Heger & Woosley (2002). Core collapse SNe with progenitor masses $\leq 13 M_{\odot}$ are believed to synthesize very few heavy elements (see, e.g., Nomoto 1987; Mayle & Wilson 1988) and are neglected here. As an estimate of the uncertainty in the results due to uncertainties in the nucleosynthesis calculations (see §5.2.4.4), we also ran a simulation using the yields of PISNe by Umeda & Nomoto (2002).

5.2.3.4 Star Formation Rates

As discussed above, the metal-free, Pop III mode of star formation likely differed from that of Pop II, occurring in metal enriched gas. We will account for this distinction by introducing one SFR for the Pop III mode and a different one for the Pop II mode. Below, these SFRs will be displayed in terms of their respective SN rate in units of $\text{kpc}^{-3} \text{ Myr}^{-1}$. Stars not ejecting

any metals, e.g., stars subject to direct black hole formation, are not included in these rates. Again, low-mass star formation is considered to occur in Pop II only, with the low-mass star formation rate closely following that of Pop II SNe.

We carried out a smoothed particle hydrodynamics (SPH) simulation of the assembly of a $10^8 M_{\odot}$ halo, including star formation without feedback, in order to estimate the star formation rate for Pop III stars forming in minihalos which are later incorporated into the larger halo. The simulation is set up similarly to those conducted in Johnson et al. (2007), employing a cosmological box of comoving length 660 kpc. We track the sites where the primordial gas is able to collapse to form Pop III stars in this simulation (Fig. 5.3), and we thereby estimate the Pop III star formation rate within the volume being assembled into the $10^8 M_{\odot}$ halo, assuming that a single Pop III star forms in each of the collapsing minihalos (e.g., Yoshida et al. 2006). In the simulation, the first star forms at a redshift of $z \simeq 23$. We find that the Pop III star formation rate, here expressed as the resulting SN rate, is $\sim 0.04 \text{ kpc}^{-3} \text{ Myr}^{-1}$ (physical) within the region which is finally virialized in this halo. We thus use this value for the normalization of the Pop III star formation rate. We note that the neglect of local radiative and mechanical feedback in this simulation is not likely to greatly affect the value that we find for the star formation rate (see Susa & Umemura 2006; Ahn & Shapiro 2007; Johnson et al. 2007; Greif et al. 2007; but see Whalen et al. 2007).

The star formation rate is assumed to be proportional to the gas density

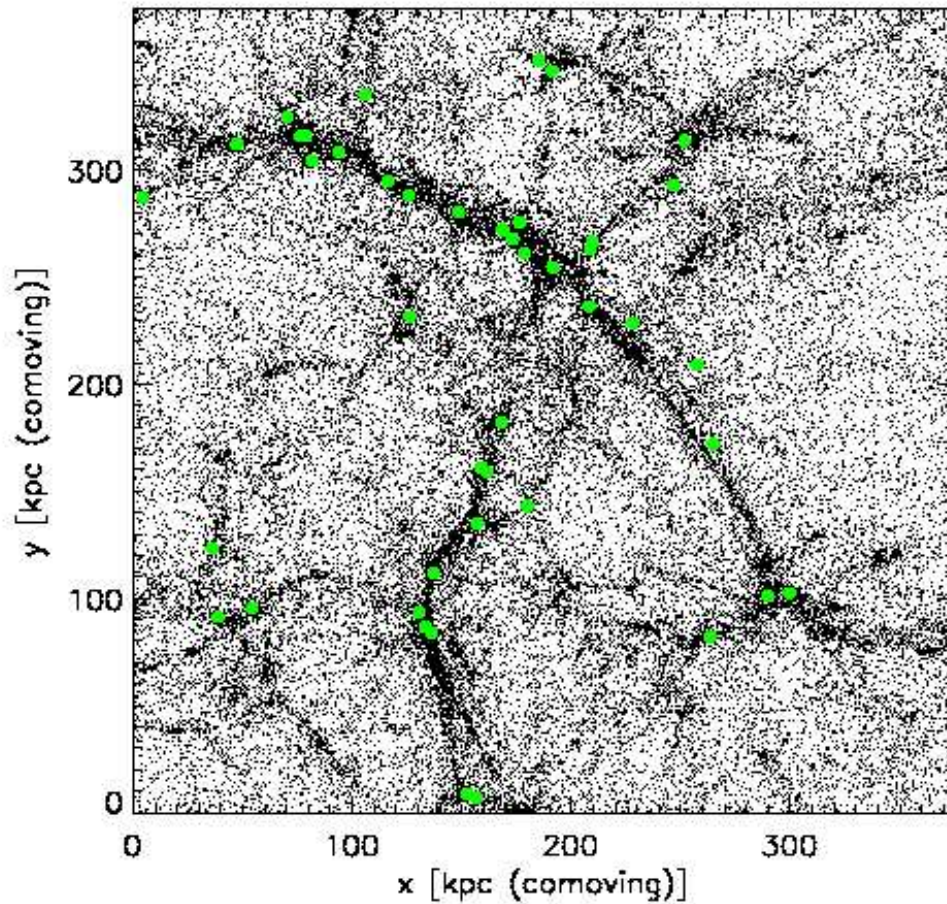


Figure 5.3: Sites of Pop III star formation in our SPH simulation. Shown here in projection is the density field around the $\sim 10^8 M_{\odot}$ system in our cosmological box at redshift $z \sim 10$. The green dots indicate the sites where the primordial gas collapses into minihalos and so allows the formation of Pop III stars. We estimate the resulting star formation rate of Pop III stars by assuming that a single Pop III star forms in each of these minihalos.

$n(t)$. Hence,

$$u_{\text{III}}(t) = u_{\text{III},0} \times Q_{\text{p}}(t) \left(\frac{n(t)}{0.1 \text{ cm}^{-3}} \right), \quad (5.7)$$

and

$$u_{\text{II}}(t) = u_{\text{II},0} \times (1 - Q_{\text{p}}(t)) \left(\frac{n(t)}{0.1 \text{ cm}^{-3}} \right), \quad (5.8)$$

where u_{III} and u_{II} denote the Pop III and Pop II SN rate, respectively (Fig. 5.4), and Q_{p} denotes the volume filling factor of primordial gas. The Pop III rate is normalized to $u_{\text{III},0} = 0.04 \text{ kpc}^{-3} \text{ Myr}^{-1}$ (see above). For metal enriched gas, the star formation efficiency is assumed to be 10 times higher. The Pop II rate is therefore normalized to $u_{\text{II},0} = 0.4 \text{ kpc}^{-3} \text{ Myr}^{-1}$ which is close to the average SN rate in the galactic halo, derived from chemodynamical modeling (Samland et al. 1997). The fraction of stars predominantly enriched by PISNe will not be very sensitive to these normalizations (see Table 5.2). We assume that star formation begins at $z = 30$, to account for the rare high- σ peaks in the dark matter distribution.

In the above expressions, the presence of the factor Q_{p} is important as it regulates the amount of gas available for both the Pop III and the Pop II mode of star formation. It is controlled by the Pop III SFR via Equation (5.5). Hence, for $k = 0$,

$$Q_{\text{p}}(t) \equiv w_{\text{III}}(0, t) = e^{-\mu_{\text{III}}(t) - \mu_{\text{III}}(t)^2/4}. \quad (5.9)$$

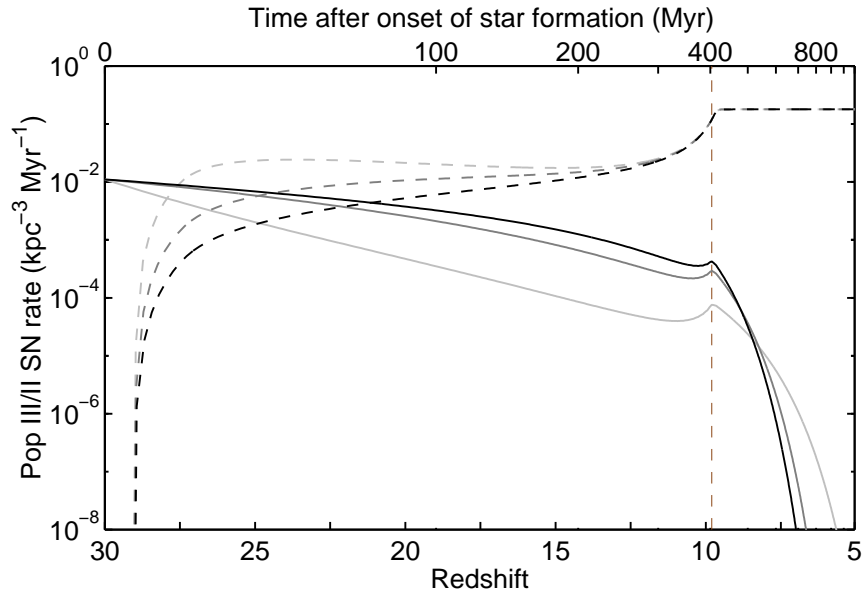


Figure 5.4: Adopted Pop III (solid lines) and Pop II (dashed lines) SN rates for $\beta = 1$, 0.1, and 0.01 (darker lines correspond to smaller β). The dashed, vertical (brown) line marks the virialization redshift of the $10^8 M_{\odot}$ halo. In general, as an increasing volume of space becomes metal enriched, the Pop III rates decrease while the Pop II rates increase. The bump in the Pop III rates at $z = 10$ is due to a sharp rise in density prior to virialization. The small delay in the rise of the Pop II rates is due to the finite lifetimes of Pop II core collapse SNe.

Since the Pop III SN rate depends on the available amount of primordial gas which, in turn, is determined by the rate of metal enrichment, u_{III} and Q_{p} are coupled via the expression for μ_{III} :

$$\begin{aligned} \mu_{\text{III}}(t) &= \beta \int_0^t V_{\text{mix}}^{\gamma}(t-t') u_{\text{III}}(t') dt' \\ &+ (1-\beta) \int_0^t V_{\text{mix}}^{\text{cc}}(t-t') u_{\text{III}}(t') dt'. \end{aligned} \quad (5.10)$$

In this expression, the contribution from PISNe and core collapse SNe are distinct since σ_E , which controls the initial expansion of the ejecta, differs between the two types of SNe (see above). Here, V_{mix}^{γ} and $V_{\text{mix}}^{\text{cc}}$ denote the mixing volumes for PISNe and core collapse SNe, respectively, while β , defined in §5.2.3.3, denotes the fraction of PISNe in Pop III.

5.2.4 Results

In this section, we shall discuss our results for the chemical enrichment during the assembly of atomic-cooling halos and compare them with recent observations. We would like to emphasize that not all stars belonging to the Milky Way halo were formed in atomic cooling halos, in particular the stars at the metal-rich end (cf. Robertson et al. 2005). However, a significant fraction of the stars below $[\text{Ca}/\text{H}] = -2$ and a majority of the second generation stars

presumably originated from this type of halo.³ If so, they are likely to be found over the entire Galactic halo (Scannapieco et al. 2006). With this in mind, we will make no distinction in origin between our simulated stars and the field stars observed in the Galactic halo.

Instead of iron, we choose calcium as the reference element for the metallicity of the stars. We do so for two reasons. First, the strong Ca II K resonance line is commonly used as metallicity indicator (Beers et al. 1990) in surveys of metal-poor stars, such as the HK survey (Beers et al. 1992) and the Hamburg/ESO survey (Wisotzki et al. 2000). The much weaker Fe lines will remain undetected in low-quality survey spectra, although they can be detected by taking high-resolution spectra. This is of importance since the vast majority of the most metal-poor stars known thus were originally recognized as being metal-poor on the basis of their Ca abundance, not their Fe abundance. The second reason we choose calcium is that the iron yield is, to a larger extent than calcium, affected by the unknown amount of fall-back in core collapse SNe and it varies by more than 3 orders of magnitude over the PISN mass range. The Ca yield, on the other hand, varies by merely 1 order of magnitude (Heger & Woosley 2002; Umeda & Nomoto 2002). For the employed observational data, either existing Ca abundances were used or, in case of the observed Galactic halo MDF, an offset of $[\text{Ca}/\text{Fe}] = +0.4$ dex was applied to convert from Fe abundances to Ca abundances. This offset is based

³ $[\text{A}/\text{B}] = \log_{10}(N_{\text{A}}/N_{\text{B}})_{\star} - \log_{10}(N_{\text{A}}/N_{\text{B}})_{\odot}$, where N_X is the number density of element X .

on the average Ca excess (Pagel & Tautvaišienė 1995) observed in Galactic halo stars (see e.g., Cayrel et al. 2004), although there are outlier stars in the lowest metallicity range which deviate from the mean $[\text{Ca}/\text{Fe}] = +0.4$. Apart from the offset, however, the shape of the Galactic halo MDF probably doesn't change much whether Fe or Ca is used as the metallicity indicator.

5.2.4.1 Comparison with Observed Metal-Poor Stars

In Figure 5.5, we show the probability density function of low-mass stars in the $[\text{Fe}/\text{Ca}] - [\text{Ca}/\text{H}]$ plane from a simulation in which 10% by number (i.e. $\beta = 0.1$), or about 50% by mass, of all Pop III stars were allowed to explode as PISNe. The agreement between the model and the observations of Galactic field stars by Cayrel et al. (2004) and Cohen et al. (2004) is satisfactory. It should be noted that the full distribution displayed in the upper panel of Figure 5.5 is effectively unaltered for any $\beta \leq 0.1$.

The surprisingly small star-to-star scatter and the lack of evolution in the scatter that is observed in various abundance ratios for well defined samples of extremely metal-poor Galactic halo stars (e.g., Cayrel et al. 2004; Arnone et al. 2005; Barklem et al. 2005) is not fully understood. Such a small scatter could be an indication of extremely short mixing timescales and a well mixed ISM already at very early times. However, as evident from Figure 5.5, the small scatter is as well reproduced by our model over the entire metallicity regime. Despite the relatively slow mixing assumed in our model, the small dispersion is explained by a selection effect favoring contributions from SNe in

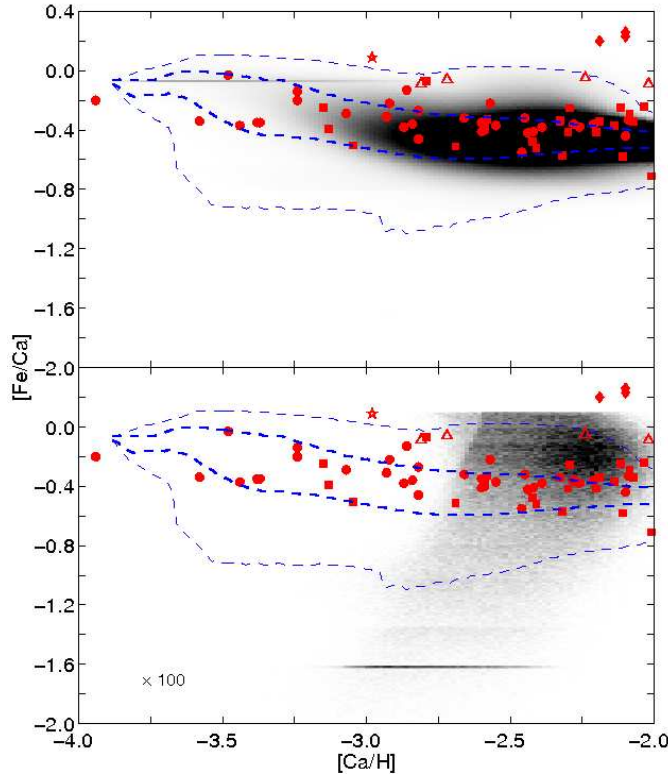


Figure 5.5: Predicted distributions (shaded areas) of low-mass stars in the $[\text{Fe}/\text{Ca}] - [\text{Ca}/\text{H}]$ plane for $\beta = 0.1$. *Upper panel:* The full distribution. Filled (red) circles are observations of giants in the Galactic halo by Cayrel et al. (2004), filled (red) squares are observations of dwarfs by Cohen et al. (2004), filled (red) diamonds are three field stars depleted in n-capture elements (Ivans et al. 2003), while open (red) triangles are observations of giants in dwarf spheroidal galaxies (Shetrone et al. 2001), and the (red) star is Draco 119 (Fulbright et al. 2004). The dashed, thick and thin (blue) lines indicate, respectively, the 1σ (innermost 68.3%) and 3σ (innermost 99.7%) cosmic scatter in the simulation. *Lower panel:* The partial distribution of simulated stars for which $> 90\%$ of the total atmospheric Ca abundance is synthesized in PISNe. This distribution is multiplied by a factor of 100. The observations and the dispersion of the full distribution are plotted for comparison. Note, the mildly enhanced density of simulated stars at $[\text{Fe}/\text{Ca}] \simeq -1.6$ originates from a nearly constant Fe/Ca yield ratio in the mass range $160 \leq m/M_{\odot} \leq 170$.

a certain mass range ($13 \leq m/M_{\odot} \leq 20$, in this particular case) for the most metal-poor stars and by the averaging of a large number of contributing SNe at higher metallicities (Karlsson & Gustafsson 2005). Ultimately depending on the stellar yields, a small star-to-star scatter can thus be realized without invoking unrealistically short mixing timescales in the early ISM.

5.2.4.2 Characteristics of PISN-Dominated Stars

In the lower panel of Figure 5.5, only those simulated low-mass stars are displayed for which $> 90\%$ of the total atmospheric calcium abundance was synthesized in PISNe. This regards the abundance originally present in the gas out of which the stars were formed and not the abundance at late-stage evolution, although the difference should be negligible for Ca. Henceforth, such stars will be referred to as PISN-dominated stars. From the results depicted in Figure 5.5, three conclusions regarding the chemical legacy of PISNe can immediately be drawn. First and foremost, the low-mass stars with a dominant contribution from PISNe, as reflected by the Ca abundance, are located at significantly higher $[\text{Ca}/\text{H}]$ than the most Ca deficient stars in the simulation, which are found at $[\text{Ca}/\text{H}] \simeq -4$. The PISN-dominated stars are instead found in the range $-3 \leq [\text{Ca}/\text{H}] \leq -2$, with a maximum around $[\text{Ca}/\text{H}] \simeq -2.3$. This prediction is at variance with the classical picture in which the chemical signatures of the first, very massive stars are anticipated to be found in the most metal-poor regime. This is exactly the effect illustrated in Figure 5.2 and described in §5.2.2. Looking for the stars with the lowest abundances of

Ca (or Fe) may thus not be the best way to find the relics of the first PISNe.

Second, the fraction of PISN-dominated stars in the halo is predicted to be small. As illustrated in the lower panel of Figure 5.5, the distribution of PISN-dominated stars has to be multiplied with a factor of 100 in order to be detected on the same scale as the total distribution, shown in the upper panel. Even for a relatively large β of 0.1 (i.e., $\sim 50\%$ by mass), the total fraction of PISN-dominated stars below $[\text{Ca}/\text{H}] = -2$ is merely $\sim 2 \times 10^{-3}$, or about one star in 500. For lower β , this fraction decreases further (see §5.2.4.3).

Third, as noted in §5.2.2, the chemical signature of PISNe distinctly differs from that of the less massive core-collapse SNe. This provides an opportunity to identify outliers, at relatively high metallicities, as possible PISN-enriched, second generation stars. As shown in Figure 5.5 (lower panel), PISN-dominated stars are predicted to be found both above and below the IMF-averaged value of $[\text{Fe}/\text{Ca}] \simeq -0.4$. Noticeably, none of the stars in the samples by Cayrel et al. (2004) and Cohen et al. (2004) show a large enough deviation from the mean $[\text{Fe}/\text{Ca}]$, and other abundance ratios, to be classified as potential PISN-enriched stars. However, the four stars belonging to the Draco, Ursa Minor, and Sextans dwarf spheroidal (dSph) galaxies have a relatively high $[\text{Fe}/\text{Ca}] \simeq -0.1$. These gas-poor satellite galaxies primarily consist of old and metal-poor stars and were presumably formed at an early stage, as a result of the collapse of dark-matter halos of $\leq 10^9 M_{\odot}$.

Could these dSph stars be second generation, PISN-dominated stars? This seems unlikely. The low α -element/iron ratios are generally attributed

to Type Ia SNe in connection to lower SFRs in these systems (e.g., Matteucci 2003), and, while no contribution of s-process elements by asymptotic giant branch stars is detected in dSph stars below $[\text{Fe}/\text{H}] \simeq -1.8$ the high Ba/Y and low Y/Eu ratios (as well as low α/Fe) could be explained by the absence of elements synthesized in the α -process (Venn et al. 2004 and references therein), suggested to occur in hypernovae (Nakamura et al. 2001). A few other, curious outliers such as Draco 119 (Fulbright et al. 2004) and BD + 80° 245, G4-36, and CS 22966-043 studied by Ivans et al. (2003), will be further discussed in §5.2.5.

In the simulations, the distribution of stars with a dominant contribution from PISNe peaks around $[\text{Ca}/\text{H}] \simeq -2.5$, or even higher (see Fig. 5.5, lower panel and Fig. 5.6, upper panel). In fact, the majority of PISN-dominated stars are predicted to be found above $[\text{Ca}/\text{H}] = -2.6$ (corresponding to $[\text{Fe}/\text{H}] = -3$). This is the upper limit for which the Hamburg/ESO survey is considered to be complete (see Fig. 5.6, upper panel). A significant fraction of the second generation stars may therefore have a chance to remain undetected in the Hamburg/ESO survey, not because they are too Ca-poor but because they are too Ca-rich. Note the deficit above $[\text{Ca}/\text{H}] = -2.6$ in the observed MDF which, to a large extent, has to be attributed to this intended observational bias against metal-rich stars (Fig. 5.6, upper panel). With this taken into account, the observed and predicted MDFs, in particular the one with $\beta = 0.01$, agree to within the stated uncertainties. The lower panel of Figure 5.6 shows the fraction of PISN-dominated stars for $\beta = 0.1$ (dark blue

line) and $\beta = 0.01$ (light blue line). Evidently, the fraction also peaks significantly above the cut-off of the observed MDF at $[\text{Ca}/\text{H}] \sim -4$ and goes to zero approaching this cut-off. We have additionally run a simulation with iron as the reference element. The corresponding distribution of PISN-dominated stars (here defined such that $> 90\%$ of the Fe is synthesized in PISNe) peaks at $[\text{Fe}/\text{H}] \simeq -2.5$, which concurs with the above result that these stars are to be found at relatively high metallicities. In this simulation, there is a weak tail of PISN-dominated stars towards low metallicities, originating from the least massive PISNe. However, for $\beta = 0.01$, merely ~ 1 star in 1000 show a clear PISN signature at $[\text{Fe}/\text{H}] = -4$, nearly a factor of 100 less than around the peak at $[\text{Fe}/\text{H}] = -2.5$.

5.2.4.3 Observational Constraints on Pop III Supernovae

As it appears from Figure 5.6, the fraction of PISN-dominated stars depends strongly on the parameter β , the fraction of Pop III stars becoming PISNe, which is to be expected. This dependence may be used to put constraints on the number of PISN-dominated stars expected to be found in the metal-poor Galactic halo and, conversely, to put observational upper limits on β itself. Figure 5.7 shows the integrated fraction of PISN-dominated stars as a function of β . This fraction, termed a_{γ} , is defined as the number of PISN-dominated stars below $[\text{Ca}/\text{H}] = -2$ divided by the total number of stars below $[\text{Ca}/\text{H}] = -2$. The fractions displayed in Figure 5.7 are based on the assumption that a distinct PISN signature is present over the entire PISN

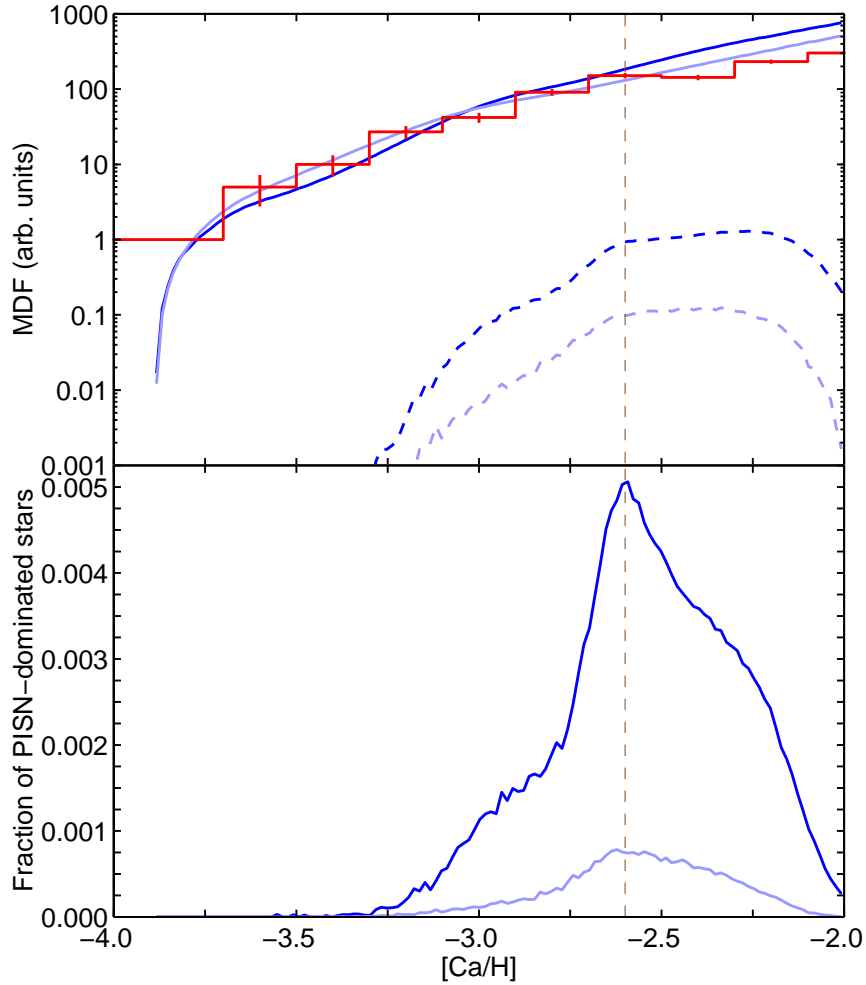


Figure 5.6: Predicted metallicity distribution functions as measured by $[\text{Ca}/\text{H}]$ for $\beta = 0.1$ (dark blue lines) and $\beta = 0.01$ (light blue lines). *Upper panel:* The solid lines denote the total MDFs while the dashed lines denote the MDFs of PISN-dominated stars, for which $> 90\%$ of the Ca originate from PISNe. The binned data (red line) are the observed (not completeness corrected) distribution of Galactic halo stars from the Hamburg/ESO survey by Beers et al. (2005), where the vertical lines indicate the (1σ) stochastic uncertainty. Note that these data are shifted $+0.4$ dex. *Lower panel:* The fraction of PISN-dominated stars. The majority of these stars fall above the upper limit of $[\text{Ca}/\text{H}] = -2.6$ (dashed brown line), the range where the Hamburg/ESO survey is incomplete.

Table 5.1: Fraction of PISN-enriched stars as a function of level of PISN-enrichment.

Level of PISN-enrichment ^a	Fraction of PISN-enriched stars ^b
> 1%	6.97×10^{-2}
> 10%	2.34×10^{-2}
> 50%	3.60×10^{-3}
> 90%	3.04×10^{-4}
> 99%	7.35×10^{-5}
> 99.9%	6.75×10^{-5}

^a As measured by the amount of Ca originating from PISNe.

^b All fractions are calculated for $\beta = 0.01$.

mass range. In the remainder of the paper, we shall further explicitly assume that this signature is detectable in stars if, and only if, > 90% of the atmospheric Ca abundance originates from the PISNe. In Figure 5.7, we have also indicated the predicted fractions $a_{\gamma\gamma}$ corresponding to 99% and 99.9% PISN-enrichment (see also Table 5.1). These results will be briefly discussed later in this section.

The number of observed Galactic halo stars below $[\text{Ca}/\text{H}] = -2$ for which abundance analyses based on high-resolution spectroscopy exists is roughly 600 (N. Christlieb, priv. comm.). None of these ~ 600 stars appear to show a dominant PISN signature. If so, we estimate that $\beta < 0.07$ (see Fig. 5.7), which corresponds to a mass fraction of very massive Pop III stars of $\leq 40\%$.

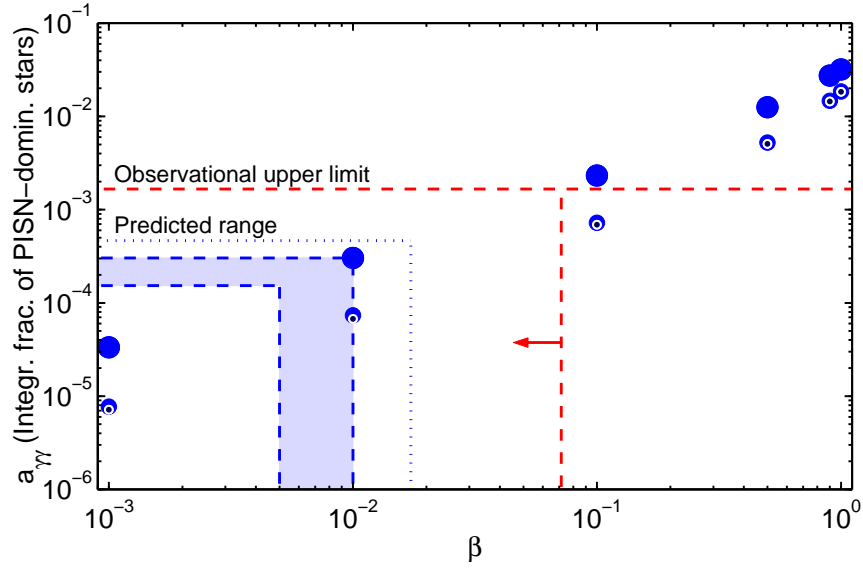


Figure 5.7: The predicted integrated (total) fraction of PISN-dominated stars below $[\text{Ca}/\text{H}] = -2$ as a function of β , corresponding to $> 90\%$ (big blue dots), $> 99\%$ (medium sized, blue dots), and $> 99.9\%$ (small, dark blue dots) PISN-enrichment. The dashed (red) lines indicate the observational upper limit of β , assuming that none of the ~ 600 Galactic halo stars with $[\text{Ca}/\text{H}] \leq -2$ for which high-resolution spectroscopy is available show any signature of PISNe (N. Christlieb, priv. comm.). The dotted (blue) line and shaded (blue) area denote the predicted range of a_{γ} anticipated from the data of Padoan et al. (2007) and Greif & Bromm (2006), respectively. If nothing else stated, it is assumed that the PISN signature is detectable in Galactic halo stars with $> 90\%$ PISN-enrichment.

Here, we disregard Draco 119 (Fulbright et al. 2004) and the group of field stars studied by Ivans et al. (2003) as PISN-dominated, second generation stars (see §5.2.5). An upper limit of $\beta = 0.07$ is consistent with the predicted range of β derived by Greif & Bromm (2006) and the β derived from the IMF by Padoan et al. (2007), which all fall in the range $0.005 \leq \beta \leq 0.02$. Conversely, as indicated in Figure 5.7, this range corresponds to a range in $a_{\gamma\gamma}$ of $1.5 \times 10^{-4} \leq a_{\gamma\gamma} \leq 5 \times 10^{-4}$, which, at face value, means that $\sim 3 - 10$ times as many metal-poor (i.e., $[\text{Ca}/\text{H}] \leq -2$) Galactic halo stars need to be analyzed in order to find a single second generation star with $> 90\%$ of its Ca originating from primordial PISNe. In §5.2.5, these results will be discussed further.

Also shown in Figure 5.7 are the predicted fractions of stars that are pre-enriched to at least 99% (medium sized, blue dots) and 99.9% (small, dark blue dots) by PISNe. These will be referred to as purely PISN-enriched stars. Although the number of such stars is smaller than the number of stars in which up to 10% of the metals (Ca) are allowed to originate from core collapse SNe, it is not radically smaller. In the range $0.005 \leq \beta \leq 0.02$, e.g., the predicted fraction of purely PISN-enriched stars is only smaller by factor of ~ 4 (see also Table 5.1). Moreover, assuming that none of the ~ 600 stars below $[\text{Ca}/\text{H}] = -2$, for which high-resolution spectroscopic data are available, are purely PISN-enriched stars, the range of possible values for β is constrained to be < 0.2 . As indicated above, a slightly stronger constraint may be placed on β if the reasonable assumption is being made that none of

these stars has a PISN-enrichment which exceeds 90%. However, due to the increasing risk of making false identifications, β may not be constrained much further by allowing for lower levels of PISN-enrichment than 90%. Table 5.1 shows the predicted fraction of stars formed from gas pre-enriched by PISNe to various levels, for $\beta = 0.01$. Clearly, the fraction of PISN-enriched stars increases with decreasing level of PISN-enrichment. However, even though the expected number of stars with, e.g., a PISN-enrichment of $> 50\%$ is ~ 10 times more than the corresponding number with $> 90\%$ PISN-enrichment, we would in practice not gain much as it would most likely be very difficult to correctly identify many of the less PISN-dominated stars. Note also that for $\beta = 0.01$, less than 10% of all stars below $[\text{Ca}/\text{H}] = -2$ are formed from gas enriched to any level by PISNe.

5.2.4.4 Parameter Dependence and Sensitivity

We have performed a number of simulations where we varied the values of several model parameters, in order to illustrate the sensitivity of our results to the uncertainties in these parameters. The SFR is a crucial ingredient in the model and we have varied both the Pop III and Pop II SN rates by changing $u_{\text{III},0}$ and $u_{\text{II},0}$, respectively. The turbulent diffusion coefficient D_t in the early ISM is difficult to estimate. According to Bateman & Larson (1993), the diffusive mixing of matter in the cold, neutral medium in the Galactic disk (e.g., through molecular cloud collisions) occurs on a similar time scale as the one adopted here, while the mixing should be substantially faster in hot,

ionized media. Alternatively, Pan & Scalo (2007) developed a "slow" mixing model with inefficient (i.e., low D_t) diffusion to explain the apparent existence of primordial gas at relatively low ($z \sim 3$) redshift. We have varied D_t in our model to map out the effect.

The results of the simulations are summarized in Table 5.2, which shows the dependence of $a_{\gamma\gamma}$ on $u_{\text{III},0}$, $u_{\text{II},0}$, and D_t , respectively. In all simulations, β is fixed to 0.01. The impact on $a_{\gamma\gamma}$ when altering the Pop III (col. 1) and Pop II (col. 2) SN rates is non-trivial, with, respectively, a local maximum and a local minimum in the value of $a_{\gamma\gamma}$ appearing within the examined ranges of the values for these rates. The dependence on D_t (col. 3) is less complex. We shall not discuss these dependences in detail but notice that $a_{\gamma\gamma}$ is roughly proportional to $\int u_{\text{III}} u_{\text{II}} dt / \int u_{\text{II}}^2 dt$ and that the Pop III and Pop II rates are coupled through Q_p (see eqs. (5.7)–(5.10)). In particular, the counter-intuitive decrease in $a_{\gamma\gamma}$ with an increasing Pop III SN rate above $u_{\text{III},0} = 1.33 \times 10^{-2} \text{ kpc}^{-3} \text{ Myr}^{-1}$ ($= 1/3$ of the adopted $u_{\text{III},0}$) may be understood from the fact that an initially high Pop III rate more efficiently suppresses subsequent formation of Pop III stars, while it simultaneously promotes the formation of Pop II stars, as a consequence of the change in the fraction of primordial gas. Note that a similar effect occurs when β is increased, indicated in Figure 5.4.

The overall change in $a_{\gamma\gamma}$ over the entire two decade range in $u_{\text{III},0}$, as well as in $u_{\text{II},0}$, is merely a factor of ~ 4 , which is quite moderate. The sensitivity on D_t is higher, a factor of ~ 30 over the examined range. We also ran one simulation where the SFR was set proportional to the square of the

Table 5.2: The dependence of $a_{\gamma\gamma}$ on model parameters. The three parameters which were varied are listed in the top row; from left to right, these are the Pop III SN rate, the Pop II SN rate, and the turbulent diffusion coefficient. The leftmost column shows the factor by which these parameters were changed from their fiducial values, and the resulting values for $a_{\gamma\gamma}$ are shown in the three rightmost columns below the specific parameter which was varied.

Parameter ^a	$u_{\text{III},0}$	$u_{\text{II},0}$	D_t
$\times 10$	1.07×10^{-4}	7.35×10^{-4}	6.89×10^{-5}
$\times 3$	1.57×10^{-4}	1.99×10^{-4}	7.98×10^{-5}
$\times 1^{b,c}$	3.04×10^{-4}	3.04×10^{-4}	3.04×10^{-4}
$\times 1/3$	4.78×10^{-4}	4.59×10^{-4}	1.02×10^{-3}
$\times 1/10$	4.01×10^{-4}	3.41×10^{-4}	1.92×10^{-3}

^aThe fiducial values of the model parameters are discussed in §5.2.3. All fractions are calculated for $\beta = 0.01$.

^b $a_{\gamma\gamma} = 4.78 \times 10^{-4}$, adopting the set of PISN yields calculated by Umeda & Nomoto (2002).

^c $a_{\gamma\gamma} = 6.03 \times 10^{-4}$, assuming that $\text{SFR} \propto \rho^2$.

density instead of the normal linear dependence, and one where we changed the set of PISN yields to those by Umeda & Nomoto (2002). In each of these two runs, $a_{\gamma\gamma}$ changed by less than a factor of 2 (see footnote b and c in Table 5.2).

The data presented in Table 5.2 are a measure of the uncertainty in our calculations. Evidently, the result is insensitive to the SFR and PISN yields, while it is relatively sensitive to the amount of mixing in the ISM. If we, e.g., adopt a 10 times smaller turbulent diffusion coefficient, the fraction of PISN-dominated stars is increased by a factor of 6. Still, even for such a low

D_t , the range of β predicted by Greif & Bromm (2006) would be consistent with the observational upper limit. We would like to emphasize that in all the runs that we have carried out, the vast majority of the PISN-dominated stars have significantly higher Ca abundances than the most Ca-poor stars in the simulations, irrespective of the predicted value of a_γ . Moreover, for all the parameters that we have varied, β remains the parameter to which the results are most sensitive (cf. Fig. 5.7). The above findings indicate two points: first, due to the sensitivity on β , we have the means to measure the frequency of very massive stars in the early universe from observations of large, homogeneous samples of metal-poor stars in the Milky Way halo. Second, due to the insensitivity on model parameters apart from β , our results and the conclusions based on these results should be relatively robust.

5.2.5 Discussion and Summary

We have shown that Milky Way halo stars born in atomic cooling halos of $M \sim 10^8 M_\odot$ and displaying a chemical abundance pattern characterized by that of Pop III PISNe are to be found at significantly higher metallicities than where the most metal-poor stars have been found. Consequently, although stars in the metal-poor tail of the MDF, like the extremely iron-deficient stars HE 0107-5240 (Christlieb et al. 2002) and HE 1327-2326 (Frebel et al. 2005), are very important for the understanding of the star formation process (e.g., Bromm & Loeb 2003; Umeda & Nomoto 2003; Tumlinson 2007) and feedback mechanisms (e.g., Karlsson 2006) in the early universe, they seem to

tell us little about primordial PISNe. The majority of Pop II stars with a dominant contribution from PISNe are predicted to have Ca abundances in excess of $[\text{Ca}/\text{H}] = -2.6$, the upper limit for which the Hamburg/ESO survey of metal-poor stars is considered to be complete. This implies that a significant fraction of the PISN-dominated stars may have escaped detection, not because they are too Ca-poor but because they are too Ca-rich. The number fraction of very massive Pop III stars exploding as PISNe is estimated to be $\beta < 0.07$ ($\leq 40\%$ by mass), assuming that currently no Galactic halo star below $[\text{Ca}/\text{H}] = -2$ with available detailed abundance analysis shows a chemical signature characteristic of PISNe. This result is consistent with the theoretical prediction of $0.005 \leq \beta \leq 0.02$, which corresponds to a handful of PISN-dominated, second generation stars in a sample of 10 000. The number of purely PISN-enriched stars is predicted to be a factor of ~ 4 smaller, assuming this range of β .

In an interesting paper, Salvadori et al. (2007) also discuss the existence of second generation stars and their location in the MDF. Their stochastic model of chemical enrichment differs from ours in a number of aspects. Firstly, they model the chemical evolution of the Galaxy as a whole based on the merger-tree approach (cf. Tumlinson 2006), while we focus on the evolution of atomic cooling halos using the mixing volume picture. They also assume that all Pop III stars are very massive, while we allow for less massive Pop III star formation as well, controlled by the parameter β . Hence, in their models with $Z_{\text{crit}} > 0$ (for $Z_{\text{crit}} = 0$, no PISNe are formed), all second

generation stars are formed from gas only enriched by PISNe. Finally, we note that while our chemical enrichment model accommodates the important contribution of metals ejected by the supernovae from Pop III stars formed in minihalos, with masses less than $10^8 M_{\odot}$ (see Bromm et al. 2003; Greif et al. 2007), this contribution is neglected in Salvadori et al. (2007) based on the assumption that strong photodissociating radiation from the first stars quenches their formation. It appears likely, however, that this effect may not have substantially lowered the Pop III star formation rate (e.g. Ricotti et al. 2001; Johnson et al. 2007; O’Shea & Norman 2007; Wise & Abel 2007; see also Yoshida et al. 2003). Despite these differences, both models generate broadly similar MDFs. However, at variance with the results presented here, Salvadori et al. predict that the highest fraction of PISN-dominated stars is to be found in the lowest metallicity regime and only a very small fraction at $[\text{Fe}/\text{H}] > -1$, provided that the host halo is able to form both first and second generation stars. This finding may be a consequence of these authors’ assumption of the instantaneous mixing of metals in the galactic medium, but should be analyzed in more detail to be fully understood.

The most characteristic and reliable chemical signature of PISNe is probably the absence of neutron-capture elements. Although this may not be a unique fingerprint (massive core collapse SN may be unable to synthesis n-capture elements as well), we have shown that stars formed from material pre-enriched by PISNe emerge in a metallicity regime where both the r-process and the s-process signatures are thoroughly established (see Burris et al. 2000).

The presence of n-capture elements in normal Pop II stars will thus serve to rule out PISN pre-enrichment. Metal-poor stars with enhanced abundances of r-process elements are certainly interesting in their own right as they, e.g., can be used as cosmochronometers and allow us to study the origin and nature of the r-process. However, as important as it is to search for r-process enhanced stars (see e.g., Christlieb et al. 2004), alternatively, the search for stars unusually depleted in r-process elements may help us locate candidates of the “missing” second stellar generation. With high-resolution follow-up spectroscopy, further signatures indicative of PISNe such as a pronounced odd-even effect and, e.g., an atypical Fe/Ca ratio (see Fig. 5.5), should then be measured to ultimately verify or refute candidates as PISN-dominated, second generation stars. Although the actual number of PISN-dominated stars is predicted to be small, perhaps only one or two in 10 000 below $[Ca/H] = -2$, the ongoing and future large-scale surveys, such as the SDSS⁴, SEGUE⁵, and LAMOST⁶, aim to find at least an order of magnitude more stars in this metallicity regime than is presently known. A few thousand of these stars should be bright enough to be successfully observed with high-resolution by 8 – 10 m class telescopes (Beers & Christlieb 2005). With the advent of 30 – 100 m class telescopes, high-resolution spectroscopic follow-up will become feasible for the majority of stars discovered below $[Ca/H] = -2$.

⁴The Sloan Digital Sky Survey

⁵The Sloan Extension for Galactic Understanding and Evolution. Operating since 2005.

⁶The Large sky Area Multi-Object fiber Spectroscopic Telescope. First spectrum delivered May 28, 2007.

There are a few examples of metal-poor stars in the Galactic halo which do show anomalous abundance patterns. Ivans et al. (2003) studied a group of three dwarf/subgiant stars with $[\text{Ca}/\text{H}] \simeq -2.2$, BD 80° 245, G 4-36, and CS 22966-043, which appears to be heavily depleted in n-capture elements (see also, e.g., HD 122563, recently studied by Mashonkina et al. 2008). These stars also display low abundances of Na, Al, and α -elements, as indicated by the relatively high $[\text{Fe}/\text{Ca}]$ ratios in Figure 5.5. Interestingly, BD 80° 245 and G 4-36 both show a particularly low $[\text{Al}/\text{Ca}]$ ratio and BD 80° 245 and CS 22966-043 have $[\text{Mg}/\text{Ca}] < 0$. However, the $[\text{Na}/\text{Ca}]$ ratio in all three stars is found to be typical for Galactic halo stars and although the heavy iron-peak elements are low in BD 80° 245, they are strongly enhanced in G 4-36, and CS 22966-043, an observation which is not understood. Ivans et al. (2003), explain the peculiar abundance patterns as a result of an early contribution by thermonuclear SNe (Type Ia) in the subsystems in which these stars were born. They do not consider PISNe as an alternative, presumably because very massive stars traditionally are believed to contribute to the chemical enrichment only at the very lowest metallicities. As intriguing as it is to envision these objects, in particular BD 80° 245, as PISN-enriched, second generation stars, the match is ambiguous. Further investigation should, however, be conducted on these peculiar stars. Another star shown in Figure 5.5 is Draco 119. This $[\text{Fe}/\text{H}] = -2.9$ giant is a member of the Draco dSph and is the only star currently known to be completely devoid of elements above Ni, to within detection limits (Fulbright et al. 2004). The upper limit on the Ba abundance,

e.g., is estimated to $[\text{Ba}/\text{Fe}] < -2.6$, more than a full dex below the next most Ba-poor stars at $[\text{Fe}/\text{H}] \sim -3$. Based on the light element abundances, Fulbright et al. (2004) conclude that Draco 119 was born out of gas primarily enriched by massive core collapse SNe, and not by PISNe, which is consistent with our finding that PISN-dominated stars generally should appear above this metallicity regime.

We have assumed that the metal-poor Galactic halo mainly consists of stars formed during the assembly of atomic cooling halos. We note, however, that a significant fraction of these halos may have ended up in the bulge of the Milky Way. With the new high-resolution infrared spectrographs on the 8 – 10 m class telescopes, detailed spectral analysis of dust-obscured Galactic bulge stars has recently become feasible (e.g., Ryde et al. 2007). The search for relics of the first stars should therefore be pursued also in this, previously inaccessible part of our Galaxy.

V. B. acknowledges support from NSF grant AST-0708795. The cosmological simulation presented here was carried out at the Texas Advanced Computing Center (TACC). We would like to thank Anna Frebel, Norbert Christlieb, Kjell Eriksson, Stefania Salvadori, and Raffaella Schneider for helpful discussions. Finally, we would like to acknowledge the anonymous referee whose comments have greatly improved the presentation of this work.

Chapter 6

Outlook

The present research has focused on the theoretical study of the formation of primordial stars during the assembly of the first galaxies, and on ways in which the properties of these stars can be constrained using observations, both direct and indirect. With the assembly of the first galaxies and the onset of the formation of stellar clusters, the process of galaxy formation becomes considerably more complex. The injection of metals and dust into the primordial gas alters the chemical and cooling properties of the gas considerably; star formation becomes driven in part by turbulence that is generated through the accretion of gas from the IGM and supernova explosions; and the rapid growth of the first massive black holes leads to feedback from the high-energy radiation that is emitted during the process of accretion. In future work, these complicating factors will be carefully considered, as the further evolution of the first galaxies to those that have been detected already at $z \geq 6$ becomes more fully understood.

The impending launch of the *James Webb Space Telescope*, with its capability to detect the radiation emitted by the first galaxies and supernovae, is a major motivation for studying the formation of the earliest galaxies. In

Chapters 3 and 4, we argued that the detection of purely primordial stellar populations may still be out of reach even of the exquisitely sensitive instruments onboard the JWST. Future theoretical studies will seek to further refine this argument, and to make detailed predictions of what the JWST will reveal. As this telescope will likely detect galaxies with masses of $\geq 10^{10} M_{\odot}$ at redshifts $z \geq 10$, simulation of the assembly of such massive galaxies is a priority for future research.

The practice of stellar archaeology will, as well, continue to provide ever better constraints on the nature of the first stars. Large-scale surveys of metal-poor stars in our Galaxy, such as the *Sloan Extension for Galactic Understanding and Exploration*, will either reveal the signature of very massive primordial stars which exploded as pair-instability supernovae or place strong constraints on the fraction of such stars which formed in the first galaxies. These surveys may also uncover stars with lower metallicities than ever before found, thereby providing further insight into how the transition to low-mass star formation took place in the early Universe.

While the direct detection of the first dwarf galaxies may remain out of reach for the foreseeable future, the first supernovae and gamma-ray bursts, with their extraordinarily high luminosities, will be detectable under currently planned missions. The JWST will be capable of detecting the supernova explosions of the first stars, while the *Energetic X-ray Imaging Survey Telescope* may detect gamma-ray bursts out to redshifts of $z \sim 20$, thereby helping to elucidate how primordial stars end their lives.

With these and other observational missions allowing to test numerous aspects of our evolving theoretical picture of the assembly of the first galaxies, one can expect exciting advances to be coming at a rapid pace in this one of the main frontiers of cosmology.

Bibliography

- [1] Abel, T., Anninos, P., Zhang, Y., & Norman, M. L. 1997, *New Astro.*, 3, 181
- [2] Abel T., Bryan G. L., Norman M. L., 2002, *Science*, 295, 93
- [3] Abel T., Wise J. H., Bryan G. L., 2006, *ApJ*, 659, L87
- [4] Adelman-McCarthy J. et al., 2008, *ApJS*, 175, 297
- [5] Ahn, K., & Shapiro, P. R. 2007, *MNRAS*, 375, 881
- [6] Ahn K., Shapiro P. R., Iliev I. T., Mellema G., Pen U.-L., 2008, *ApJ*, accepted (arXiv:0807.2254)
- [7] Alvarez, M. A., Bromm, V., & Shapiro, P. R. 2006, *ApJ*, 639, 621
- [8] Alvarez M. A., Wise J. H., Abel T. 2008, *ApJ*, submitted (arXiv:0811.0820)
- [9] Arnone, E., Ryan, S. G., Argast, D., Norris, J. E., & Beers, T. C. 2005, *A&A*, 430, 507
- [10] Ballero, S. K., Matteucci, F., & Chiappini, C. 2006, *NewA*, 11, 306
- [11] Barkana, R., & Loeb, A. 2001, *Phys. Rep.*, 349, 125
- [12] Barkana R., Loeb A., 2007, *Rep. Prog. Phys.*, 70, 627

- [13] Barklem, P. S., et al. 2005, *A&A*, 439, 129
- [14] Barton E. J., et al. 2004, *ApJ*, 604, L1
- [15] Bate M. R. 2009, *MNRAS*, 392, 1363
- [16] Bateman, N. P. & Larson, R. B. 1993, *ApJ*, 407, 634
- [17] Beers, T. C., & Christlieb, N. 2005, *ARA&A*, 43, 531
- [18] Beers, T. C., Kage, J. A., Preston, G. W., & Shectman, S. A. 1990, *AJ*, 100, 849
- [19] Beers, T. C., Preston, G. W., & Shectman, S. A. 1992, *AJ*, 103, 1987
- [20] Beers, T. C., et al. 2005, in *IAU Symp. 228, From Lithium to Uranium: Elemental Tracers of Early Cosmic Evolution*, ed. V. Hill, P. François, & F. Primas (Cambridge: Cambridge University Press), 175
- [21] Bond, H. E. 1981, *ApJ*, 248, 606
- [22] Bondi H., 1952, *MNRAS*, 112, 195
- [23] Bouwens, R. J., & Illingworth, G. D. 2006, *Nature*, 443, 189
- [24] Brinchmann J., Pettini M., Charlot S., 2008, *MNRAS*, 385, 769
- [25] Bromm V., Larson R. B., 2004, *ARA&A*, 42, 79
- [26] Bromm V., Loeb A., 2003a, *ApJ*, 596, 34
- [27] Bromm V., Loeb A., 2003b, *Nat*, 425, 812

- [28] Bromm V., Loeb A., 2004, *New Astron.*, 9, 353
- [29] Bromm V., Coppi P. S., Larson R. B., 1999, *ApJ*, 527, L5
- [30] Bromm V., Coppi P. S., Larson R. B., 2002, *ApJ*, 564, 23
- [31] Bromm V., Ferrara A., Coppi P. S., Larson R. B., 2001a, *MNRAS*, 328,969
- [32] Bromm V., Kudritzki R. P., Loeb A., 2001b, *ApJ*, 552, 464
- [33] Bromm V., Yoshida N., Hernquist L., 2003, *ApJ*, 596, L135
- [34] Burris, D. L., Pilachowski, C. A., Armandroff, T. E., Sneden, C., Cowan, J. J., Roe, H. 2000, *ApJ*, 544, 302
- [35] Carollo D. et al., 2007, *Nat*, 450, 1020
- [36] Cayrel, R., et al. 2004, *A&A*, 416, 1117
- [37] Cen R., Riquelme M. A., 2008, *ApJ*, 674, 644
- [38] Chiappini C., Ekstrom S., Meynet G., Maeder A., Hirschi R. 2008, *First Stars III*, AIPC, 990, 325
- [39] Choudhury T. R., Ferrara A. 2007, *MNRAS*, 380, L6
- [40] Christlieb, N. et al. 2002, *Nature*, 419, 904
- [41] Christlieb, N., et al. 2004, *A&A*, 428, 1027
- [42] Chuzhoy L., Kuhlen M., Shapiro P. R., 2007, *ApJL*, 665, 85

- [43] Chuzhoy L., Shapiro P. R., 2007, ApJ, 655, 843
- [44] Ciardi B., Ferrara A., 2005, Space Sci. Rev., 116, 625
- [45] Ciardi, B., Ferrara, A., Governato, F., & Jenkins, A. 2000, MNRAS, 314, 611
- [46] Ciardi B., Salvaterra R., 2007, MNRAS, 381, 1137
- [47] Ciardi, B., Scannapieco, E., Stoehr, F., Ferrara, A., Iliev, I. T., & Shapiro, P. R. 2006, MNRAS, 366, 689
- [48] Cioffi, D. F., McKee, C. F., & Bertschinger, E. 1988, ApJ, 334, 252
- [49] Clark P. C., Glover S. C. O., Klessen R. S., 2008, ApJ, 672, 757
- [50] Cohen, J. G., et al. 2004, ApJ, 612, 1107
- [51] Collet R., Asplund M., Trampedach R., 2006, ApJ, 644, L121
- [52] Dale J. E., Bonnell I. A., Clarke C. J., Bate M. R. 2005, MNRAS, 358, 291
- [53] Dale J. E., Clark P. C., Bonnell I. A. 2007, MNRAS, 377, 535
- [54] Davé, R., Finlator, K., & Oppenheimer, B. D. 2006, MNRAS, 370, 273
- [55] Dawson S., et al. 2004, ApJ, 617, 707
- [56] de Jong, T. 1972, A&A, 20, 263
- [57] Dekel A., Rees M. J., 1987, Nat, 326, 455

- [58] Dijkstra M., Haiman Z., Mesinger A., Wyithe J. S. B. 2008, MNRAS, 391, 1961
- [59] Dijkstra M., Lidz A., Wyithe J. S. B. 2007, MNRAS, 377, 1175
- [60] Dijkstra M., Wyithe J. S. B. 2007, MNRAS, 379, 1589
- [61] Draine B., Bertoldi F., 1996, ApJ, 468, 269
- [62] Dunn, G. H. 1968, Phys. Rev., 172, 1
- [63] Ekström, S., Meynet, G., & Maeder, A. 2006, in ASP Conf. Ser. 353, Stellar Evolution at Low Metallicity: Mass Loss, Explosions, Cosmology, ed. H. J. G. L. M. Lamers, N. Langer, T. Nugis, & K. Annuk (San Fransisco: ASP), 141
- [64] Fan X. et al., 2004, AJ, 128, 515
- [65] Fan X. et al., 2006, AJ, 131, 1203
- [66] Fernandez E. R., Komatsu E., 2006, ApJ, 646, 703
- [67] Ferrara, A. 1998, ApJ, 499, L17
- [68] Frebel, A. et al. 2005, Nature, 434, 871
- [69] Frebel A., Johnson J. L., Bromm V., 2007, MNRAS, 380, L40
- [70] Frebel A., Collet R., Eriksson K., Christlieb N., Aoki W., 2008, ApJ, 684, 588

- [71] Freeman K., Bland-Hawthorn J., 2002, *ARA&A*, 40, 487
- [72] Fryer, C. L., Woosley, S. E., & Heger, A. 2001, *ApJ*, 550, 372
- [73] Fulbright J. P., 2000, *AJ*, 120, 1841
- [74] Fulbright, J. P., Rich, R. M., & Castro, S. 2004, *ApJ*, 612, 447
- [75] Galli, D., & Palla, F. 1998, *A&A*, 335, 403
- [76] Galli D., Palla F., 2002, *Planet. Space Sci.*, 50, 1197
- [77] Gao, L., Abel, T., Frenk, C. S., Jenkins, A., Springel, V., Yoshida, N., 2007, *MNRAS*, 378, 449
- [78] Gardner, J. P. et al. 2006, *Sp. Sci. Rev.*, 123, 485
- [79] Glover S. C. O., Brand P. W. J. L., 2001, *MNRAS*, 321, 385
- [80] Glover S. C. O., Brand P. W. J. L., 2003, *MNRAS*, 340, 210
- [81] Glover, S. C. O. 2005, *SSRv*, 117, 445
- [82] Glover S. C. O., Savin D. W., Jappsen A.-K., 2006, *ApJ*, 640, 553
- [83] Gnedin N. Y., Kravtsov A. V., Chen H.-W. 2008, *ApJ*, 672, 765
- [84] Greif T. H., Bromm V., 2006, *MNRAS*, 373, 128
- [85] Greif T. H., Johnson J. L., Bromm V., Klessen R. S., 2007, *ApJ*, 670, 1

- [86] Greif T. H., Johnson J. L., Klessen R., Bromm V., 2008, MNRAS, 387, 1021
- [87] Greif T. H., Johnson J. L., Klessen R. S., Bromm V., 2009, MNRAS, in prep.
- [88] Haiman Z., 2008, *Astrophysics in the Next Decade: JWST and Concurrent Facilities*. Springer, Dordrecht (arXiv:0809.3926)
- [89] Haiman, Z., Abel, T., & Rees, M. J. 2000, ApJ, 534, 11
- [90] Haiman, Z., & Loeb, A. 2001, ApJ, 552, 459
- [91] Haiman, Z., Rees, M. J., & Loeb, A. 1996, ApJ, 467, 522
- [92] Haiman Z., Rees M., Loeb A., 1997, ApJ, 476, 458
- [93] Heger, A., Fryer, C. L., Woosley, S. E., Langer, N., & Hartmann, D. H. 2003, ApJ, 591, 288
- [94] Heger, A. & Woosley, S. E. 2002, ApJ, 567, 532
- [95] Iben I., 1983, Mem. Soc. Astron. Ital., 54, 321
- [96] Ivans, I. I., Sneden, C., James, C. R., Preston, G. W., Fulbright, J. P., Höflich, P. A., Carney, B. W., & Wheeler, J. C. 2003, ApJ, 592, 906
- [97] Iwamoto N., Umeda H., Tominaga N., Nomoto K., Maeda K., 2005, Science, 309, 451

- [98] Iye, M., et al. 2006, Nature, 443, 186
- [99] Jasche J., Ciardi B., Ensslin T. A., 2007, MNRAS, 380, 417
- [100] Jappsen, A.-K., Glover, S. C. O., Klessen, R. S., MacLow M.-M. 2007, ApJ, 660, 1332
- [101] Jappsen A.-K., Klessen R. S., Glover S. C. O., Mac Low M.-M. 2009a, ApJ, in press (arXiv:0709.3530)
- [102] Jappsen A.-K., Mac Low M.-M., Glover S. C. O., Klessen R. S., Kitsionas S. 2009b, ApJ, in press (arXiv:0810.1867)
- [103] Jimenez, R., & Haiman, Z. 2006, Nature, 440, 501
- [104] Johnson J. L., Bromm V., 2006, MNRAS, 366, 247
- [105] Johnson J. L., Bromm V., 2007, MNRAS, 374, 1557
- [106] Johnson J. L., Greif T. H., Bromm V., 2007, ApJ, 665, 85
- [107] Johnson J. L., Greif T. H., Bromm V. 2008, MNRAS, 388, 26
- [108] Johnston K. V., 1998, ApJ, 495, 297
- [109] Kang, H., & Shapiro, P. R. 1992, ApJ, 386, 432
- [110] Karlsson, T., Johnson J. L., Bromm V. 2008, ApJ, 679, 6
- [111] Karlsson, T. 2005, A&A, 439, 93
- [112] Karlsson, T. 2006, ApJ, 641, L41

- [113] Karlsson, T. & Gustafsson, B. 2005, *A&A*, 436, 879
- [114] Karpas, Z., Anicich, V., & Huntress, W. T. 1979, *J. Chem. Phys.*, 70, 2877
- [115] Kashlinsky, A., Arendt, R. G., Mather, J., & Moseley, S. H. 2007, *ApJ*, 654, L5
- [116] Kawata, D., Arimoto, N., Cen, R., & Gibson, B. K. 2006, *ApJ*, 641, 785
- [117] Kawata D., Gibson B. K., 2003, *MNRAS*, 346, 135
- [118] Kennicutt, R. C., Jr. 1983, *ApJ*, 272, 54
- [119] Kitayama T., Yoshida N., 2005, *ApJ*, 630, 675
- [120] Kitayama, T., Yoshida, N., Susa, H., & Umemura, M. 2004, *ApJ*, 613, 631
- [121] Kroupa, P. 2001, *MNRAS*, 322, 231
- [122] Krumholz M. R., Klein R. I., McKee C. F. 2007, *ApJ*, 656, 959
- [123] Kuhlen M., Madau P. 2005, *MNRAS*, 363, 1069
- [124] Lacey C., Cole S., 1993, *MNRAS*, 262, 627
- [125] Langer, N., Norman, C. A., de Koter, A., Vink J., Cantiello M., & Yoon S.-C. 2007, *A&A*, 475, L19
- [126] Larson, R. B. & Starrfield, S. 1971, *A&A*, 13, 190

- [127] Larson R. B., 1998, MNRAS, 301, 569
- [128] Larson R. B., 2005, MNRAS, 359, 211
- [129] Lee Y. S. et al., 2007, AJ, 136, 2022
- [130] Lepp S., Shull J. M., 1984, ApJ, 280, 465
- [131] Li Y., et al., 2007, ApJ, 665, 187
- [132] Loeb A. 2008, Phys. Rev. submitted (arXiv:0811.2222)
- [133] Loeb A., Rybicki G. B., 1999, ApJ, 524, 527
- [134] Mac Low M.-M., Toraskar J., Oishi J. S. 2007, ApJ, 668, 980
- [135] Machacek, M. E., Bryan, G. L., & Abel, T. 2001, ApJ, 548, 509
- [136] Machacek, M. E., Bryan, G. L., & Abel, T. 2003, MNRAS, 338, 273
- [137] Machida M., Tomisaka K., Nakamura F., Fujimoto M., 2005, ApJ, 622, 39
- [138] Mackey J., Bromm V., Hernquist L., 2003, ApJ, 586, 1
- [139] Madau P., Rees M. J., 2001, ApJ, 551, L27
- [140] Malhotra S., Rhoads J. E. 2002, ApJ, 565, L71
- [141] Marigo P., Girardi L., Chiosi C., Wood P. R., 2001, A&A, 371, 152
- [142] Mashonkina, L., et al. 2008, A&A, 478, 529

- [143] Matteucci, F. 2003, *Ap&SS*, 284, 539
- [144] Mayle, R. & Wilson, J. R. 1988, *ApJ*, 334, 909
- [145] McKee C. F., Tan J. C., 2008, *ApJ*, 681, 771
- [146] Mesinger A., Bryan G. L., Haiman Z., 2006, *ApJ*, 648, 835
- [147] Milosavljević M., Bromm V., Couch S. M., Oh S. P. 2008, *ApJ*, in press
(arXiv:0809.2404)
- [148] Milosavljević M., Couch S. M., Bromm V. 2009, *ApJ*, submitted (arXiv:0812.2516)
- [149] Mobasher, B., et al. 2005, , 635, 832
- [150] Mori M., Ferrara A., Madau P., 2002, *ApJ*, 571, 40
- [151] Munn J. A. et al., 2004, *AJ*, 127, 3034
- [Murray et al.(1993)] Murray, S. D., White, S. D. M., Blondin, J. M., Lin,
D. N. C., 1993, *ApJ*, 407, 588
- [152] Nagakura T., Omukai K., 2005, *MNRAS*, 364, 1378
- [153] Nagao T., et al. 2008, *ApJ*, 680, 100
- [154] Nagao T., et al., 2007, *AA*, 468, 877
- [155] Nagao T., et al. 2005, *ApJ*, 631, L5
- [156] Nakamura, T., Umeda, H., Iwamoto, K., Nomoto, K., Hashimoto, M.,
Hix, W. R., & Thielemann, K.-F. 2001, *ApJ*, 555, 880

- [157] Nomoto, K. 1987, *ApJ*, 322, 206
- [158] Nomoto, K., Tominaga, N., Umeda, H., Kobayashi, C., & Maeda, K. 2006, *Nucl. Phys. A*, 777, 424
- [159] Norris J. E., Christlieb N., Korn A. J., Eriksson K., Bessell M. S., Beers T. C., Wisotzki L., Reimers D., 2007, *ApJ*, 670, 774
- [160] Oey, M. S. 2003, *MNRAS*, 339, 849
- [161] Oh S. P., Haiman Z., 2002, *ApJ*, 569, 558
- [162] Oh S. P., Haiman Z., 2003, *MNRAS*, 346, 456
- [163] Oh S. P., Haiman Z., Rees M. J. 2001, *ApJ*, 553, 73
- [164] Omukai K., Palla F., 2001, *ApJ*, 561, L55
- [165] Omukai K., Palla F., 2003, *ApJ*, 589, 677
- [166] Omukai K., Schneider R., Haiman Z. 2008, *ApJ*, 686, 801
- [167] Omukai K., Tsuribe T., Schneider R., Ferrara A., 2005, *ApJ*, 626, 627
- [168] O'Shea, B. W., Abel, T., Whalen, D., & Norman, M. L. 2005, *ApJ*, 628, L5
- [169] O'Shea B. W., Norman, M. L., 2008, *ApJ*, 673, 14
- [170] Osterbrock D., Ferland G., 2006, *Astrophysics of Gaseous Nebulae and Active Galactic Nuclei*. University Science Books, Sausalito

- [171] Padmanabhan, T. 2002, *Theoretical Astrophysics, Volume III: Galaxies and Cosmology* (Cambridge, UK: Cambridge University Press)
- [172] Padoan, P., Nordlund, A., Kritsuk, A. G., Norman, M. L., & Li, P. S. 2007, *ApJ*, 661, 972
- [173] Pagel B. E. J., 1997, *Nucleosynthesis and Chemical Evolution of Galaxies*. Cambridge University Press, Cambridge
- [174] Pagel, B. E. J. & Tautvaišienė, G. 1995, *MNRAS*, 276, 505
- [175] Palla, F. 2002, in *Physics of Star Formation in Galaxies*, ed. A. Maeder & G. Meynet (Berlin: Springer)
- [176] Pan, L. & Scalo, J. 2007, *ApJ*, 654, L29
- [177] Panagia N. 2004, arXiv:0410235
- [178] Peebles, P. J. E., & Dicke R. H., 1968, *ApJ*, 154, 891
- [179] Pelupessy, F. I., Di Matteo, T., Ciardi, B., 2007, *ApJ*, 665, 107
- [180] Pflamm-Altenburg J., Weidner C., Kroupa P. 2007, *ApJ*, 671, 1550
- [181] Prantzos, N. 2005, *Nucl. Phys. A*, 758, 249
- [182] Razoumov A. O., Sommer-Larsen J., 2009, *ApJ*, submitted (arXiv:0903.2045)
- [183] Read J. I., Pontzen A. P., Viel M., 2006, *MNRAS*, 371, 885
- [184] Refsdal S. 1964, *MNRAS*, 128, 295

- [185] Regan J. A., Haehnelt M. G. 2009, MNRAS, 393, 858
- [186] Ricotti M., Gnedin N., & Shull J. M., 2001, ApJ, 560, 580
- [187] Ricotti M., Gnedin N., & Shull J. M., 2002a, ApJ, 575, 33
- [188] Ricotti M., Gnedin N., Shull J. M., 2002b, ApJ, 575, 49
- [189] Ricotti M., Gnedin N., Shull J. M., 2008, ApJ, 685, 21
- [190] Robertson, B., Bullock, J. S., Font, A. S., Johnston, K. V., & Hernquist, L. 2005, ApJ, 632, 872
- [191] Ryan, S. G., Norris, J. E., & Beers, T. C. 1996, ApJ, 471, 254
- [192] Ryde, N., Edvardsson, B., Gustafsson, B., & Käufel, H. U. 2007, in IAU Symp. 241, Stellar Populations as Building Blocks of Galaxies, ed. A. Vazdekis & R. F. Peletier (Cambridge: Cambridge University Press), 260
- [193] Sakuma M., Susa H. 2009, ApJ, accepted (arXiv:0904.2355)
- [194] Salvadori S., Schneider R., Ferrara A., 2007, MNRAS, 381, 647
- [195] Salvaterra R., Ferrara A., Schneider R., 2004, New Astron., 10, 113
- [196] Samland, M., Hensler, G., & Theis, C. 1997, ApJ, 476, 544
- [197] Santoro F., Shull J. M., 2006, ApJ, 643, 26
- [198] Santos M. R., Bromm V., Kamionkowski M., 2002, MNRAS, 336, 1082

- [199] Scannapieco, E., Kawata, D., Brook, C. B., Schneider, R., Ferrara, A., & Gibson, B. K. 2006, *ApJ*, 653, 285
- [200] Schaerer D., 2002, *A&A*, 382, 28
- [201] Schaerer D., 2003, *A&A*, 397, 527
- [202] Schaerer D., Vacca W. D., 1998, *ApJ*, 497, 618
- [203] Schneider R., Ferrara A., Salvaterra R., Omukai K., Bromm V., 2003, *Nat*, 422, 869
- [204] Schneider R., Omukai K., Inoue A. K., Ferrara A., 2006, *MNRAS*, 369, 1437
- [205] Shapiro P. R., Iliev I. T., Raga A. C., 2004, *MNRAS*, 348, 753
- [206] Shapiro P. R., Kang H., 1987, *ApJ*, 318, 32
- [207] Shapley A. E., Steidel C. C., Pettini M., Adelberger K. L. 2003, *ApJ*, 588, 65
- [208] Sheth R. K., Mo H. J., Tormen G., 2001, *MNRAS*, 323, 1
- [209] Shetrone, M. D., Côté, P., & Sargent, W. L. W. 2001, *ApJ*, 548, 592
- [210] Shull J. M., McKee C. F., 1979, *ApJ*, 227, 131
- [211] Silk, J. & Langer, M. 2006, *MNRAS*, 371, 444
- [212] Smith B. D., Sigurdsson S., 2007, *ApJ*, 661, L5

- [213] Smith, N., et al. 2007, ApJ, 666, 1116
- [214] Spergel D. N., et al. 2003, ApJS, 148, 175
- [215] Spergel D. N., et al. 2007, ApJS, 170, 377
- [216] Springel V., Hernquist L., 2002, MNRAS, 333, 649
- [217] Springel V., Yoshida N., White S. D. M., 2001, New Astron., 6, 79
- [218] Stacy A., Bromm V., 2007, MNRAS, 382, 229
- [219] Stark D. P., et al. 2007, ApJ, 663, 10
- [220] Susa H., 2007, ApJ, 659, 908
- [221] Susa H., Umemura M., 2006, ApJ, 645, L93
- [222] Talbot Jr., R. J., Newman M. J., 1977, ApJS, 34, 295
- [223] Tan J. C., McKee C. F., 2004, ApJ, 603, 383
- [224] Tassis, K., Abel, T., Bryan, G. L., & Norman, M. I. 2003, ApJ, 587, 13
- [225] Tassis, K., Kravtsov, A. V., & Gnedin, N. Y. 2008, ApJ, 672, 888
- [226] Tegmark M., Silk J., Rees M. J., Blanchard A., Abel T., Palla F., 1997, ApJ, 474, 1
- [227] Tornatore L., Ferrara A., Schneider R. 2007, MNRAS, 382, 945
- [228] Trenti M., Stiavelli M. 2009, ApJ, accepted (arXiv:0901.0711)

- [229] Tumlinson J., Giroux M. L., Shull M. J. 2001, ApJ, 550, L1
- [230] Tumlinson, J. 2006, ApJ, 641, 1
- [231] Tumlinson, J. 2007, ApJ, 665, 1361
- [232] Tumlinson, J., Venkatesan, A., & Shull, J. M. 2004, ApJ, 612, 602
- [233] Umeda, H. & Nomoto, K. 2002, ApJ, 565, 385
- [234] Umeda, H., Nomoto, K., 2003, Nat, 422, 871
- [235] Vazquez G. A., Leitherer C., Schaerer D., Meynet G., Maeder A. 2007, ApJ, 663, 995
- [236] Venn, K. A., Irwin, M., Shetrone, M. D., Tout, C. A., Hill, V., & Tolstoy, E. 2004, AJ, 128, 1177
- [237] Volonteri, M., & Rees, M. J. 2006, ApJ, 650, 669
- [238] Walter, F. & Carilli, C. 2008, Ap&SS, 313, 313
- [239] Whalen, D., Abel, T., & Norman, M. L. 2004, ApJ, 610, 14
- [240] Whalen D., O'Shea B. W., Smidt J., Norman M. L. 2008, ApJ, 679, 925
- [241] Windhorst R. A., Cohen S. H., Jansen R. A., Conselice C., Yan H. 2006, New Astron. Rev., 50, 113
- [242] Wise J. H., Abel T., 2005, ApJ, 629, 615
- [243] Wise J. H., Abel T., 2008, ApJ, 684, 1

- [244] Wise J. H., Abel T., 2007b, ApJ, 671, 1559
- [245] Wise J. H., Abel T., 2007c, ApJ, 665, 899
- [246] Wise J. H., Cen R. 2008, ApJ, submitted (arXiv:0808.2477)
- [247] Wise J. H., Turk M. J., Abel T. 2008, ApJ, 682, 745
- [248] Wisotzki, L., Christlieb, N., Bade, N., Beckmann, V., Köhler, T., Vanelle, C., & Reimers, D. 2000, A&A, 358, 77
- [249] Wood D. O. S., Churchwell E., 1989, ApJS, 69, 831
- [250] Woosley S. E., Heger A. 2006, ApJ, 637, 914
- [251] Wyithe, J. S. B., Cen, R., 2007, ApJ, 659, 890
- [252] Xie T., Mundy L. G., Vogel S. N., 1996, ApJ, 473, L131
- [253] Yoon S.-C., Langer N. 2005, AA, 443, 643
- [254] Yoshida N., Abel T., Hernquist L., Sugiyama N., 2003, ApJ, 592, 645
- [255] Yoshida N., 2006, New Astron. Rev., 50, 19
- [256] Yoshida N., Oh S. P., Kitayama T., Hernquist L., 2007, ApJ, 663, 687
- [257] Yoshida N., Omukai, K., Hernquist, L., Abel, T., 2006, ApJ, 652, 6
- [258] Yoshida N., Omukai K., Hernquist L., 2008, Sci, 321, 669
- [259] Yoshii Y., 1981, A&A, 97, 280

Vita

Jarrett Lawrence Johnson was born in Lawrence, Kansas on November 11, 1981, the son of Michael and Kathleen Johnson. After graduating from Baldwin High School, Baldwin City, Kansas, in 2000, he entered Truman State University in Kirksville, Missouri, as a General John J. Pershing Scholar. He received the degree of Bachelor of Science in Physics, with minors in Mathematics and Spanish, in May, 2004, graduating as a valedictorian of his class at Truman State University. In August, 2004, he started graduate studies in Astronomy at the University of Texas at Austin. He received the degree of Master of Arts in Astronomy in August, 2006, and was awarded the Outstanding Thesis Award by the Graduate School of the University of Texas at Austin for his thesis *Towards the First Galaxies*.

Permanent address: 7630 Wood Hollow Dr., Apt. 334
Austin, Texas 78731

This dissertation was typeset with L^AT_EX[†] by the author.

[†]L^AT_EX is a document preparation system developed by Leslie Lamport as a special version of Donald Knuth's T_EX Program.